Profile analysis: Retrieval of physical parameters

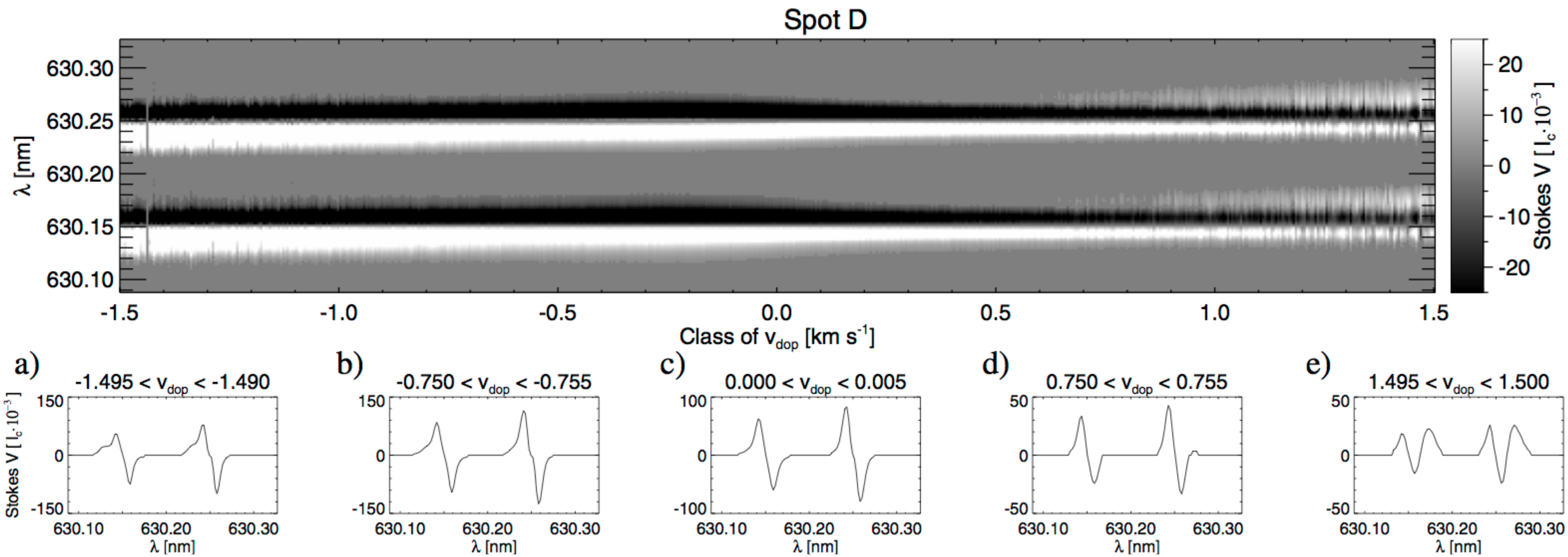

Fig. 4. *Top*: average Stokes *V* profiles of different bins of Doppler velocity for the penumbra of dataset Spot D. White represents the positive lobe, black the negative lobe. The picture is saturated at a continuum intensity of 2.5% and all measurements below the 3σ noise level were artificially set to zero. *Bottom*: examples of averaged profiles in various velocity bins.

(Franz & Schl. 2013)

1st SOLARNET Week above the Clouds
August 5 – 9, 2019 at Observatorio del Teide in Tenerife

Rolf Schlichenmaier
Leibniz-Institut für Sonnenphysik, Freiburg, Germany

Leibniz-Institut für Sonnenphysik (KIS)

The phase of the radial mean field in the solar dynamo

R. Schlichenmaier* **and M. Stix**

Kiepenheuer-Institut für Sonnenphysik, Schöneckstr. 6, D-79104 Freiburg, Germany

A&A 302, 264-270 (1995)

Received 20 December 1994 / Accepted 25 February 1995

Abstract. Observations indicate that the radial and azimuthal components of the mean solar magnetic field oscillate with a phase shift of approximately 180° during the 22-year cycle. In order to calculate such phase shifts we construct a simple two-dimensional, nonlinear $\alpha^2\Omega$ dynamo, which operates in the overshoot region beneath the convection zone. Like previous models, our model predicts an almost in-phase oscillation for most parameter choices. Special configurations, in which the two components of the mean field have different distributions in latitude, may resolve the dilemma. Alternative conclusions are that our knowledge of the α effect is insufficient, or that the observational result is not reliable.

Key words: MHD – Sun: activity – Sun: magnetic fields

$$\partial_t A = D \sin 2x \ \sin z\, B + \nabla^2 A - CB \ ,$$

$$\partial_t B = \sin x \ \sin z\, \partial_x A - (1 - \cos z) \cos x\, \partial_z A - \frac{C_\alpha}{C_\Omega} \nabla \cdot [\sin 2x \ \sin z\, \nabla A] + \frac{1}{C_\Omega^2} \nabla \cdot C \nabla A + \nabla^2 B \ ,$$

and

$$\partial_t C = AB + \nu \nabla^2 C \ .$$

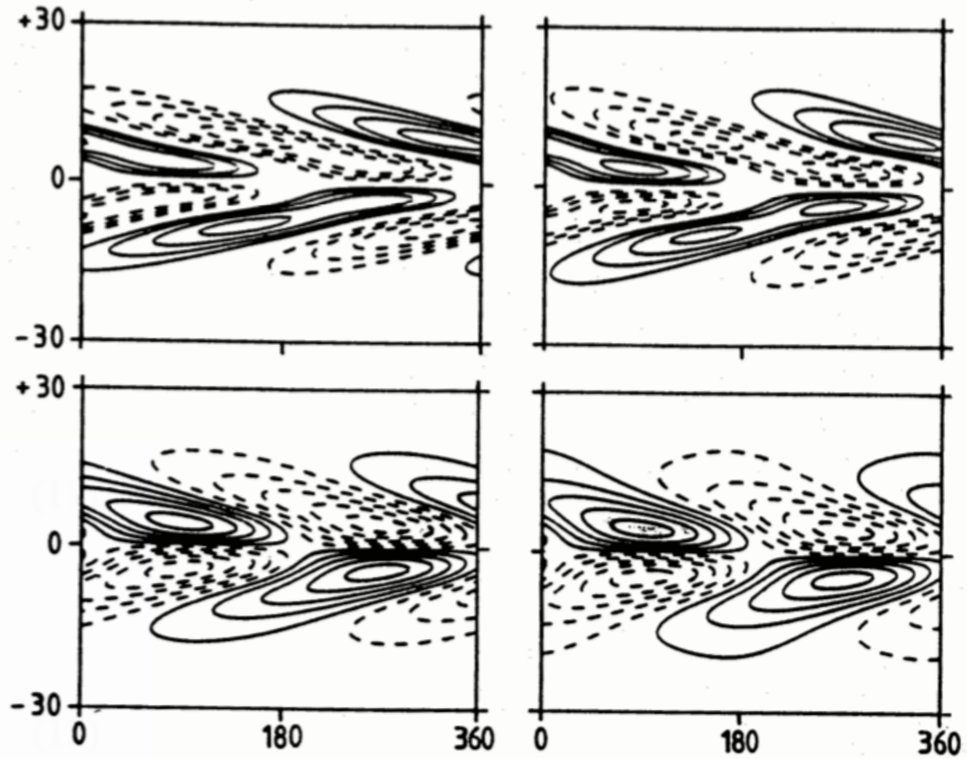

Fig. 3. Butterfly diagrams for marginally stable oscillatory magnetic fields of dipolar symmetry in the case $Q = 12.5$: Contours of the radial and toroidal field components (*upper* and *lower* panels, resp.), for $C_\alpha/C_\Omega = -10^{-5}$ (*left*) and $C_\alpha/C_\Omega = -0.01$ (*right*). *Solid* curves mark positive, *dashed* negative values. The depth is $z_0 = \pi/2$, the middle of the dynamo layer

Magnetic flux tubes evolving in sunspots

A model for the penumbral fine structure and the Evershed flow

R. Schlichenmaier[1]⋆, K. Jahn[2], and H.U. Schmidt[3]

[1] Max-Planck-Institut für extraterrestrische Physik, D-85748 Garching, Germany
[2] Warsaw University Observatory, Al. Ujazdowskie 4, PL-00 478 Warsaw, Poland (crj@astrouw.edu.pl)
[3] Max-Planck-Institut für Astrophysik, Karl-Schwarzschild-Str. 1, D-85748 Garching, Germany

Received 29 January 1998 / Accepted 26 June 1998

A&A 337, 897 (1998)

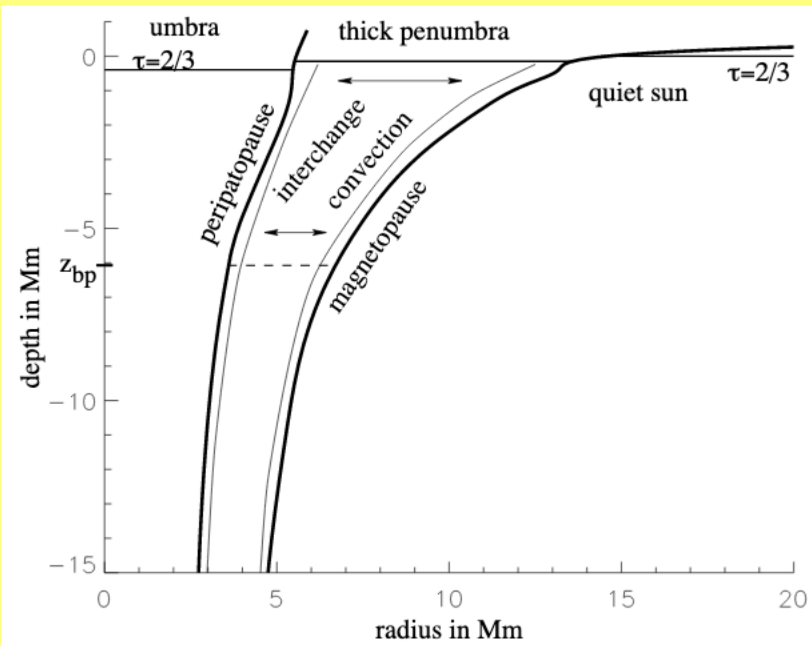

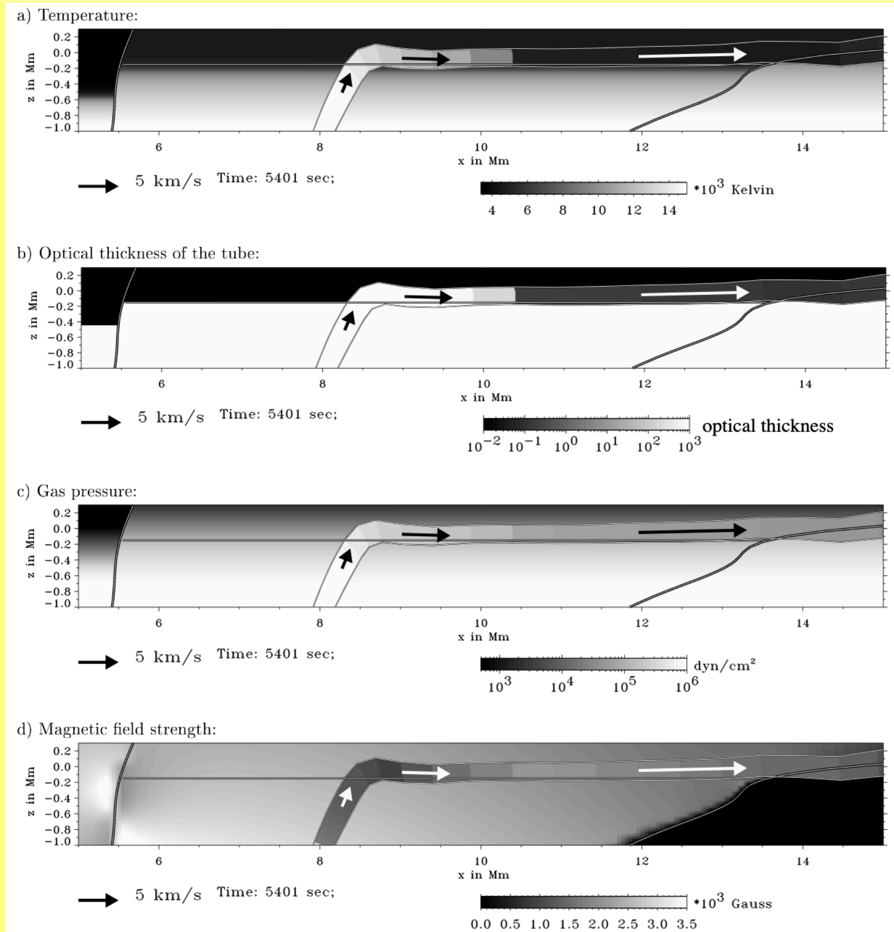

Radiative transfer
in a magnetic atmosphere

Magnetic field measurements: The Zeeman effect

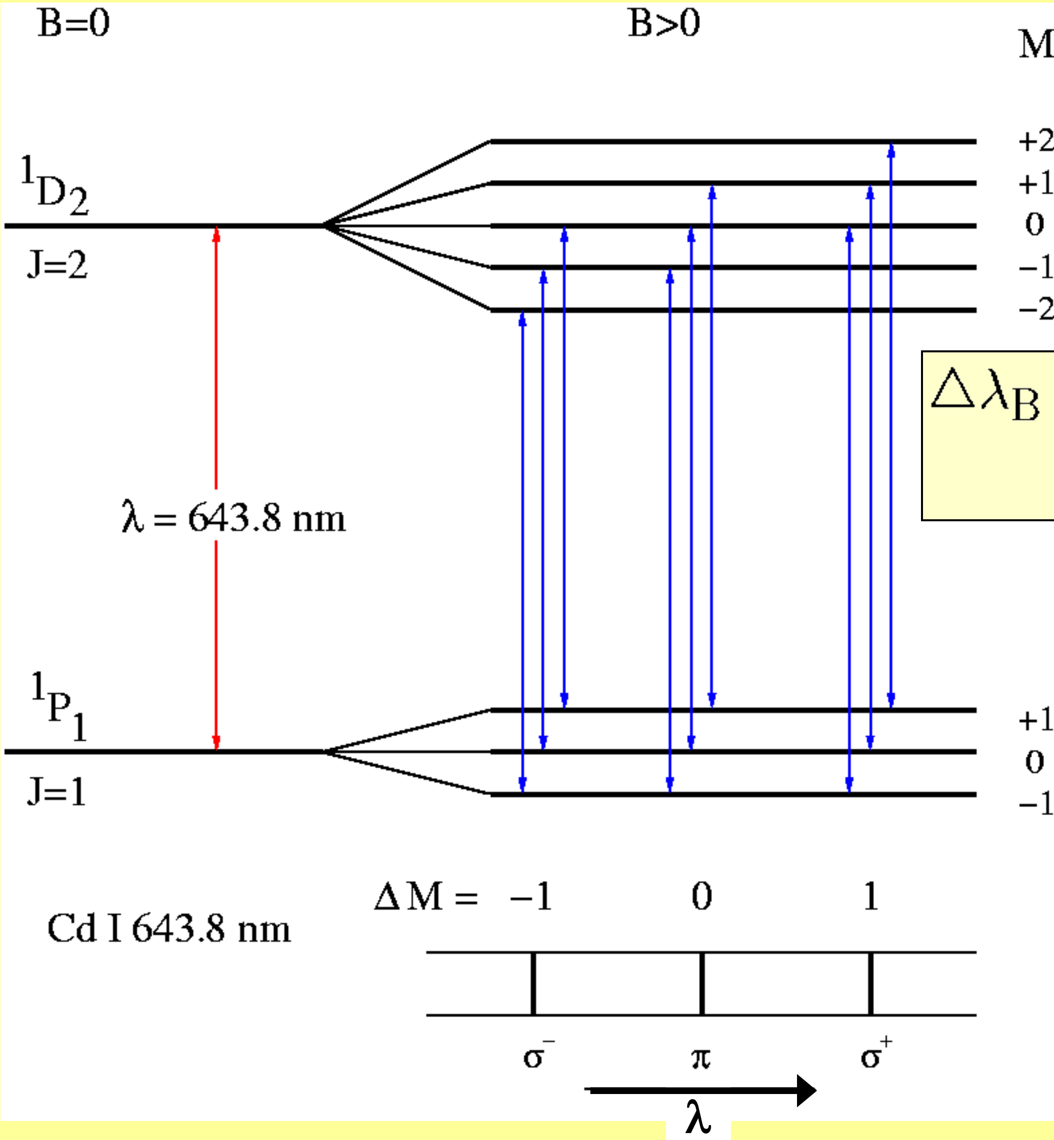

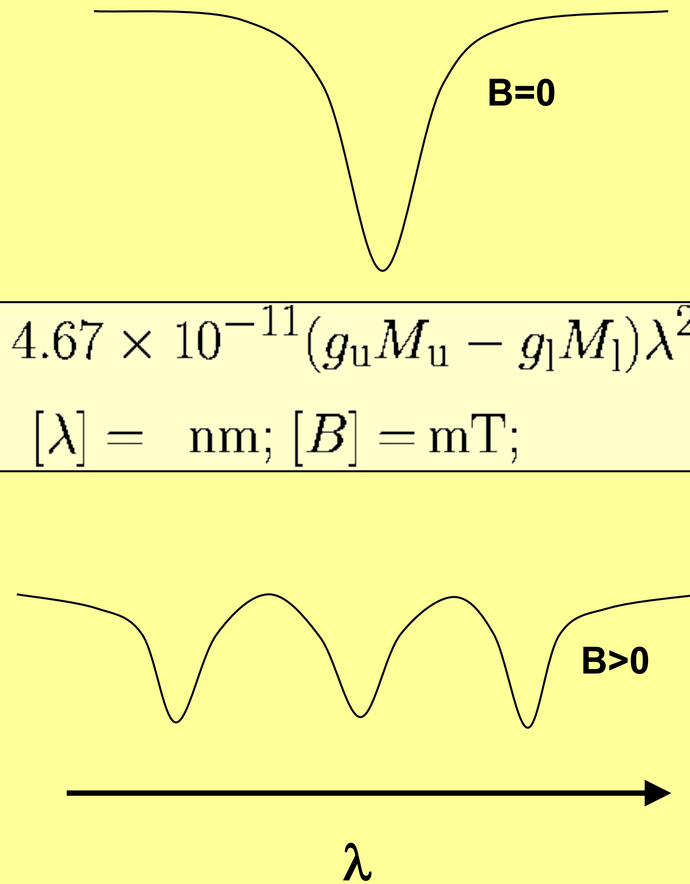

$$\Delta\lambda_{\mathrm{B}} = 4.67 \times 10^{-11} (g_{\mathrm{u}} M_{\mathrm{u}} - g_{\mathrm{l}} M_{\mathrm{l}}) \lambda^2 B$$

$$[\lambda] = \ \mathrm{nm}; \ [B] = \mathrm{mT};$$

Weak field limit:

Polarized light: The Stokes Parameter

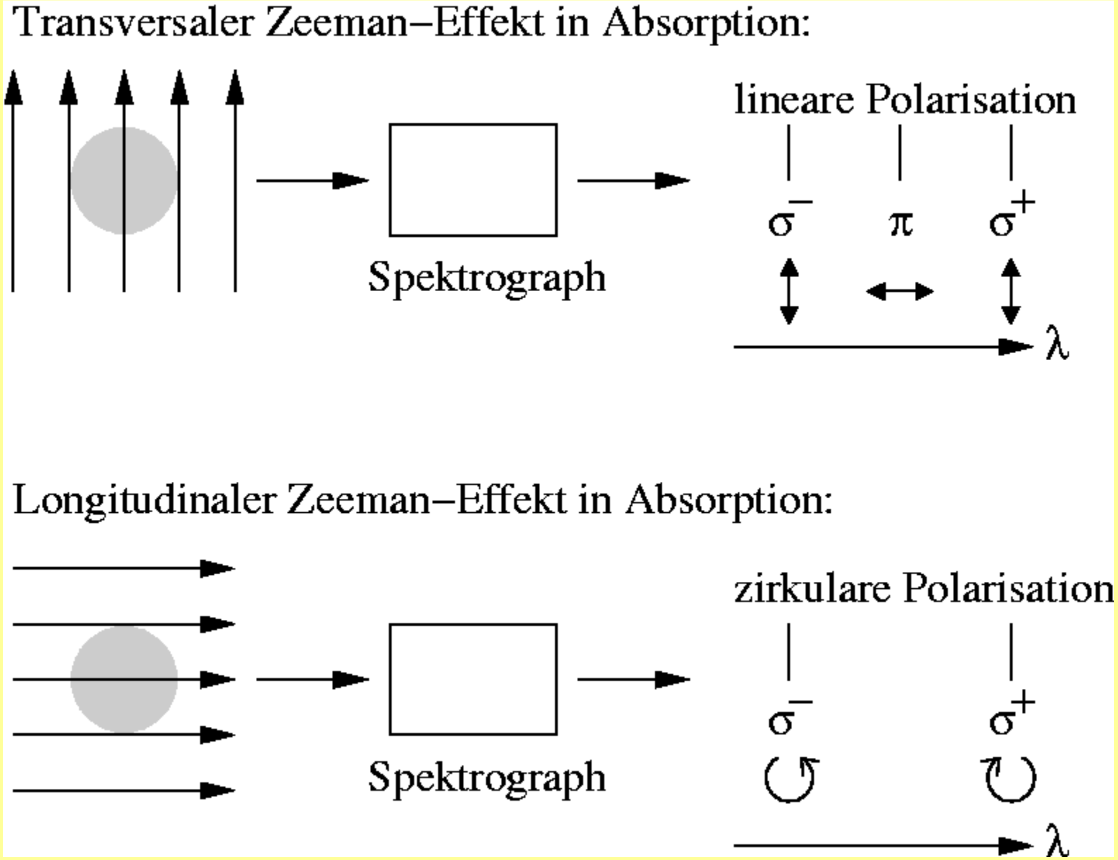

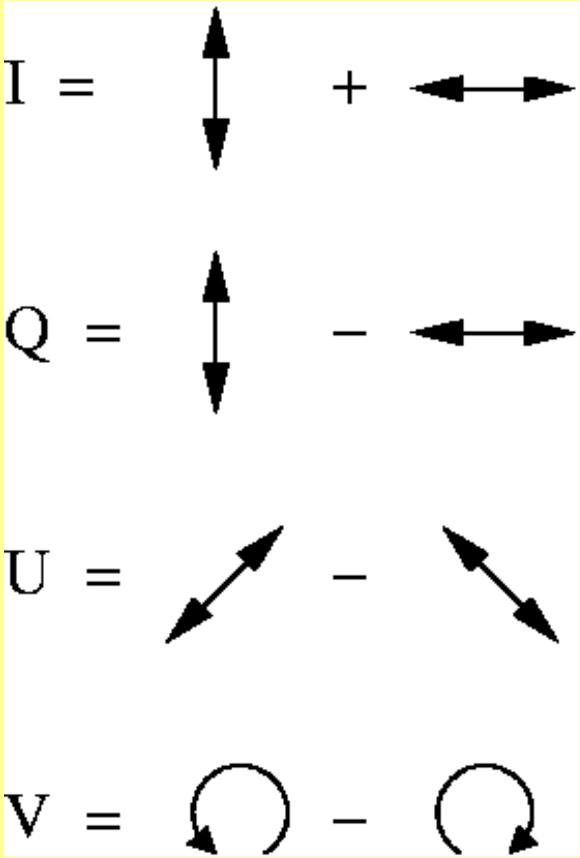

Attention: Zeeman effect in emission causes sign reversal in Stokes V.

Reversal of Sokes V: opposite polarity **or** emission instead of absorption

The radiation transfer equation for the Stokes vector $\mathbf{S}$ in the solar atmosphere is given by

$$\cos\theta \frac{d\mathbf{S}_\nu(\tau)}{d\tau} = \mathcal{M} \cdot \left(\mathbf{S}_\nu(\tau) - (B_\nu(\tau),0,0,0)^{\mathrm{T}}\right) . \tag{B.1}$$

The total absorption matrix $\mathcal{M}$ is given by

$$\kappa_c \cdot \mathcal{M} = \kappa_0 \cdot \eta + \kappa_c \cdot \mathbb{1} = \begin{pmatrix} \eta_I & \eta_Q & \eta_U & \eta_V \\ \eta_Q & \eta_I & \rho_V & -\rho_U \\ \eta_U & -\rho_V & \eta_I & \rho_Q \\ \eta_V & \rho_U & -\rho_Q & \eta_I \end{pmatrix} + \kappa_c \cdot \mathbb{1} , \tag{B.2}$$

The entries of η can be derived from the properties of the electric transition in the presence of magnetic fields (Landi degl'Innocenti & Landi degl'Innocenti 1972). They are given by

$$\eta_I = \frac{1}{2}\left[\eta_p \sin^2\gamma + \frac{1}{2}(\eta_r + \eta_b)(1+\cos^2\gamma)\right] \tag{B.3}$$

$$\eta_Q = \frac{1}{2}\left[\eta_p - \frac{1}{2}(\eta_r + \eta_b)\right] \sin^2\gamma \cos 2\phi \tag{B.4}$$

$$\eta_U = \frac{1}{2}\left[\eta_p - \frac{1}{2}(\eta_r + \eta_b)\right] \sin^2\gamma \sin 2\phi \tag{B.5}$$

$$\eta_V = \frac{1}{2}\left[\eta_p - \frac{1}{2}(\eta_r + \eta_b)\right] \sin^2\gamma \cos 2\phi \tag{B.6}$$

$$\rho_Q = \frac{1}{2}\left[\rho_p - \frac{1}{2}(\rho_r + \rho_b)\right] \sin^2\gamma \cos 2\phi \tag{B.7}$$

$$\rho_Q = \frac{1}{2}\left[\rho_p - \frac{1}{2}(\rho_r + \rho_b)\right] \sin^2\gamma \sin 2\phi \tag{B.8}$$

$$\rho_V = \frac{1}{2}\left[\rho_p - \rho_r\right] \cos\gamma \tag{B.9}$$

γ denotes the inclination between magnetic field and the line of sight (LOS), ϕ the field azimuth in the plane perpendicular to the LOS, $\eta_{p,b,r}$ and $\rho_{p,b,r}$ the general profile functions for absorption and anormal dispersion.

The profile functions are defined as the energy emission of a damped oscillator with a finite life time, Γ, that is additionally smeared out by the random distribution of the absorber velocities. The profile function is then given by the convolution of a Lorentz profile ($\propto \frac{\Gamma}{1+\Gamma^2}$) with a Gaussian ($\propto e^{-\nu^2}$):

$$\Phi(\nu) = \frac{\Gamma}{\sqrt{\pi}\Delta\nu_D} \int_{-\infty}^{+\infty} \frac{\exp\left[-(\nu-\nu')^2/\Delta\nu_D^2\right]}{(2\pi)^2(\nu'-\nu_0)^2 + \Gamma^2/4} d\nu' , \tag{B.10}$$

Beck (2005, after Landi degl'Innocenti & Landi degl'Innocenti 1972)

with the thermally induced Doppler width, $\Delta\nu_D = \nu_0/c\sqrt{2kT/m}$, and the frequency of the transition, ν_0.
Using

$$y = (\nu - \nu')/\Delta\nu_D, \tag{B.11}$$
$$a = \Gamma 4\pi\Delta\nu_D, \text{ and} \tag{B.12}$$
$$v = (\nu - \nu_0)/\Delta\nu_D, \tag{B.13}$$

Eq. (B.10) can be written as

$$\Phi(\nu) = \frac{1}{\sqrt{\pi}\Delta\nu_D} H(v,a), \tag{B.14}$$

with the *Voigt function* $H(v,a)$ given by

$$H(v,a) = \frac{a}{\pi}\int_{-\infty}^{+\infty} \frac{e^{-y^2}dy}{(v-y)^2+a^2} \,. \tag{B.15}$$

With the indices p for the π-component of a Zeeman triplet at the rest wavelength, b for the σ^--component, and r for the σ^+-component (cf. Sect. 3.1) the quantities $\eta_{p,b,r}$ and $\rho_{p,b,r}$ are given by

$$\eta_i = \sum w_i H(v - v_i, a) \tag{B.16}$$
$$\rho_i = \sum w_i F(v - v_i, a) \,, \tag{B.17}$$

with the *Faraday-Voigt function*

$$F(v,a) = \frac{a}{2\pi}\int_{-\infty}^{+\infty} \frac{(v-y)e^{y^2}dy}{(v-y)^2+a^2} \,. \tag{B.18}$$

w_i are the statistical weights for the transition probability, and v_i is determined by the strength of the magnetic field by

$$v_i = v_0 \pm \frac{e}{4\pi m_e c^2}\frac{\lambda_0^2}{\Delta\lambda_D} \cdot B \,. \tag{B.19}$$

Doppler shifts due to the flow velocity in the atmosphere are added to v_i. The effect of the microturbulent velocity, v_{mic}, is added to the collision broadening coefficient, $\Gamma_{\text{tot}} = \Gamma + \Gamma_{v_{mic}}$. The effect of the macroturbulent velocity, v_{mac}, is added to the thermal Doppler width.

Beck (2005, after Landi degl'Innocenti & Landi degl'Innocenti 1972)

Line profile: profile function $\phi(\lambda)$

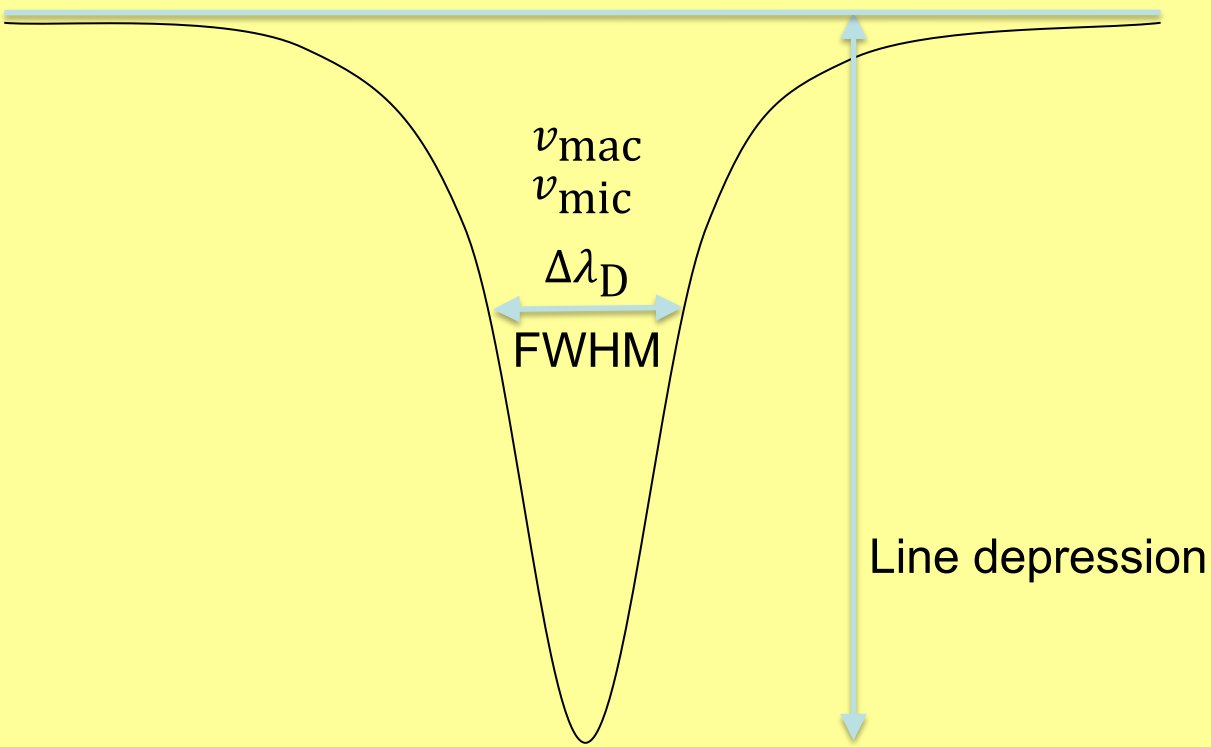

FWHM => Doppler broadening:
Temperature, $\Delta\lambda_{\mathrm{D}}$, and micro- and macroturbulence

Line depression contribution functions
Response functions

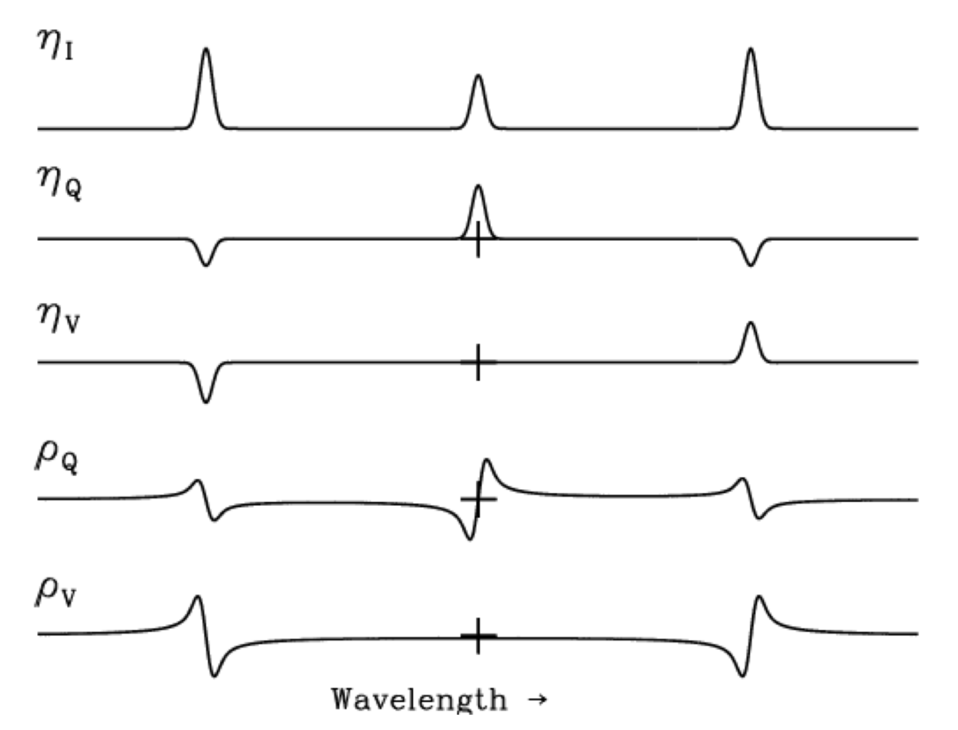

Zeeman triplet

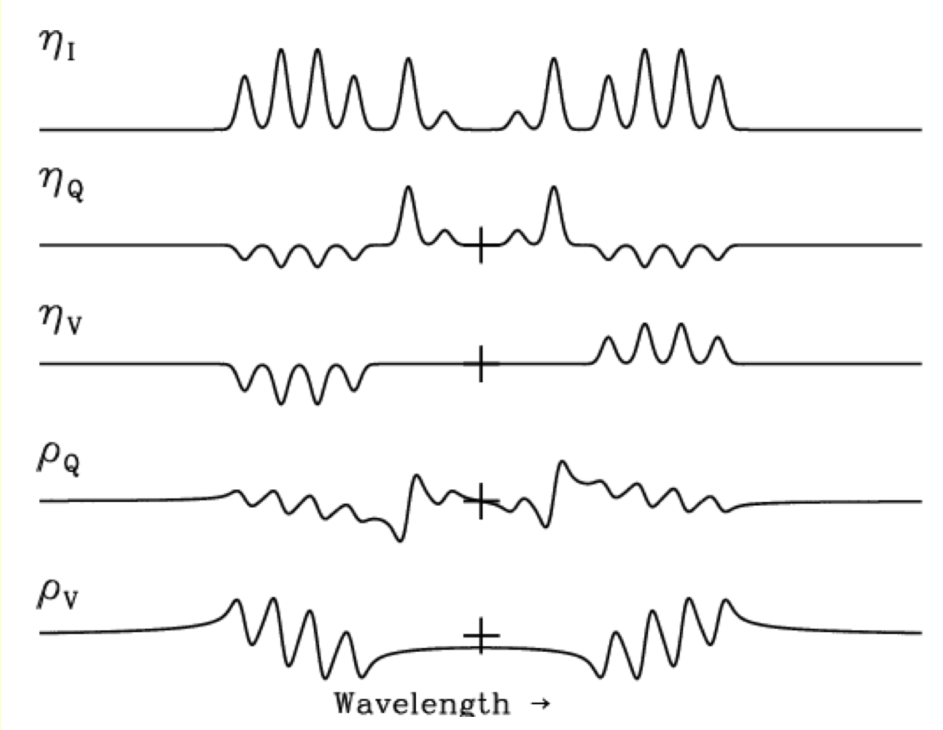

more complicated Zeeman pattern

Sanchez Almeida

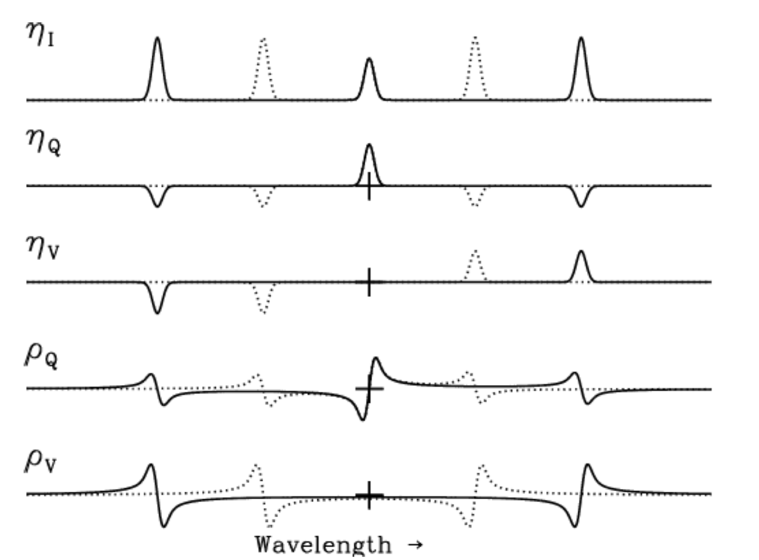

effect of a change in magnetic field strength

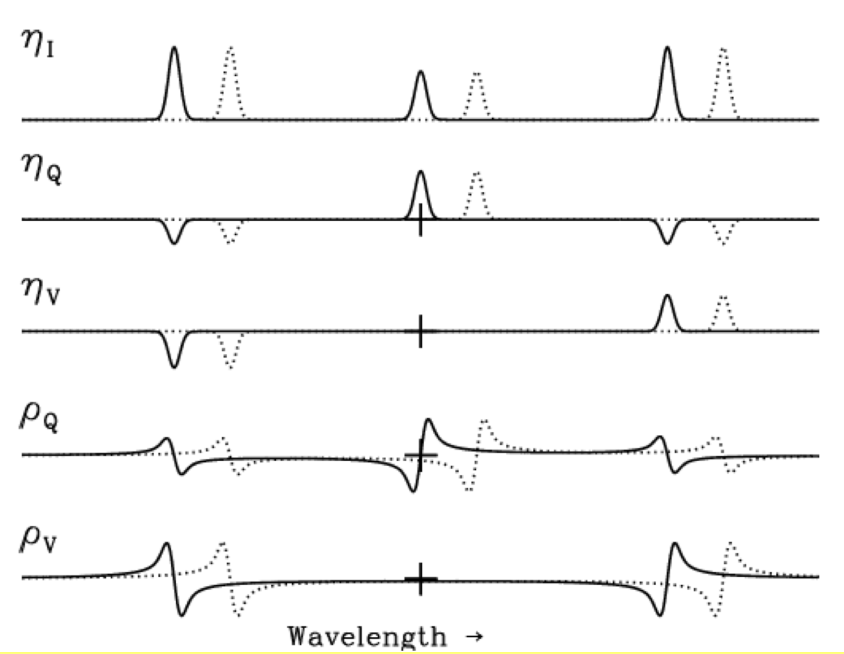

effect of a change in macroscopic velocity

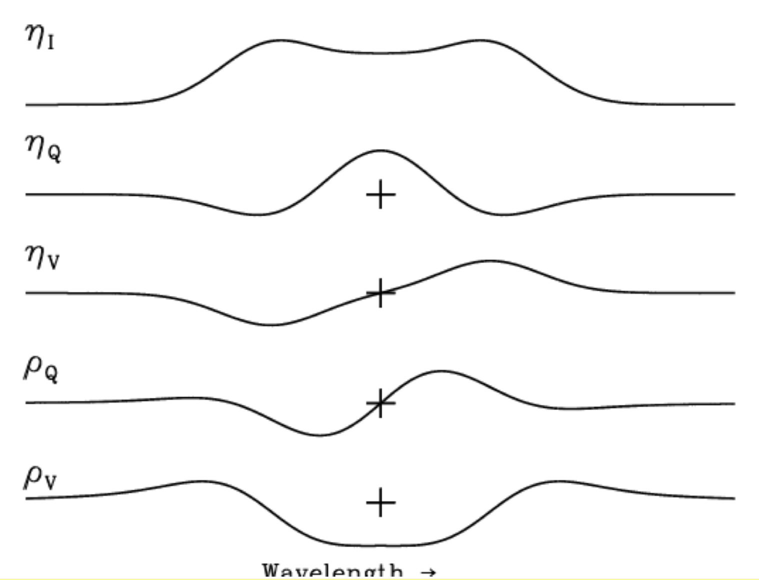

regime of weak magnetic field

Sanchez Almeida

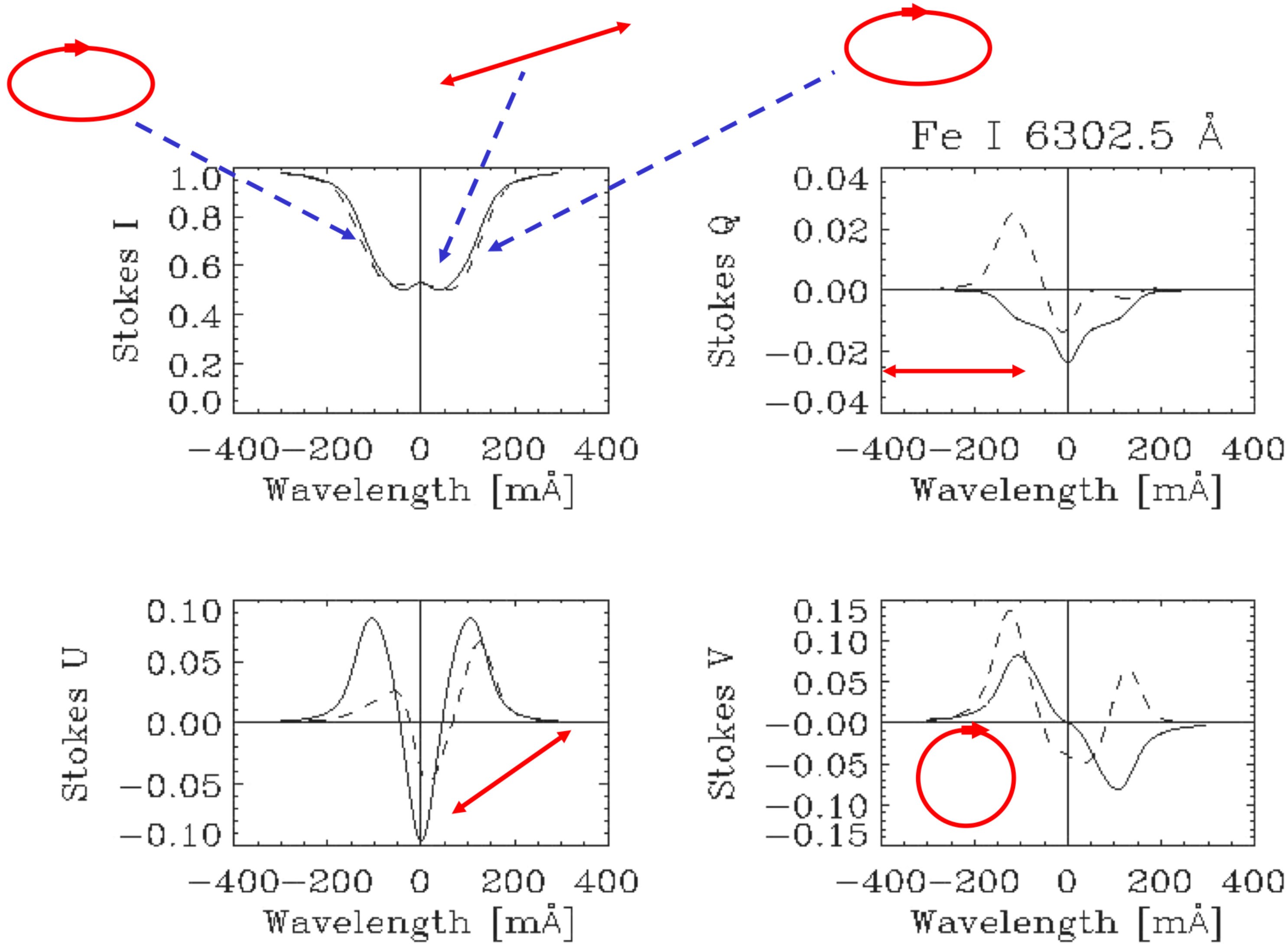

Stokes Profiles

Play with various parameters at:
http://www.iac.es/proyecto/inversion/online/milne_code/milne.php

Sanchez Almeida

Equation of transfer for polarized light

$$\frac{\mathrm{d}}{\mathrm{d}s}\begin{pmatrix} I \\ Q \\ U \\ V \end{pmatrix} = \begin{pmatrix} \eta_I & \eta_Q & \eta_U & \eta_V \\ \eta_Q & \eta_I & \rho_V & -\rho_U \\ \eta_U & -\rho_V & \eta_I & \rho_Q \\ \eta_V & \rho_U & -\rho_Q & \eta_I \end{pmatrix}\begin{pmatrix} I \\ Q \\ U \\ V \end{pmatrix} + \begin{pmatrix} j_I \\ j_Q \\ j_U \\ j_V \end{pmatrix}$$

η_I: Absorption $\longrightarrow$ absorption coefficient for unpolarized light.

η_Q, η_U, η_V: Dichroism $\longrightarrow$ the absorption property of the medium depends on the polarization of radiation.

ρ_Q, ρ_U, ρ_V: Anomalous dispersion $\longrightarrow$ the velocity of propagation of the wave in the medium depends on its polarization properties.

Landi degl'Innocenti in "Astrophysical Spectropolarimetry", (eds.) Trujillo-Bueno, Moreno-Insertis, Sanchez, Cambridge University Press, 2002.

Magneto-optical effect: Off, uniform B=3500 Gauss in umbral atmosphere

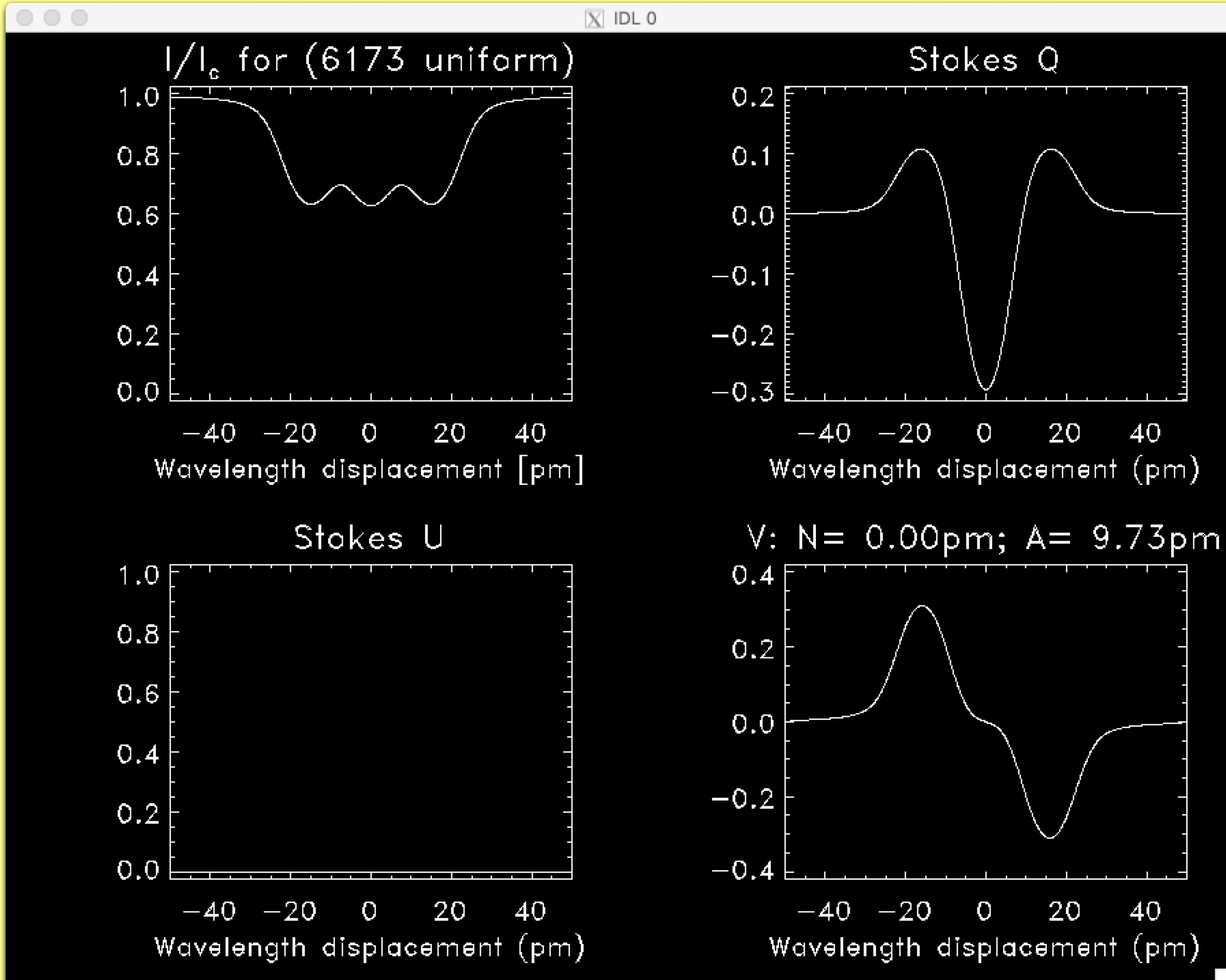

Magneto-optical effect: ON, uniform B=3500 Gauss in umbral atmosphere

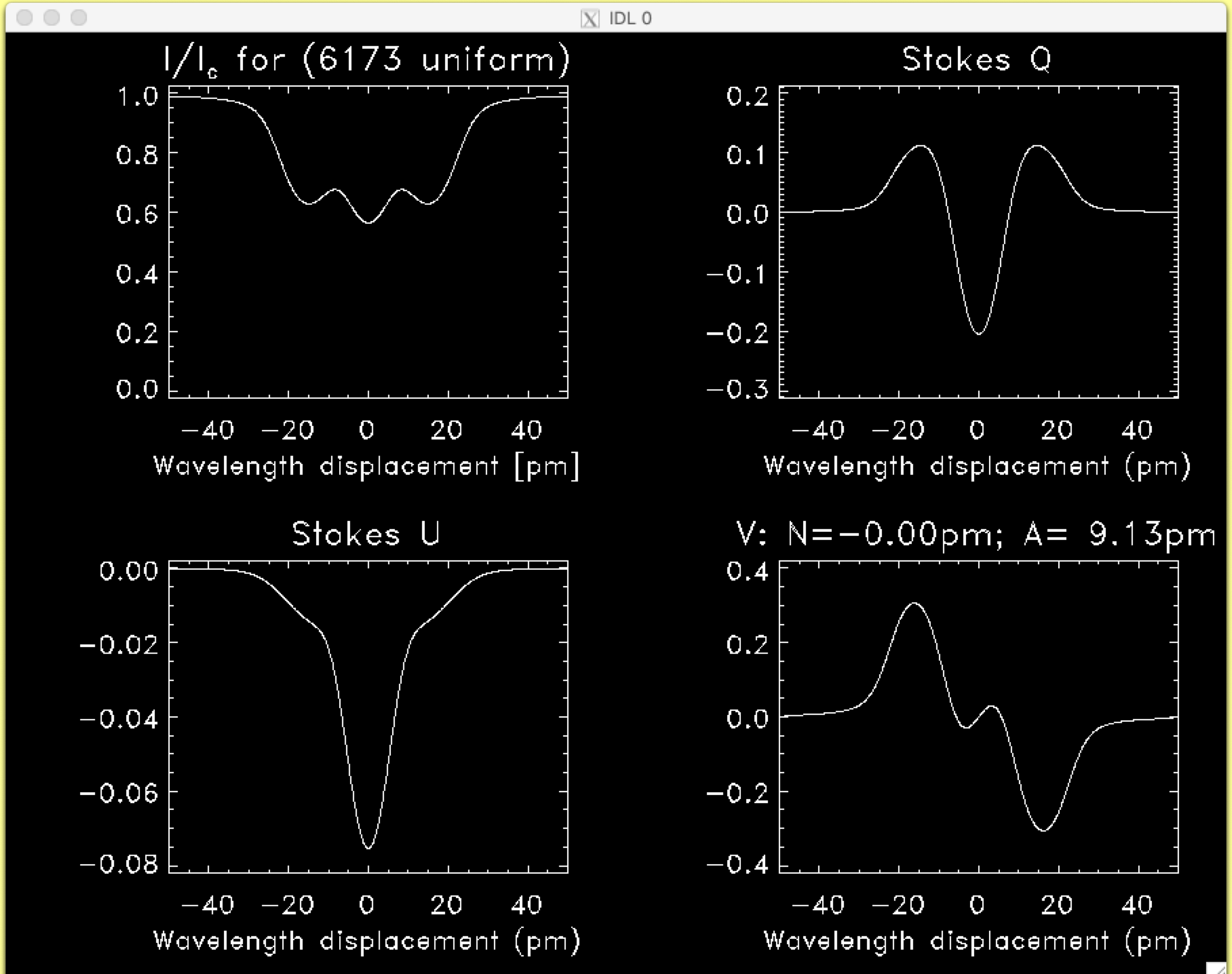

Polarized light: spectro-polarimetry

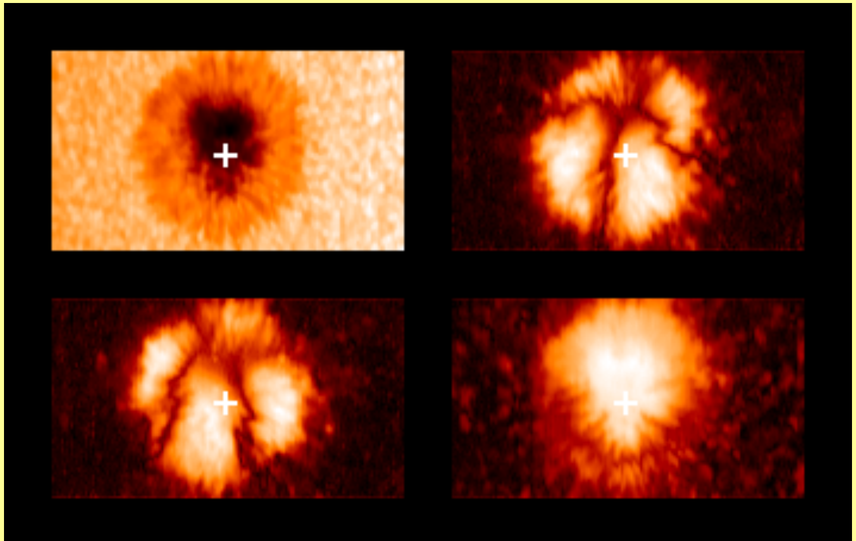

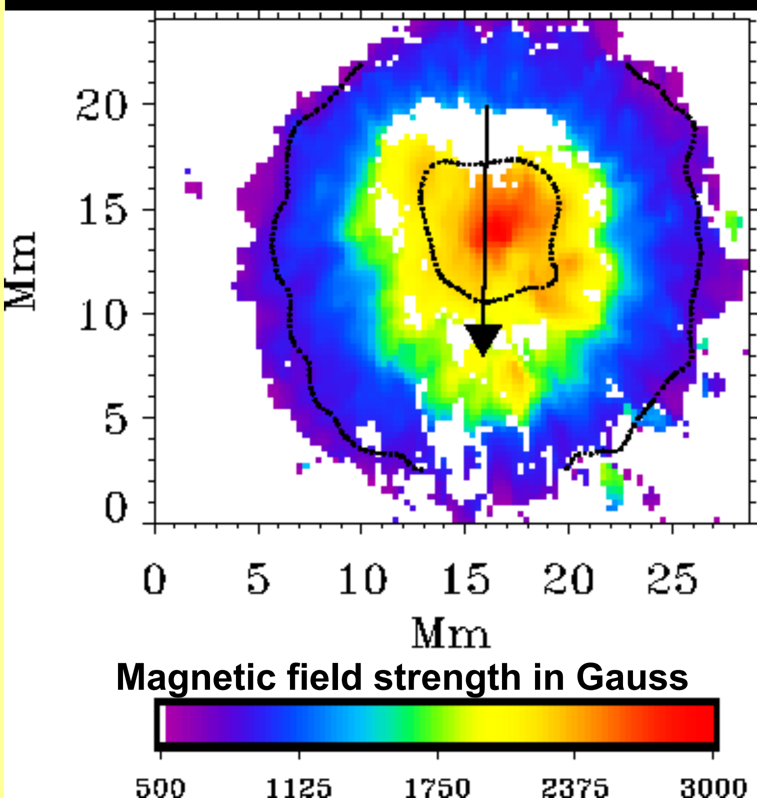

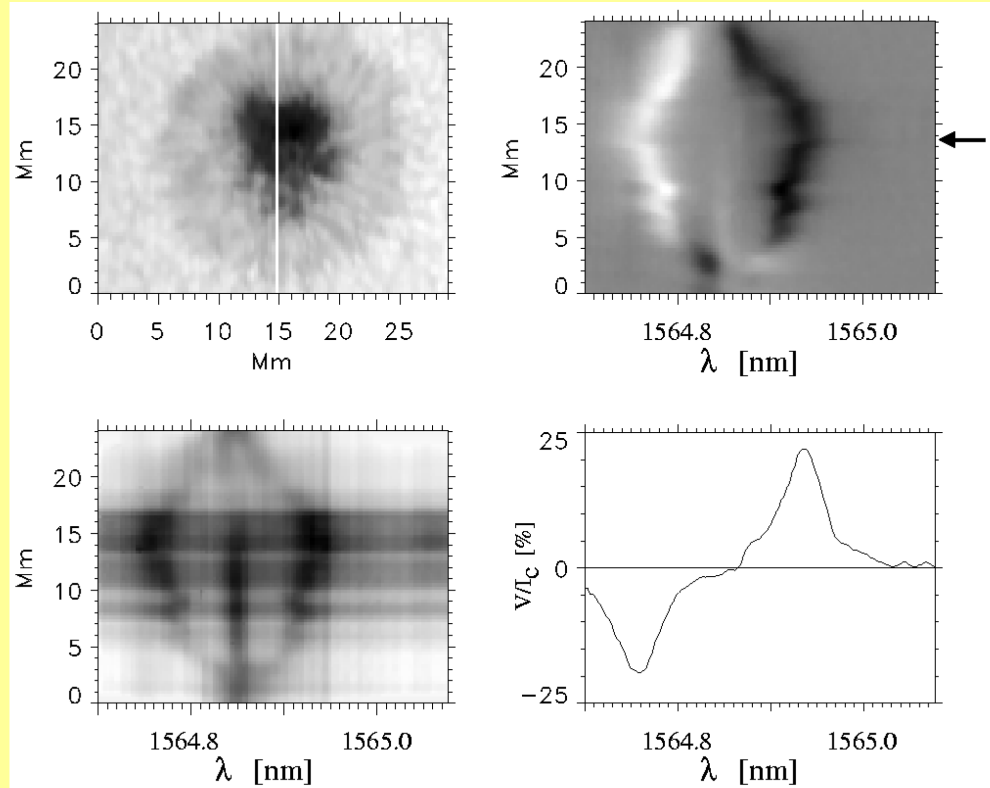

For homogeneous magnetic field:

Line splitting → **Magnetic field strength**

Amplitudes → **Field inclination**

(Strong field regime, different in weak field regime)

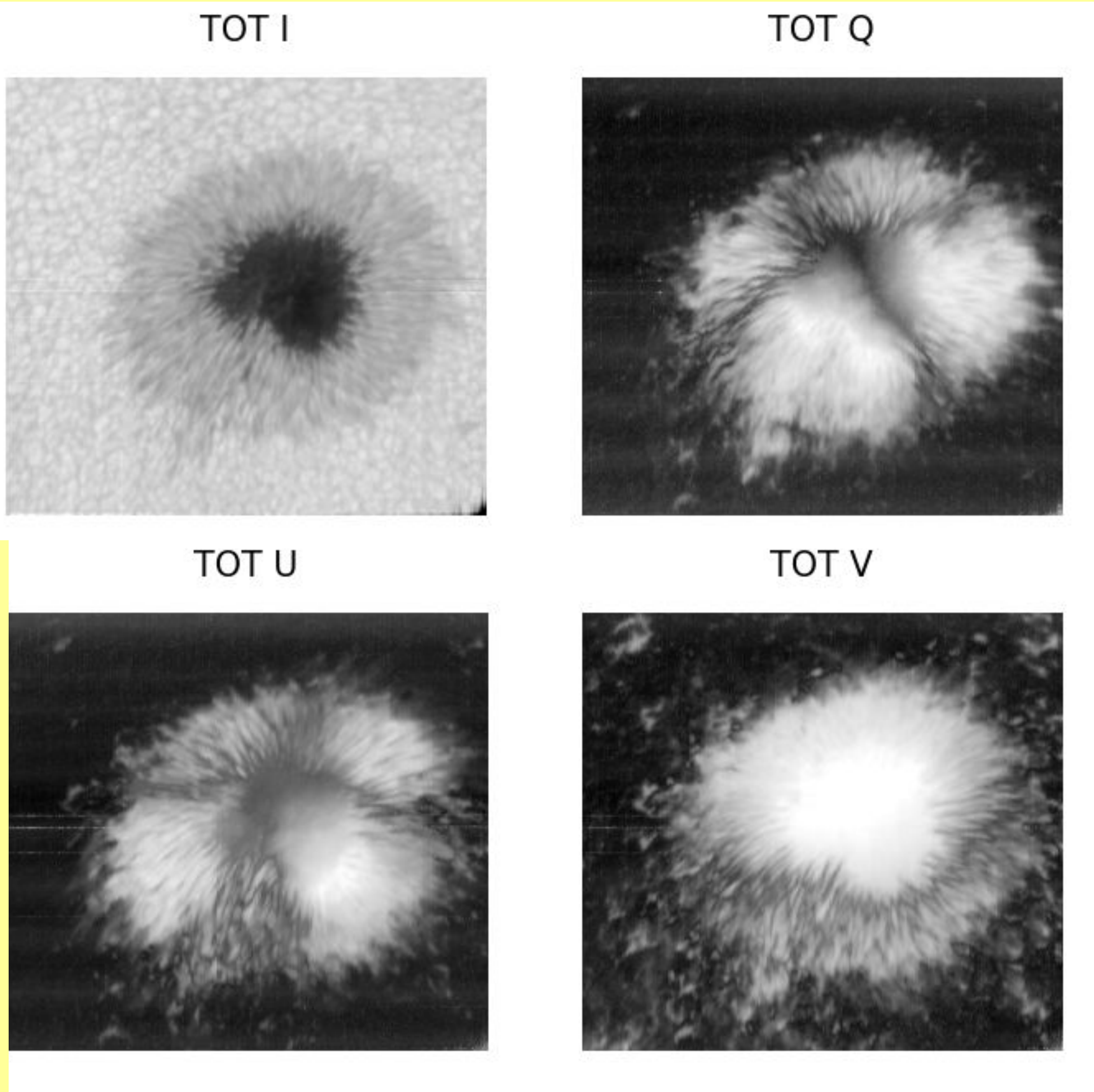

GRIS
@
GREGOR

17Sep2015

GRIS archive:
sdc.leibniz-kis.de

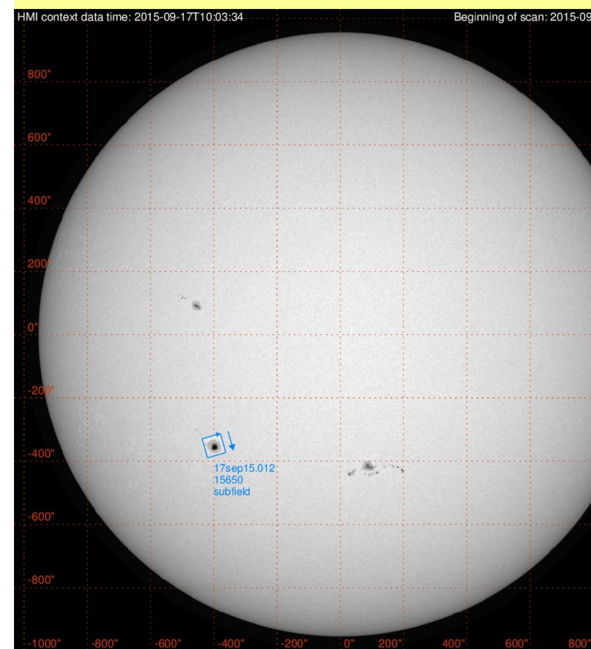

Show 'STOKES' program and demonstrate how line profiles change with various parameter:

stokes.pro

wrapper around fortran 77 code: 'dmg_wys' (Grossmann-Doerth 1984)

Line asymmetries in Stokes I

Mean quite Sun profiles are asymmetric and show a 'C'-shape

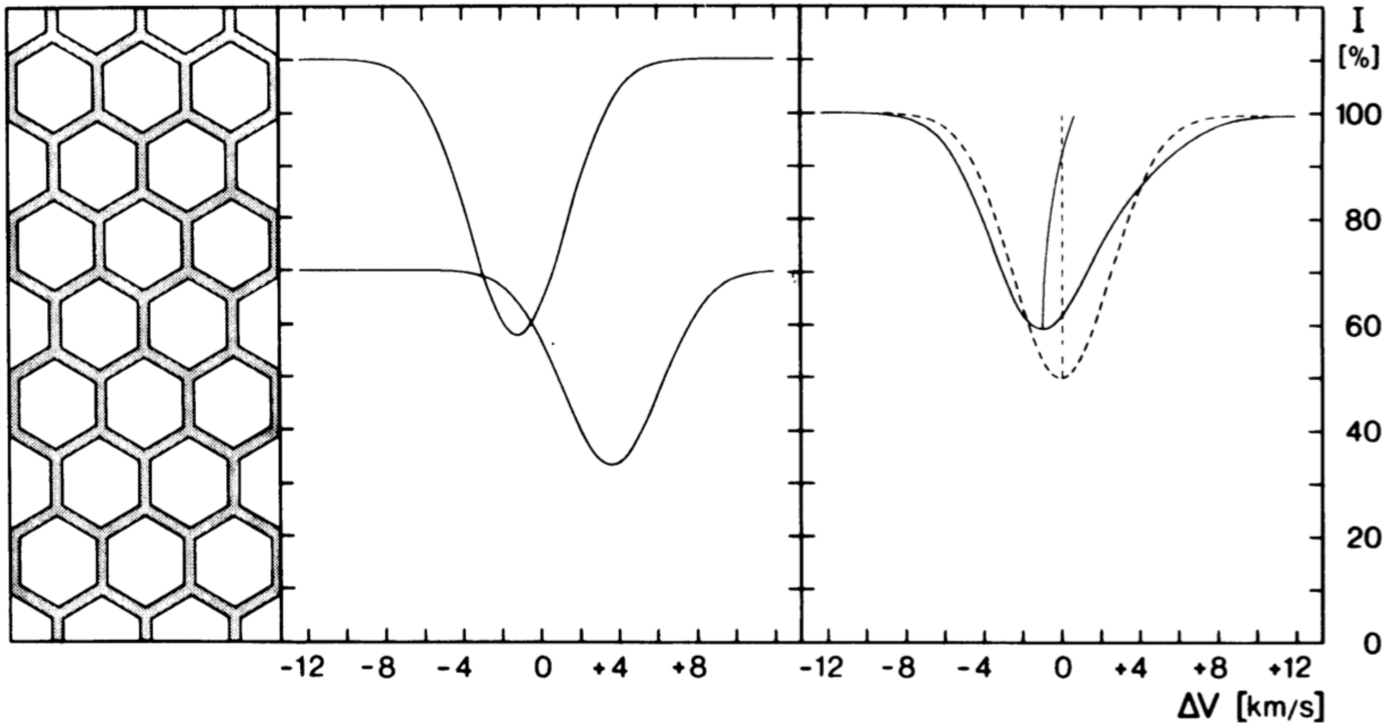

Fig. 6.14. Origin of the line asymmetry. Granular and intergranular regions (*left*) contribute different profiles (*center*). The average is an asymmetric line, with a C-shaped bisector (*right, solid*). The *dashed*, symmetric, line would result in the absence of convection. From Dravins et al. (1981)

Stix: 'The Sun' (2002)

The Evershed flow

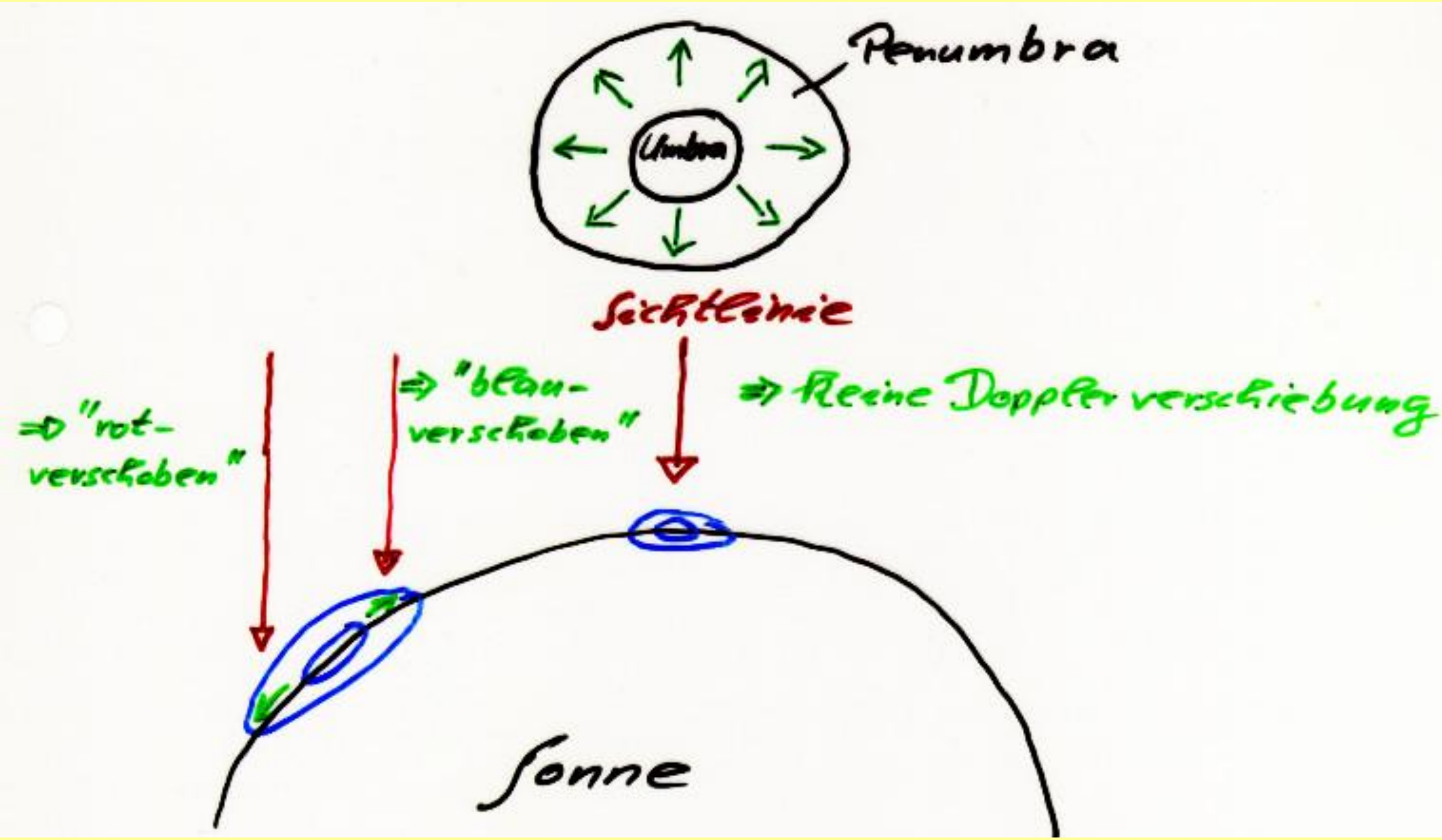

→ **Evershed (1909):**

- **horizontal flow,**
- **radially outwards.**

2D Spectroscopy of Fe I 557.6 nm

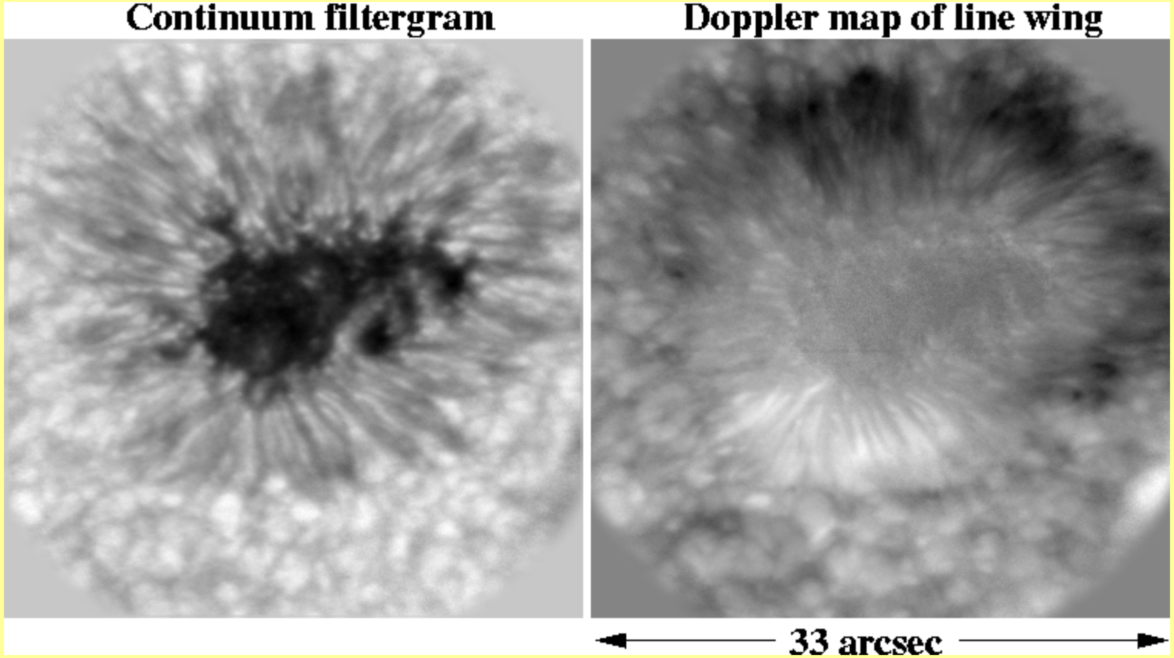

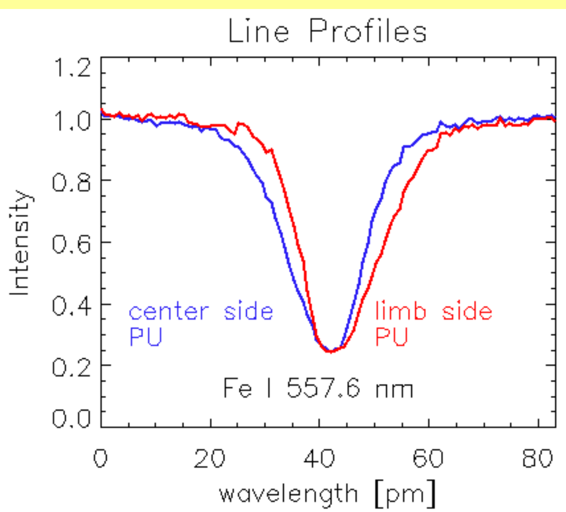

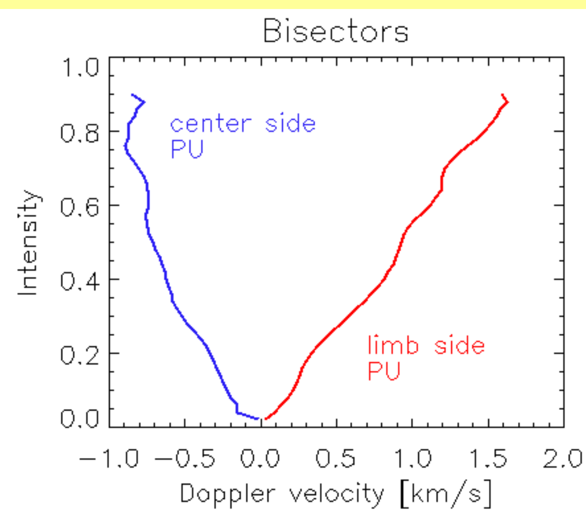

TESOS@VTT in Fe I 557.6 nm:

- **g=0,**
- **formation height up to $\log\tau = -3$**
- $\boldsymbol{\lambda/\triangle\lambda = 250\,000}$ $\boldsymbol{\Rightarrow \; \triangle\lambda = 2.2\,\mathrm{pm}}$
- **100 steps@0.84 pm in 30 s**
- **KAOS: $0.5''$ spatial resolution**
- **Spot at $\theta = 23°$**

(Tritschler, Schl., Bellot Rubio, & KAOS team 2004)

Line asymmetries of *unmagnetic* lines

High forming lines:

- **Small line core shift**
- **Large asymmetry**

Deep forming lines:

- **Large line core shift**
- **Small asymmetry**

(Maltby 1964, Stellmacher & Wiehr 1980)

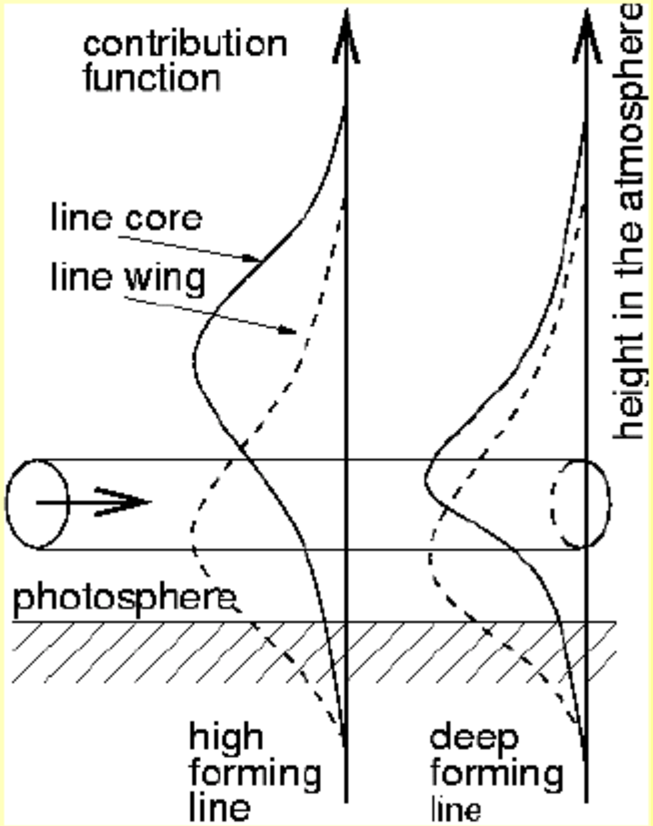

- **Mean bisectors inclined → Flow in deep layers.**
- **Different slopes of mean bisectors on center and limb side interpreted as projection effects of non-horizontal flow channels.**

  → Mean downflow component.

(Schl., Bellot Rubio, Tritschler 2004)

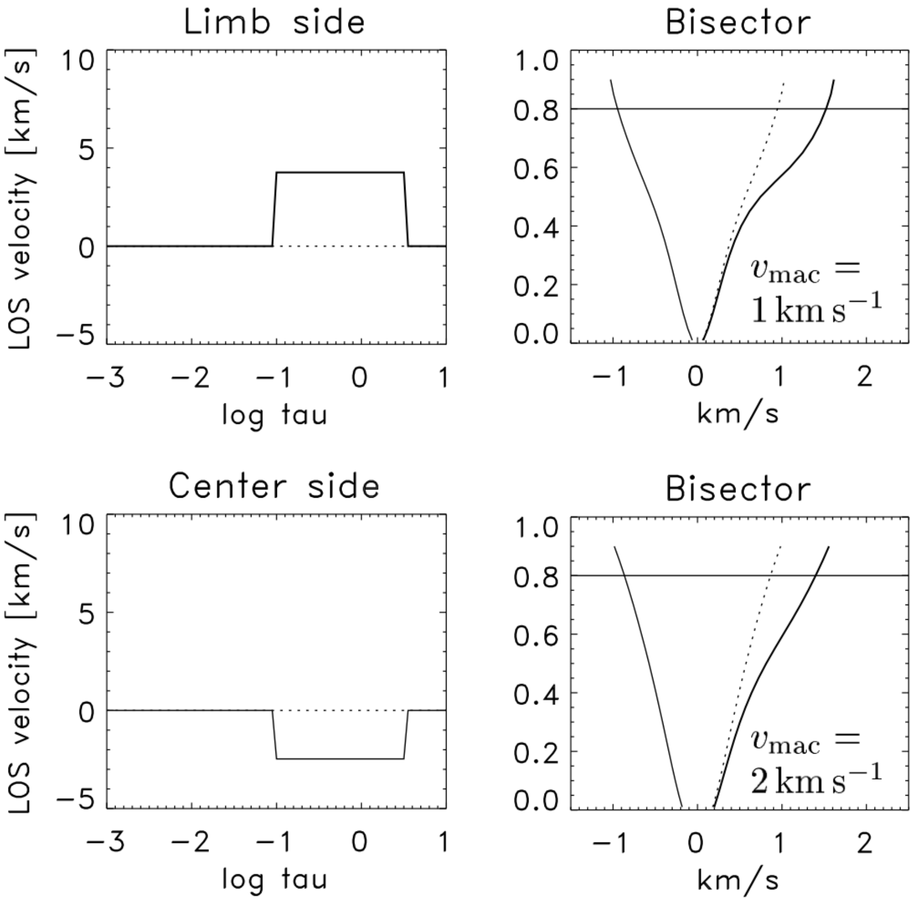

Fig. 4. Synthetic bisectors with different slopes: the upper and lower left panel show the LOS velocities of a flow channel in the deep photosphere for the limb and center side, respectively. The flow has an absolute velocity of 8 km s^{-1} and a downward angle with respect to the horizontal of 5°. The solid line traces the flow component, while the dotted line reflects the background component at rest. The right panels show the corresponding synthetic bisectors for a macro-turbulence of 1 km s^{-1} (top) and 2 km s^{-1} (bottom). The red-shifted (thick) solid lines correspond to the limb side bisectors and the blue shifted (thin) solid lines correspond the the center side bisector. For better comparison with the limb side bisector, the dotted line represents a reflection of the center side bisector.

The mean bisectors

- **Flow channel with v = 8 km/s**
- **Inclination 95 degrees**

- **Line core stronger shifted than line wing**
- **Larger bisector inclination on limb side**

Schl., Tritschler, Bellot Rubio 2004

Penumbral line asymmetries: bisectors

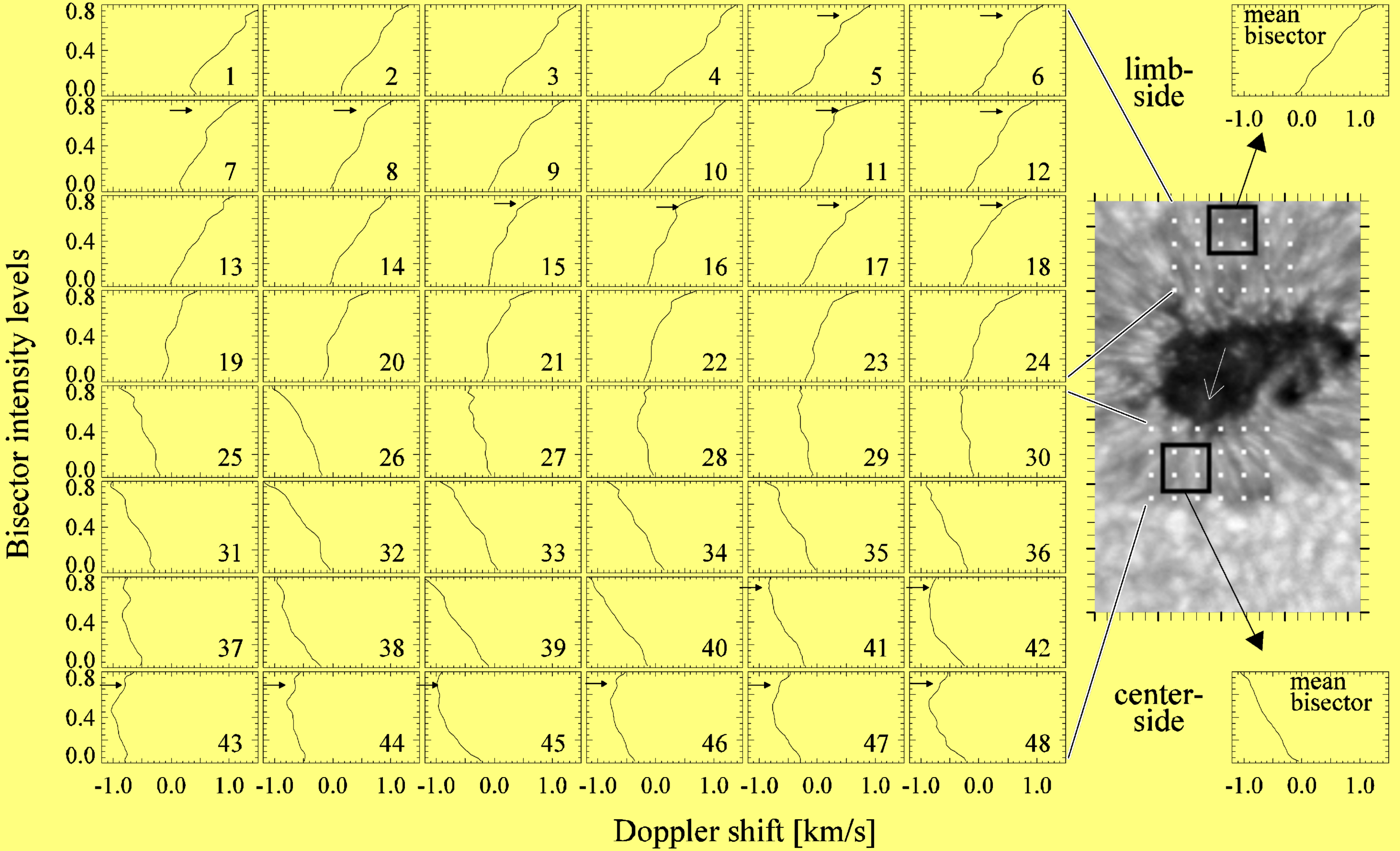

- **Bisector reversals on center side.**
- **Bisector kinks on limb side.**

(Schl., Bellot Rubio, Tritschler 2004)

Individual flow filament

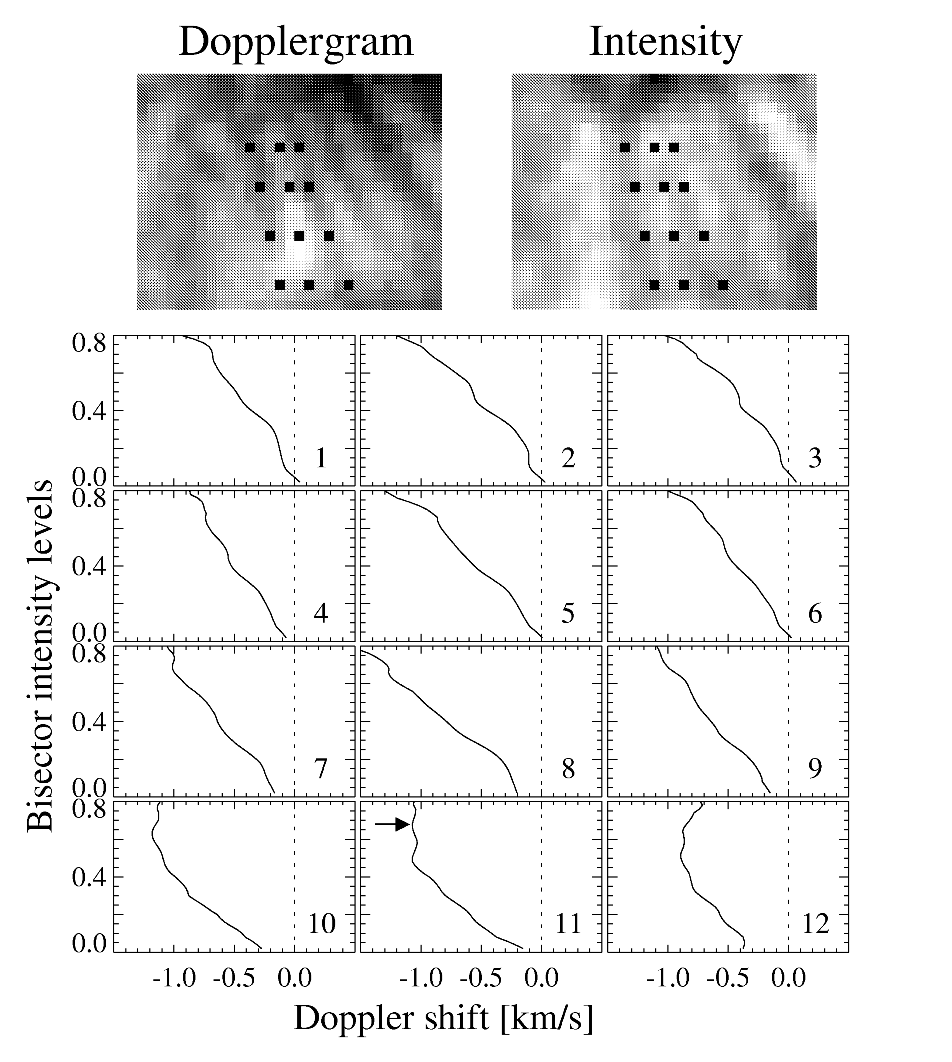

- **Upflow at inner end of flow filament (#2).**
- **Horizontal outflow in deep layers (#5, #8).**
- **Downflow at outer end of filament (#11).**

⇒ **Compatible with sea serpent and estimates on energy transport (Schl. & Solanki 2003).**

Interpretation of bisector reversal and kink

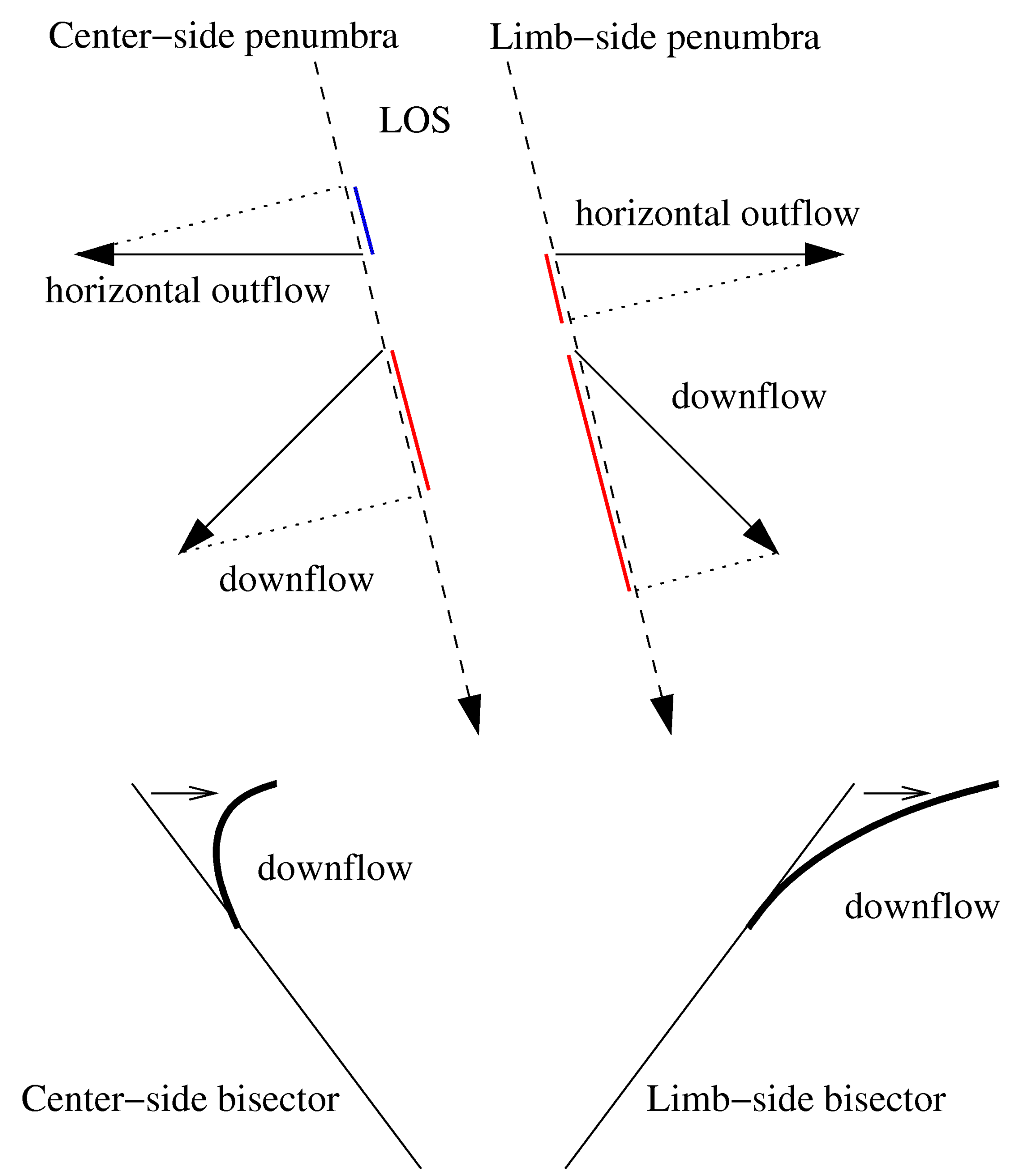

Synthetic line profiles

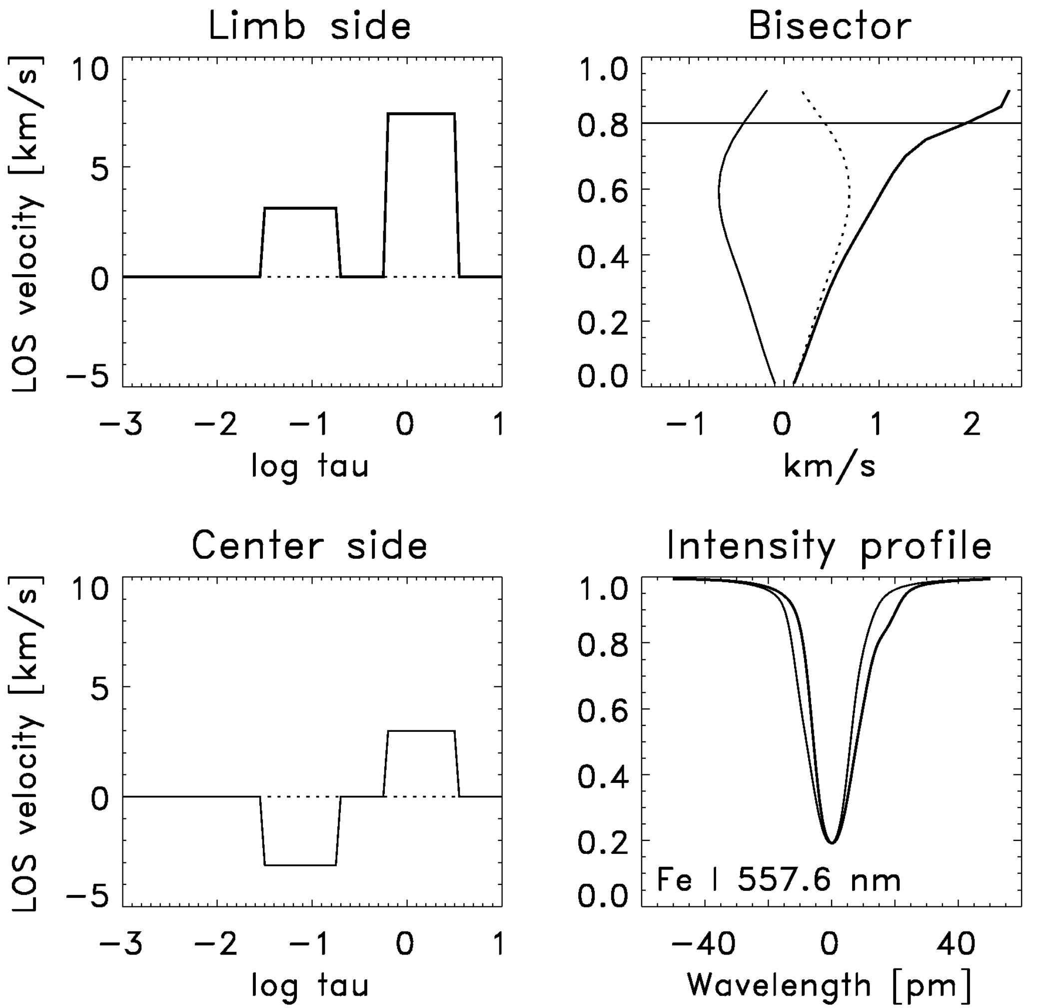

Model input:

- Penumbral atmosphere (L. Bellot).
- Macro-turbulence of 1 km/s.
- Microturbulence of 1.5 km/s.
- Instrumental broadening of 2.2 pm.
- Two-components ($f = 50\%$):
  1. "Background component" at rest.
  2. Flows along the LOS (v=8 km/s):
     (a) horizontal flow at $\log\tau \approx -1$.
     (b) 45°-downflow in continuum forming layers.

Bisector reversals are due to the presence of downflows

Standard filament

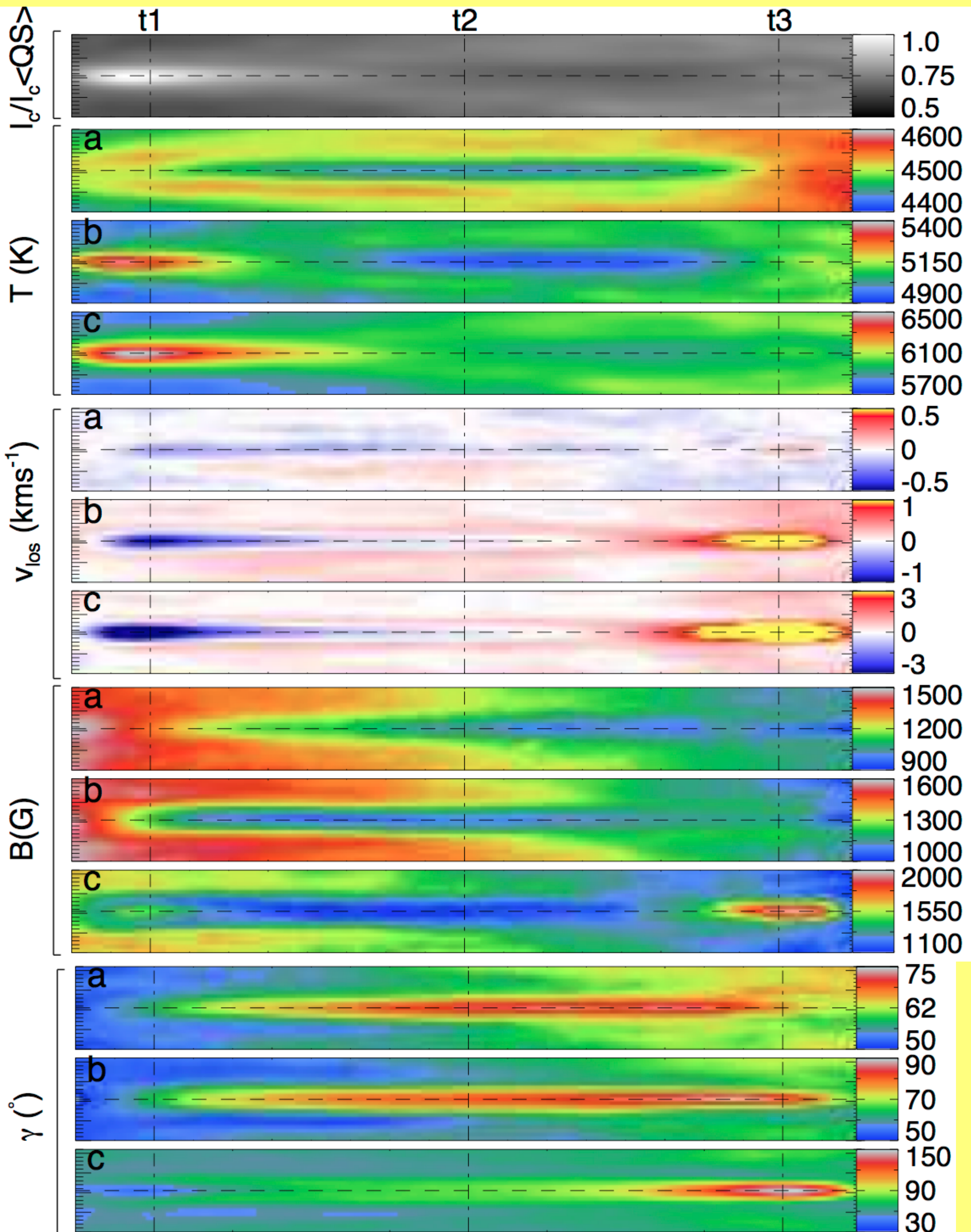

(SP@SOT Hinode)

Tiwari, van Noort, Lagg, & Solanki 2013

- **SP@SOT Hinode**
- **Depth-dependent inversion coupled with straylight deconvolution.**
- **Word of caution:**
  "However, it is difficult to precisly establish the error in the fitted atmospheric parameters. [...] In this paper, therefore, we refrain from presenting error estimates of the inversion."
- **Uniformity of penumbral filaments: consider averages!**

(a) → log tau = - 2.5
(b) → log tau = - 0.9
(c) → log tau = 0

Modelling the penumbra

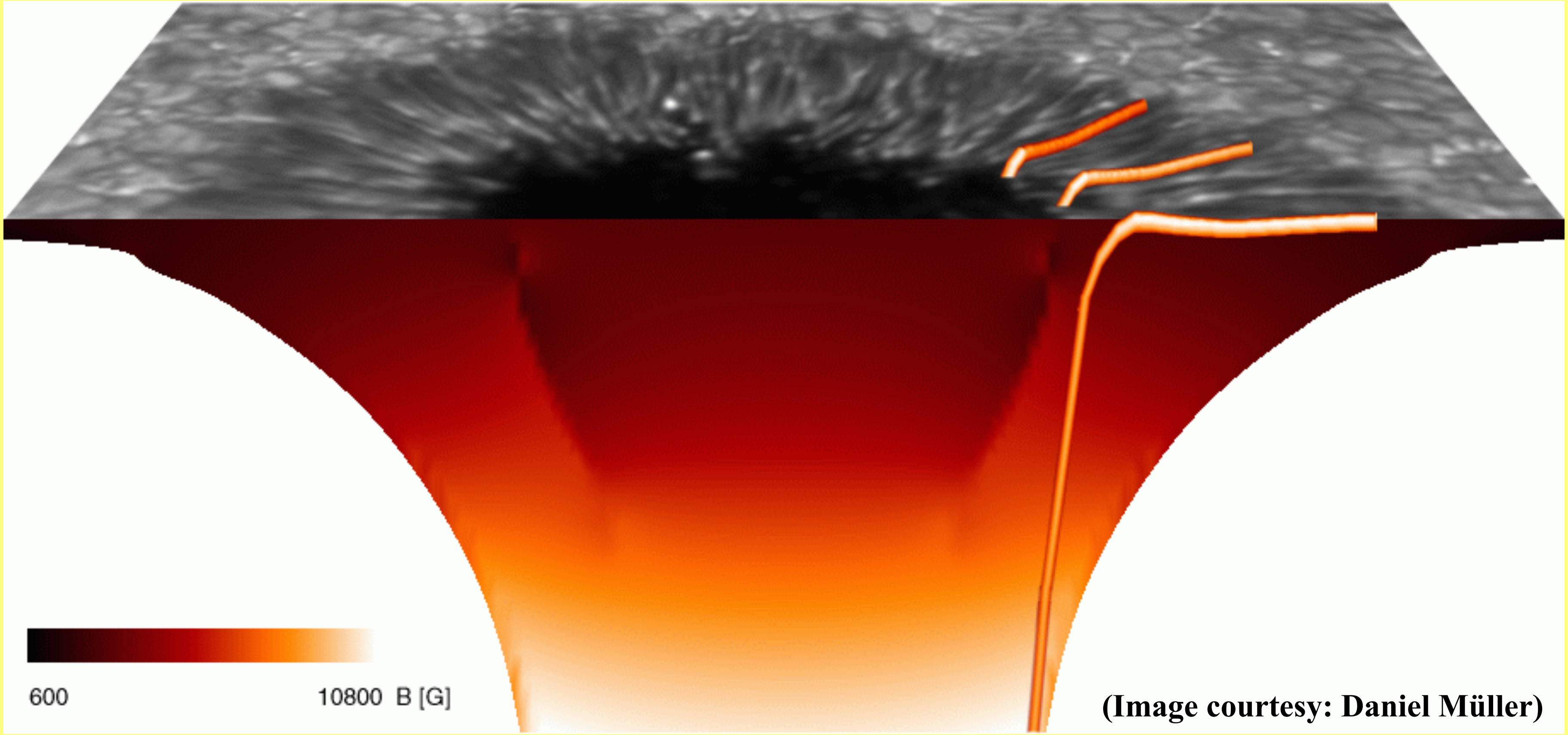

(Image courtesy: Daniel Müller)

Dynamic flux tubes embedded in a sunspot

Modelling a sunspot

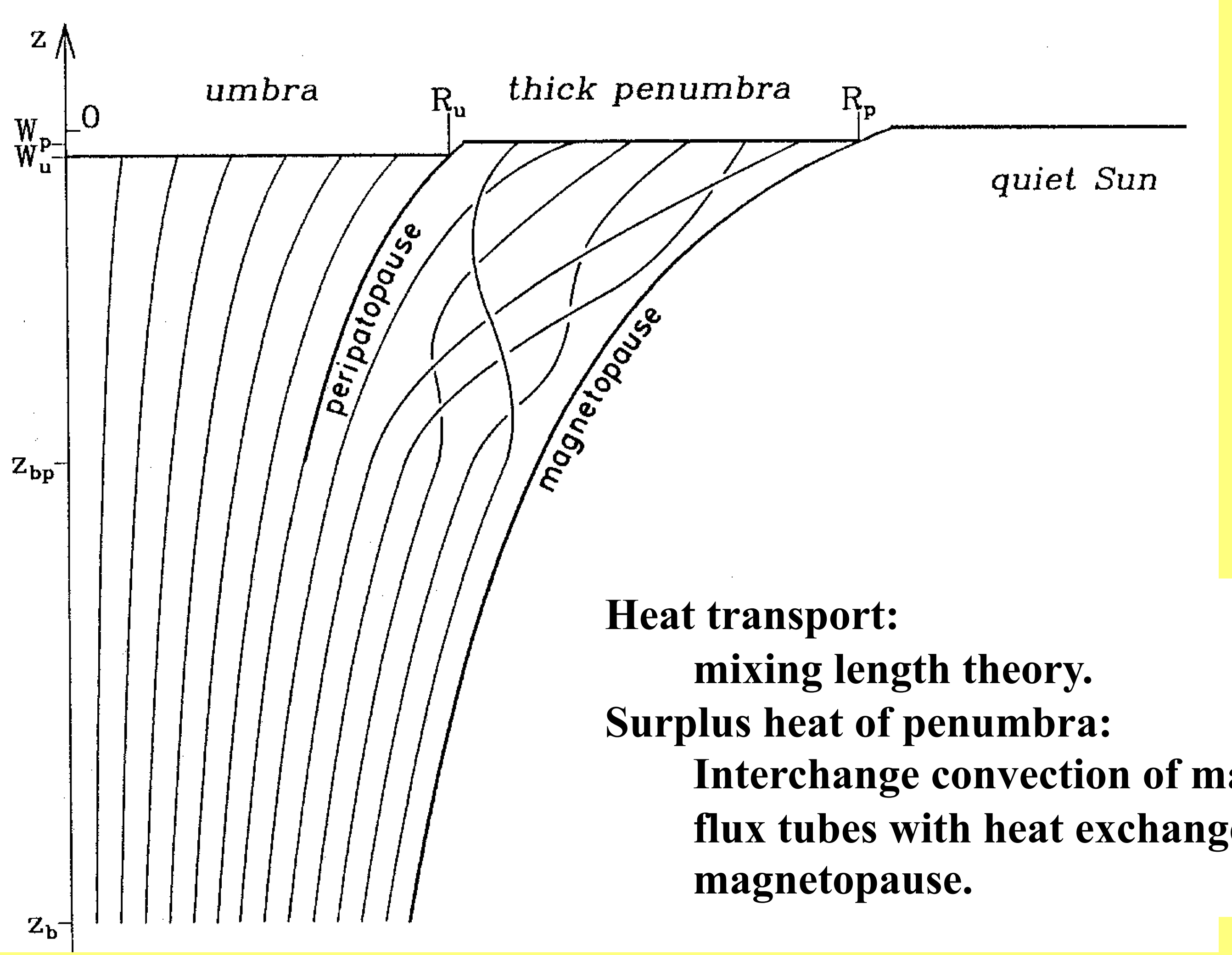

Heat transport:

mixing length theory.

Surplus heat of penumbra:

Interchange convection of magnetic flux tubes with heat exchange at magnetopause.

Tripartite sunspot (Jahn & Schmidt 1994)

The tripartite sunspot model

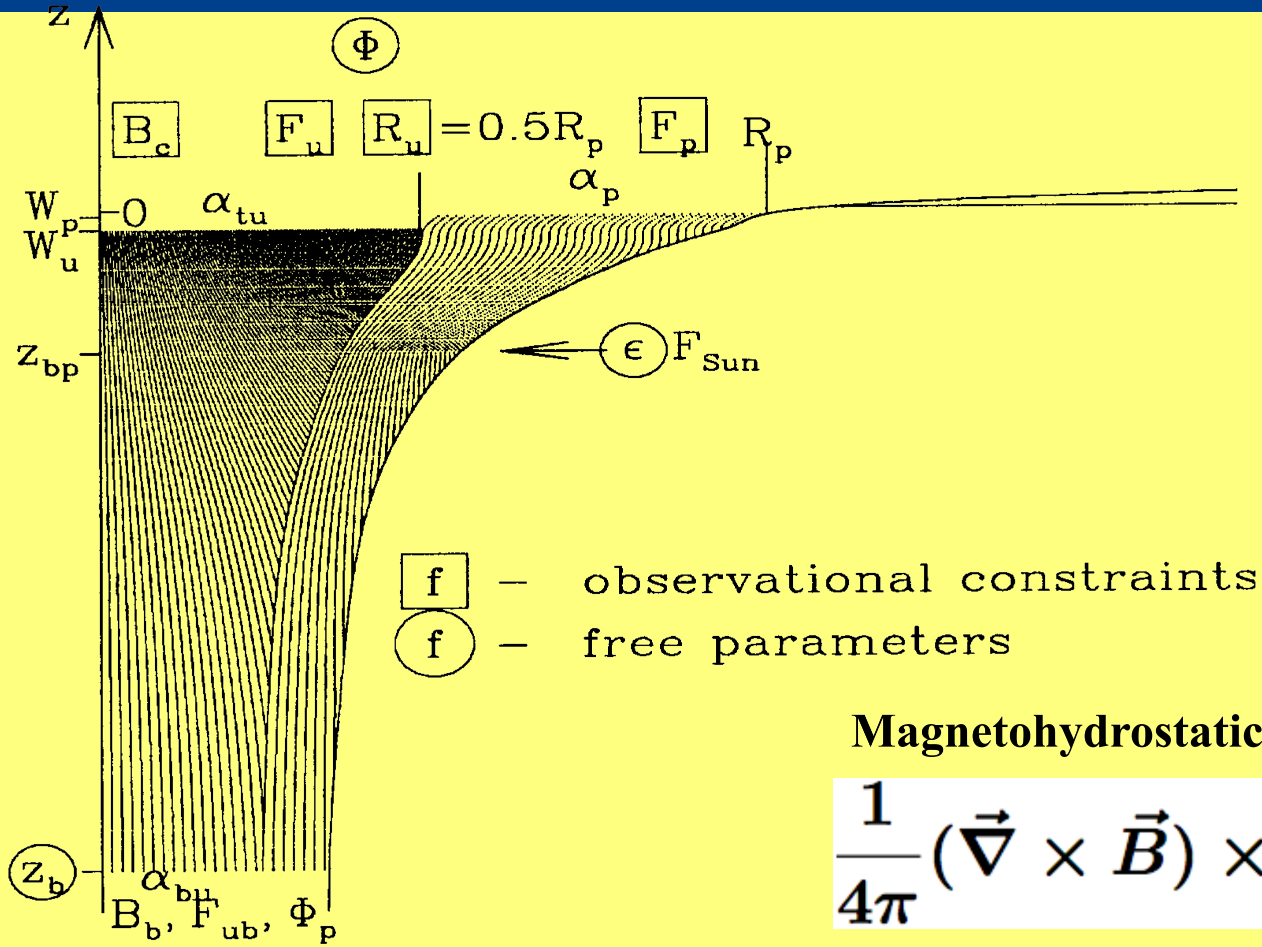

Magnetohydrostatic equilibrium:

$$\frac{1}{4\pi}(\vec{\nabla} \times \vec{B}) \times \vec{B} = \vec{\nabla} p - \rho \vec{g}$$

- **Electric currents along two sheets.**
- **Horizontal pressure balance: gas pressure + magnetic pressure.**

(Jahn & Schmidt 1994)

Gleichungen der idealen MHD

Continuity: $$\frac{\mathrm{d}}{\mathrm{d}t}\rho = -\rho\vec{\nabla}\cdot\vec{v}$$

Induction: $$\frac{\partial}{\partial t}\vec{B} = \vec{\nabla}\times(\vec{v}\times\vec{B})$$

Motion: $$\rho\frac{\mathrm{d}}{\mathrm{d}t}\vec{v} = -\vec{\nabla}p + \vec{g}\rho + \frac{1}{4\pi}(\vec{\nabla}\times\vec{B})\times\vec{B}$$

Entropy: $$\rho T\frac{\mathrm{d}}{\mathrm{d}t}S = \vec{\nabla}\cdot\vec{F} = \rho T\left(\frac{\mathrm{d}}{\mathrm{d}t}S\right)_{\mathrm{Strahlung}}$$

Maxwell: $$\vec{\nabla}\cdot\vec{B} = 0$$

Eq. of state: $$p = \frac{\mathcal{R}}{\mu}\rho T$$

Dynamics of a thin magnetic flux tube

$$\frac{\mathrm{d}}{\mathrm{d}t}\frac{\vec{B}}{\rho} = \frac{B}{\rho}\frac{\partial \vec{v}}{\partial s}$$

s: **arc length (Lagrange coordinate)**

$$\rho\left(\frac{\mathrm{d}}{\mathrm{d}t}\vec{v}\right)_{\parallel} = -\frac{\partial p}{\partial s} - g\,\rho\,\cos\vartheta$$

$$\rho\left(\frac{\mathrm{d}}{\mathrm{d}t}\vec{v}\right)_{\perp} = g\,\sin\vartheta\,(\rho - \rho_{\mathrm{back}}) + \frac{\kappa\,B^2}{4\pi} - \frac{(\nabla B^2_{\mathrm{back}})_{\perp}}{8\pi}$$

$$\rho T\frac{\mathrm{d}}{\mathrm{d}t}S = \rho T\left(\frac{\mathrm{d}}{\mathrm{d}t}S\right)_{\mathrm{Strahlung}} = \frac{\rho\,c_p\,(T - T_{\mathrm{back}})}{t_{\mathrm{rad}}}$$

$$\phi = B\,A = \mathrm{konstant}$$

$$p = \frac{\mathcal{R}}{\mu}\rho T$$

$$p + \frac{B^2}{8\pi} = p_{\mathrm{back}} + \frac{B^2_{\mathrm{back}}}{8\pi}$$

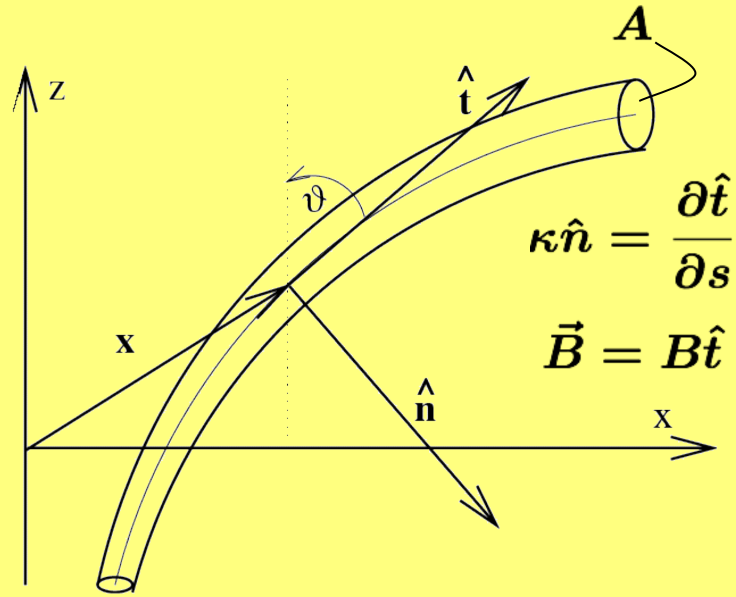

$$\kappa\hat{n} = \frac{\partial \hat{t}}{\partial s}$$

$$\vec{B} = B\hat{t}$$

The moving tube model: simulation

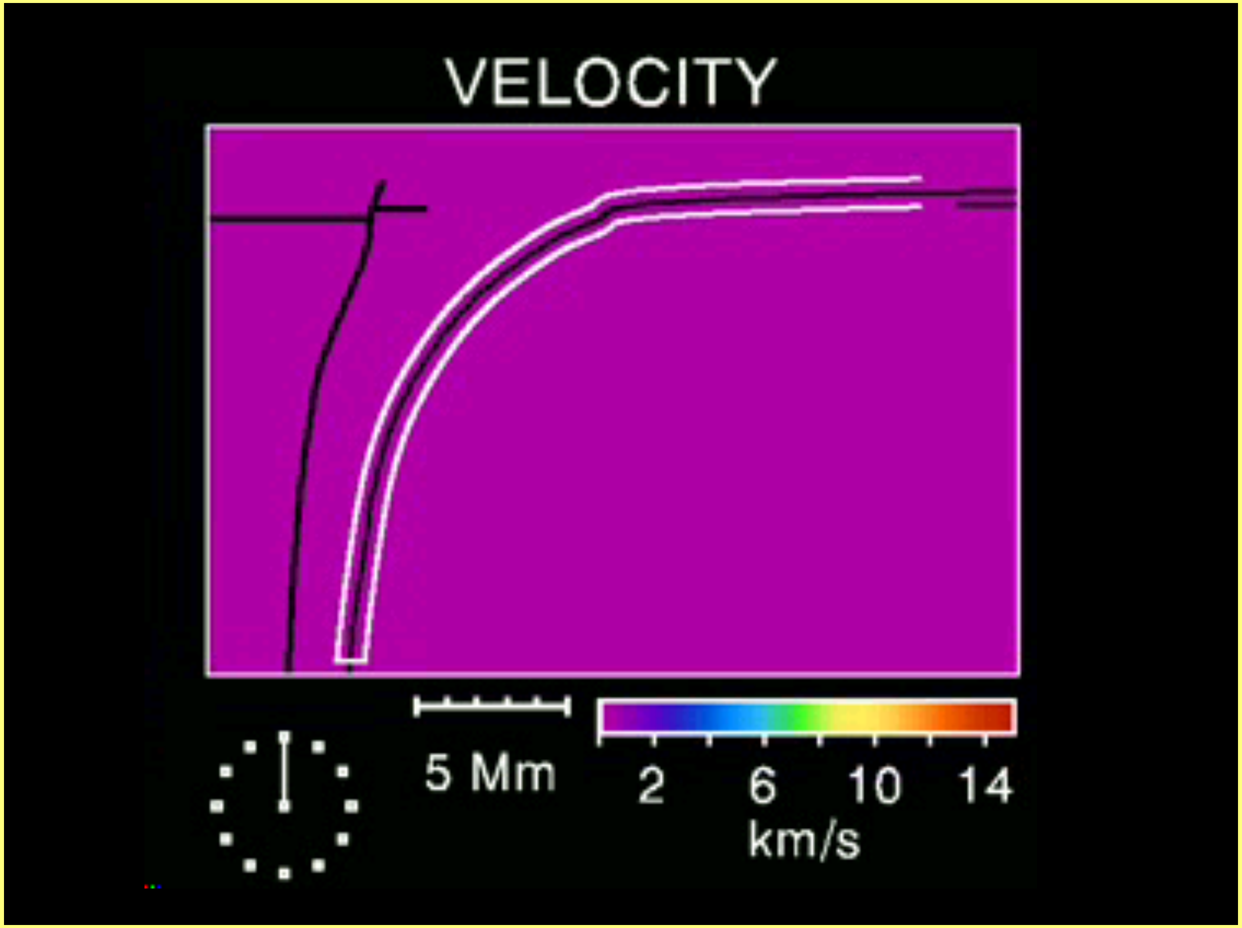

Equations:

- Ideal MHD
- Thin flux tube approximation.
- Evolution of thin magnetic flux tube embedded in a model sunspot.
- Partial ionization of H and He.
- Radiative heat exchange (Radiative relaxation time, Spiegel 1957).

The moving tube model in photosphere

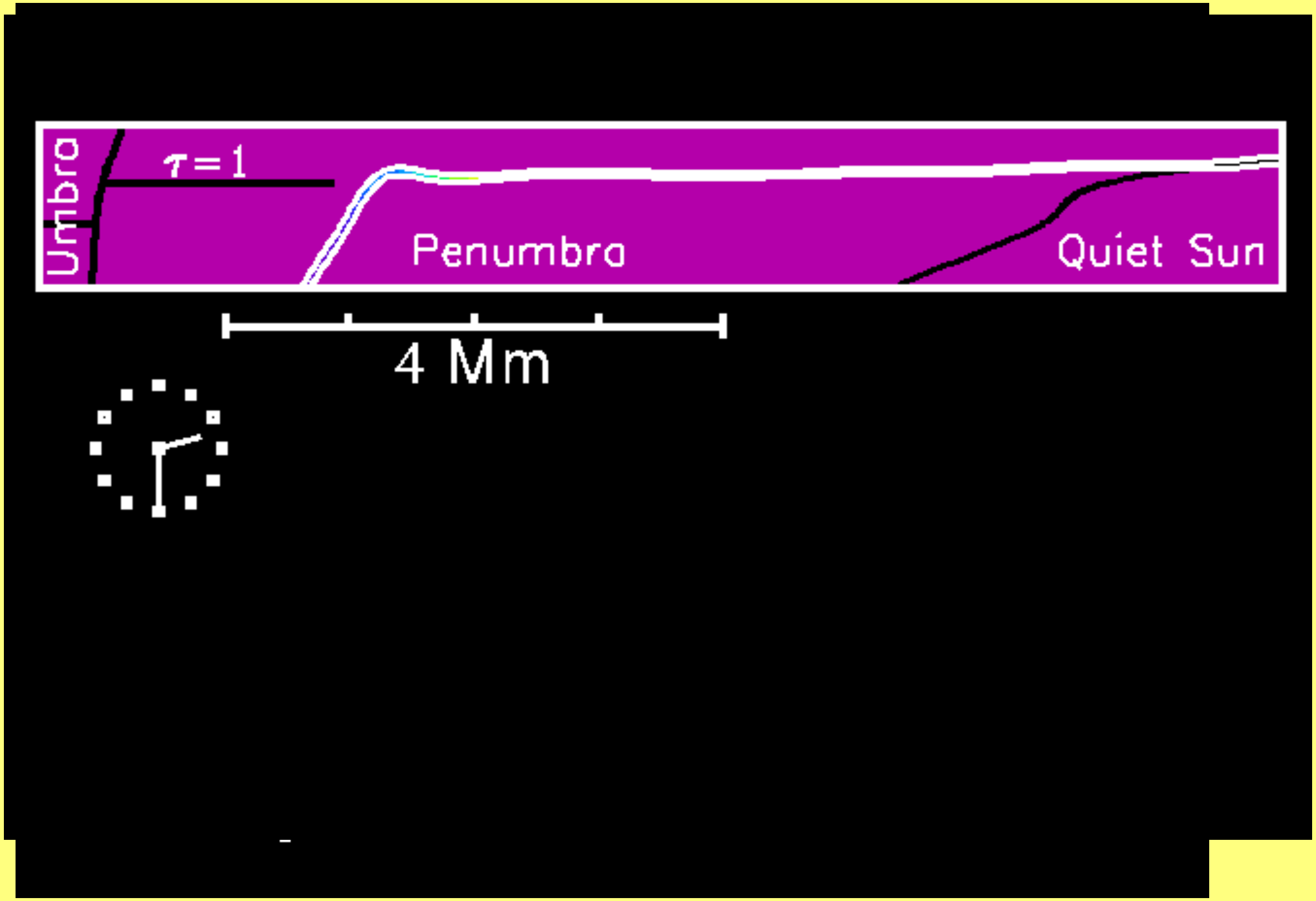

The moving tube model in photosphere: simulation

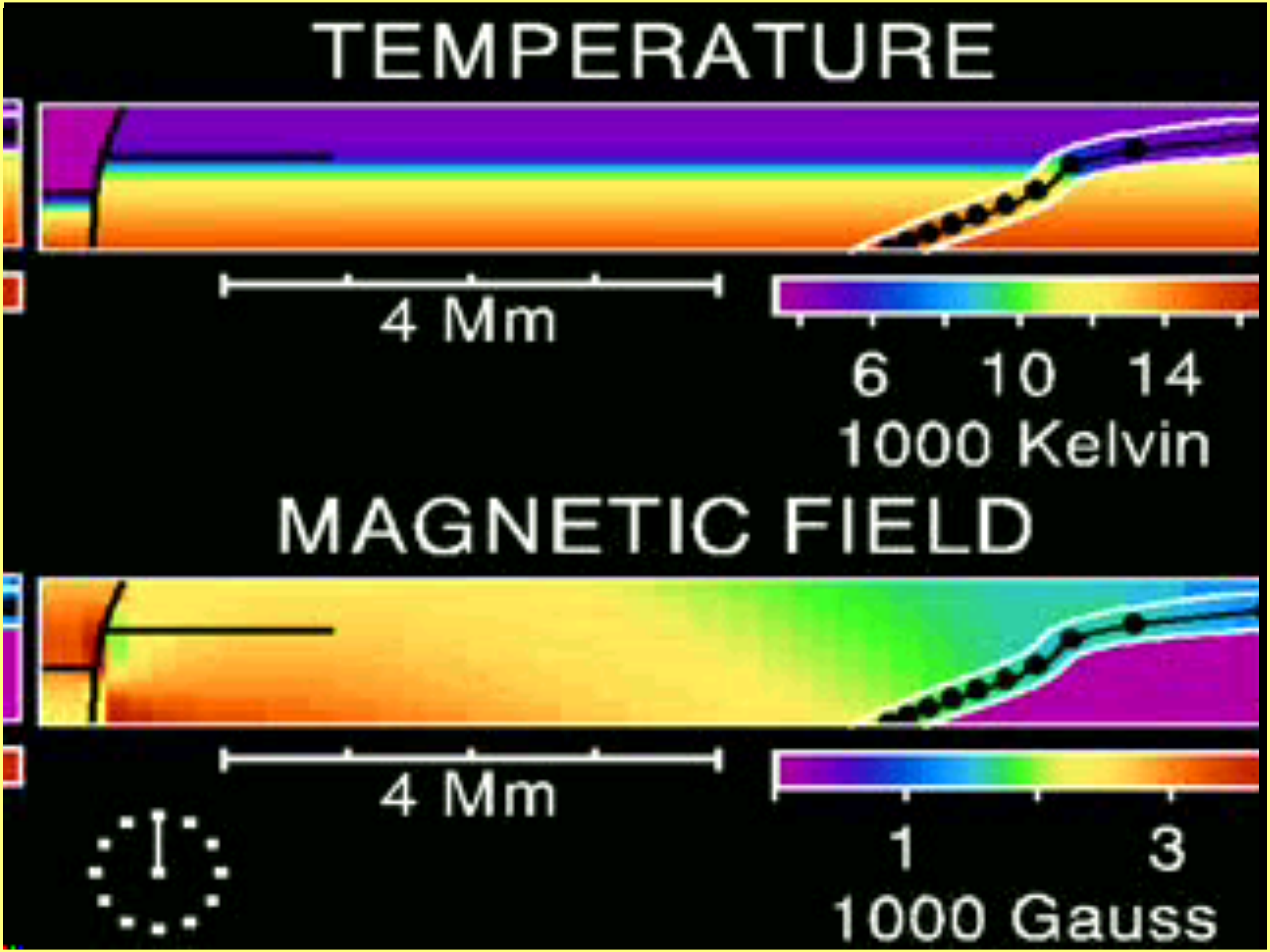

Rempel 2012: Magneto-convective cell

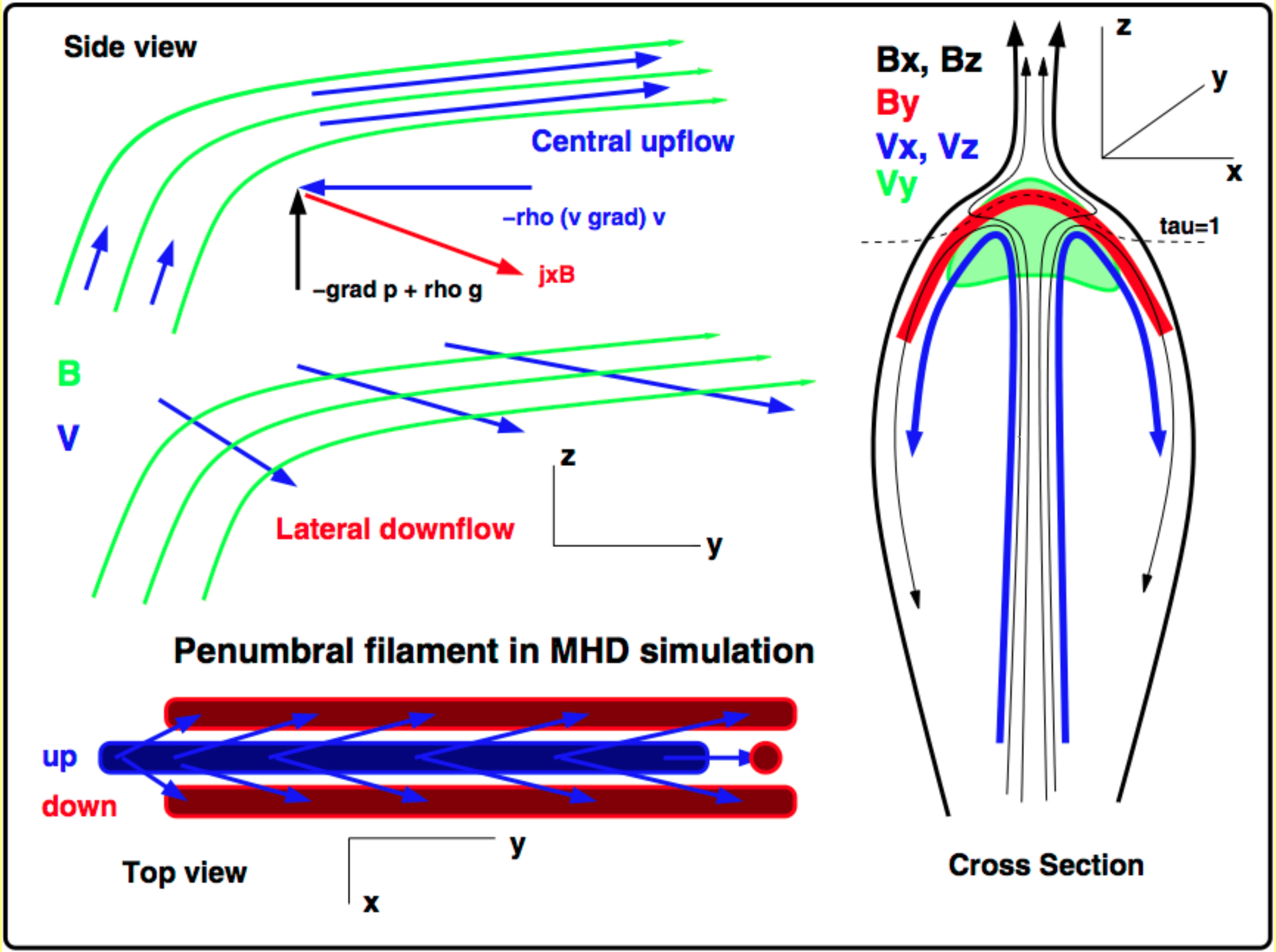

The sea serpent

Simulation of moving tube model with less dissipative numerical scheme

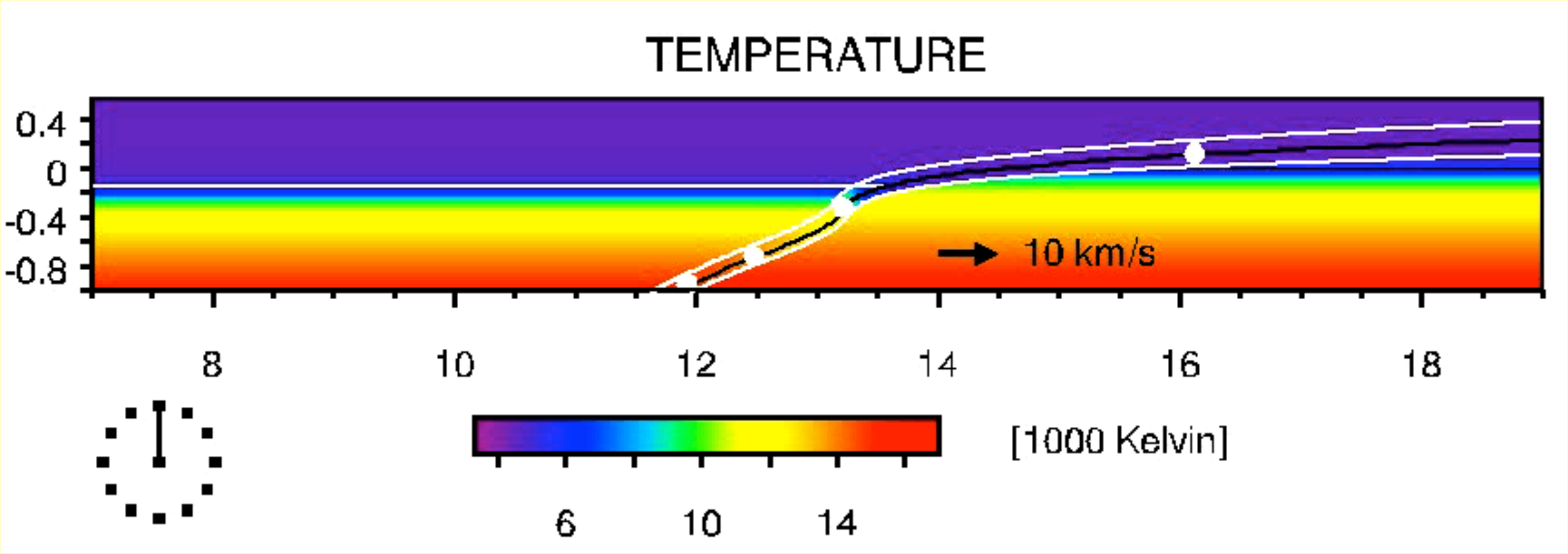

- **Penumbral grains that migrate outwards (e.g., Bovelet & Wiehr 2003)**
- **Downflows and opposite polarity in outer penumbra (e.g., Ichimoto et al. PASJ, 2007)**
- **Outward migrating pair of polarity (Sainz Dalda & Bellot Rubio A&A, 2008)**

(Schl. 2002)

Downflows in the penumbra: the sea serpent

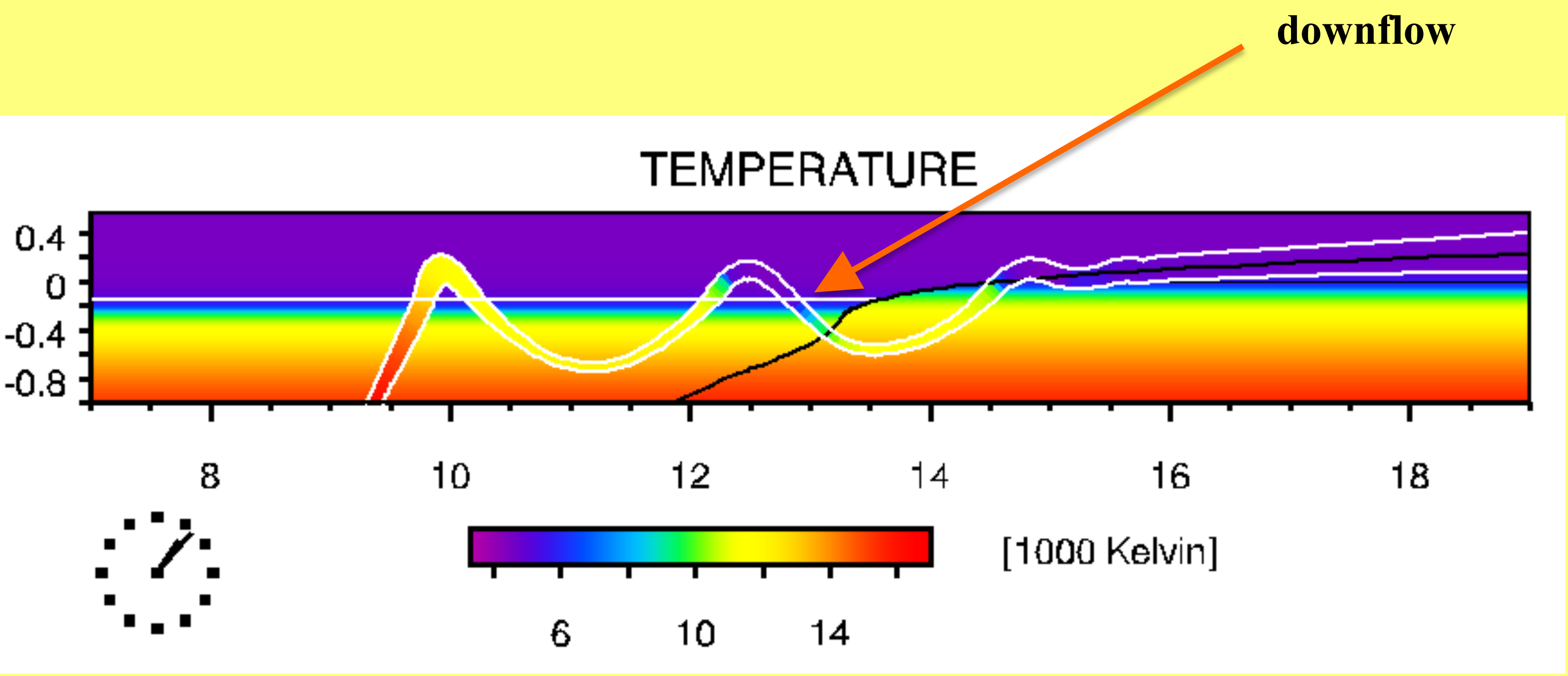

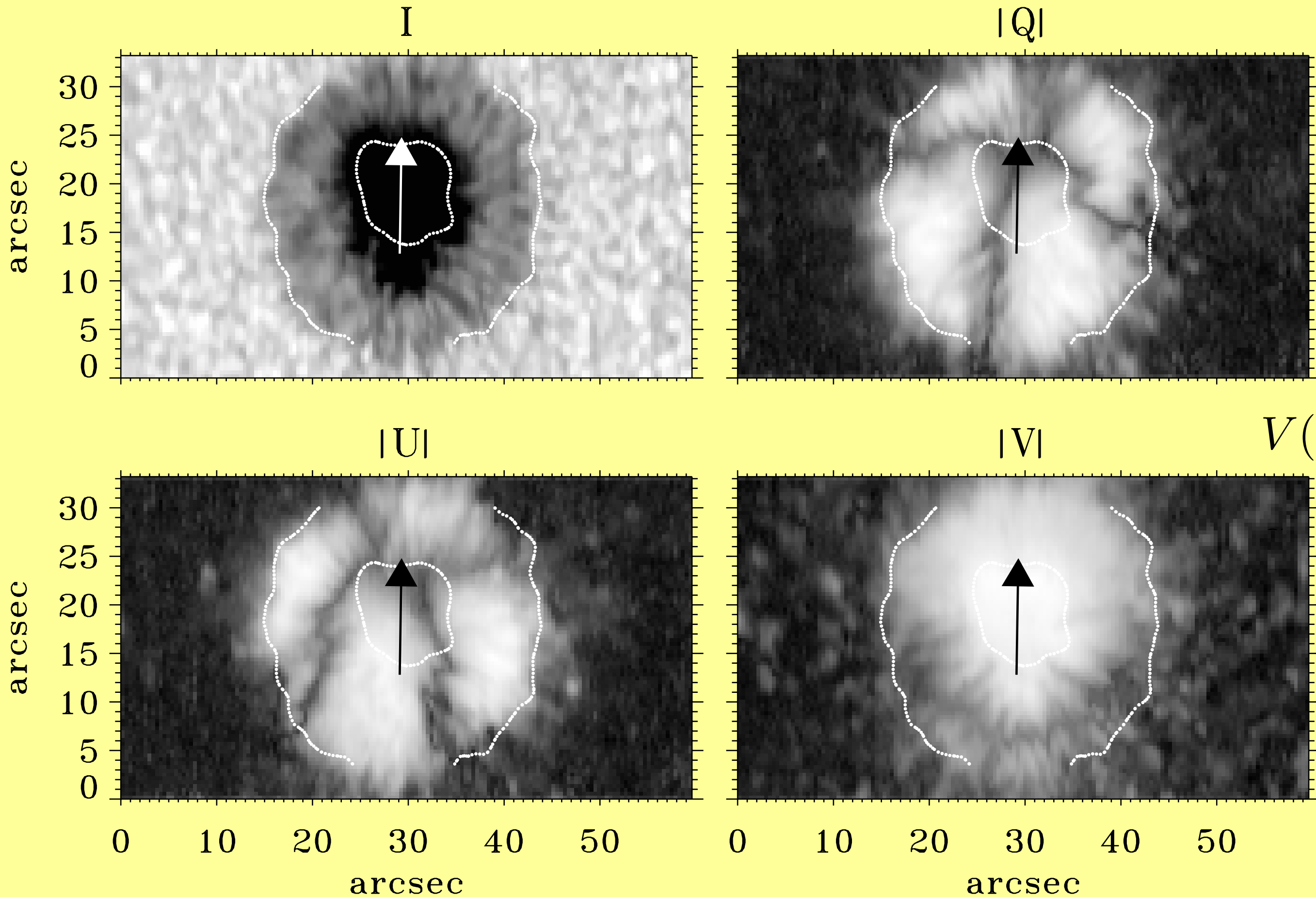

$$V(\lambda) \equiv 100 \cdot \frac{V_{\mathrm{measured}}(\lambda)}{I_{\mathrm{c}}}$$

$$\mathrm{NCP} \equiv \int V(\lambda)\mathrm{d}\lambda$$

Fig. 1. Maps of the spectrally integrated Stokes profiles $\log(I)$, $\log|Q|$, $\log|U|$, and $\log|V|$ for the spot on Nov. 9 1999, at a heliocentric angle of 30°. The arrow points towards disk center.

$$\mathrm{d}a \equiv |a_{\mathrm{b}}| - |a_{\mathrm{r}}|$$

$$L(\lambda) \equiv \sqrt{Q(\lambda)^2 + U(\lambda)^2}$$

$$P(\lambda) \equiv \sqrt{Q(\lambda)^2 + U(\lambda)^2 + V(\lambda)^2}.$$

$$a_{\mathrm{b}} \equiv \begin{cases} \max(V(\lambda)) & \text{for } \lambda_{\max} < \lambda_{\min} \\ |\min(V(\lambda))| & \text{for } \lambda_{\min} < \lambda_{\max} \end{cases}$$

$$a_{\mathrm{r}} \equiv \begin{cases} |\min(V(\lambda))| & \text{for } \lambda_{\max} < \lambda_{\min} \\ \max(V(\lambda)) & \text{for } \lambda_{\min} < \lambda_{\max} \end{cases}$$

Amplitude difference of V

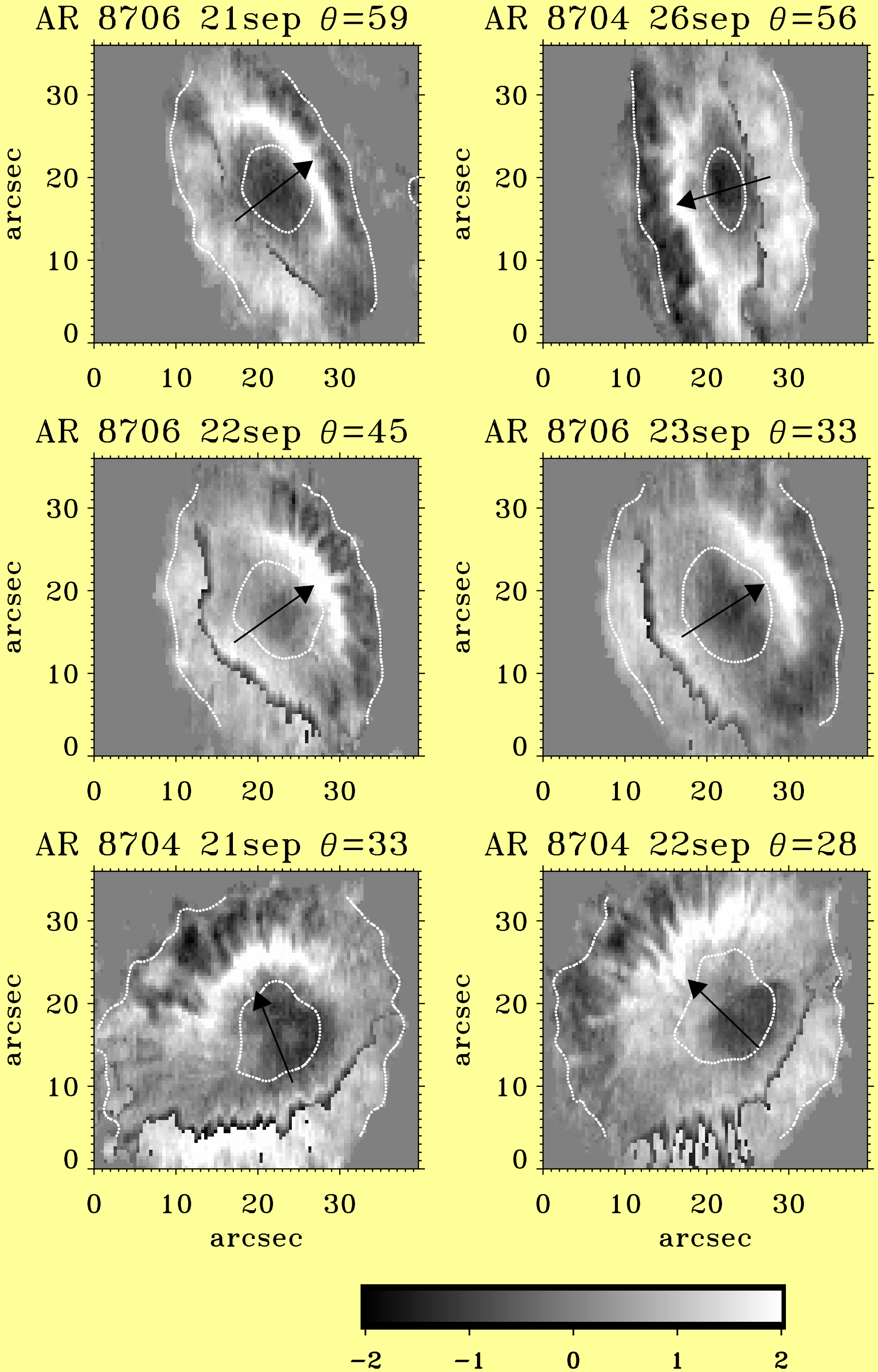

Center-side penumbra: Profiles along radial cut from inner to outer

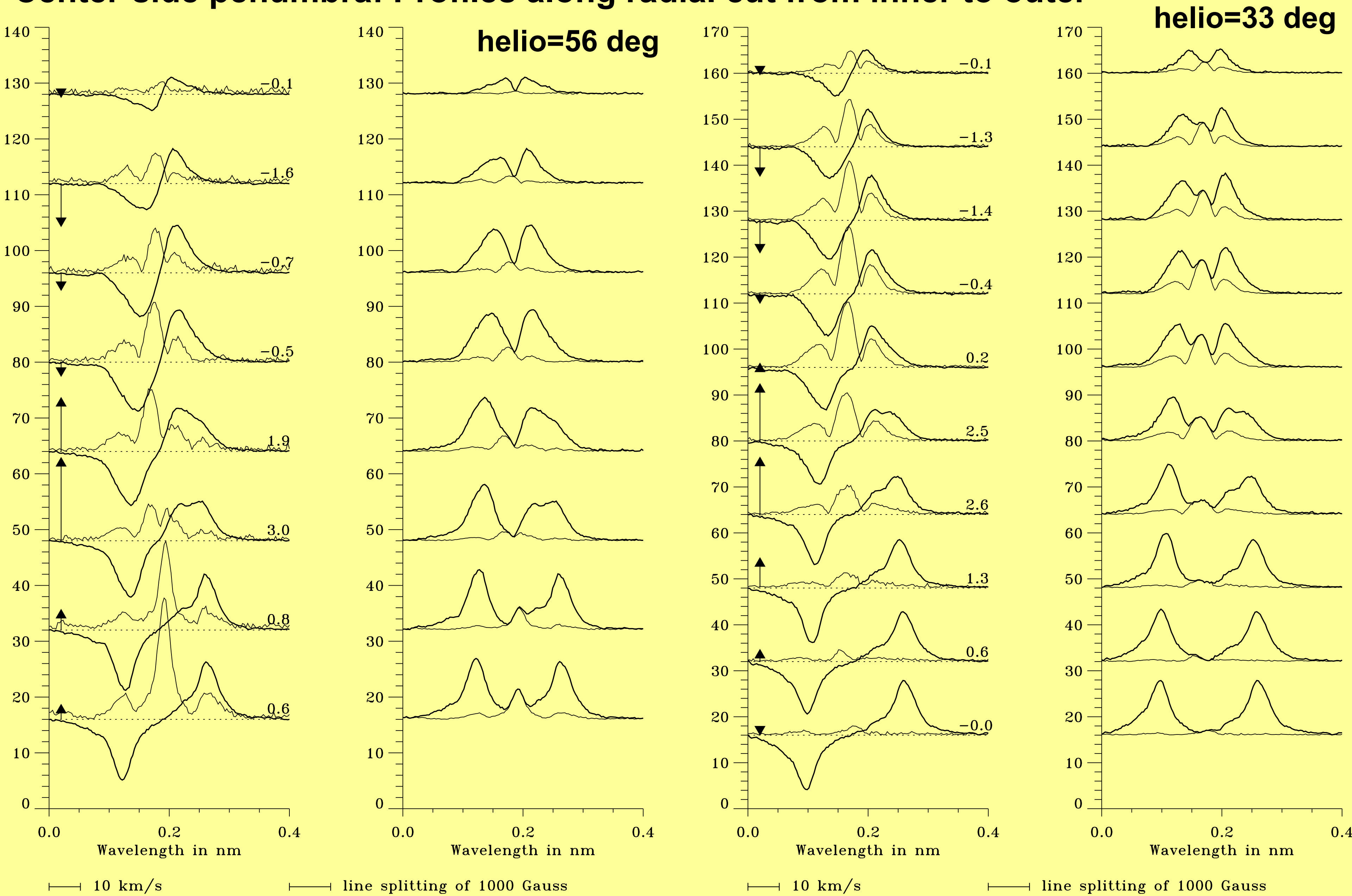

$$V(\lambda) \equiv 100 \cdot \frac{V_{\mathrm{measured}}(\lambda)}{I_{\mathrm{c}}}.$$

$$L(\lambda) \equiv \sqrt{Q(\lambda)^2 + U(\lambda)^2}$$

$$P(\lambda) \equiv \sqrt{Q(\lambda)^2 + U(\lambda)^2 + V(\lambda)^2}.$$

Limb-side penumbra: Profiles along radial cut from inner to outer

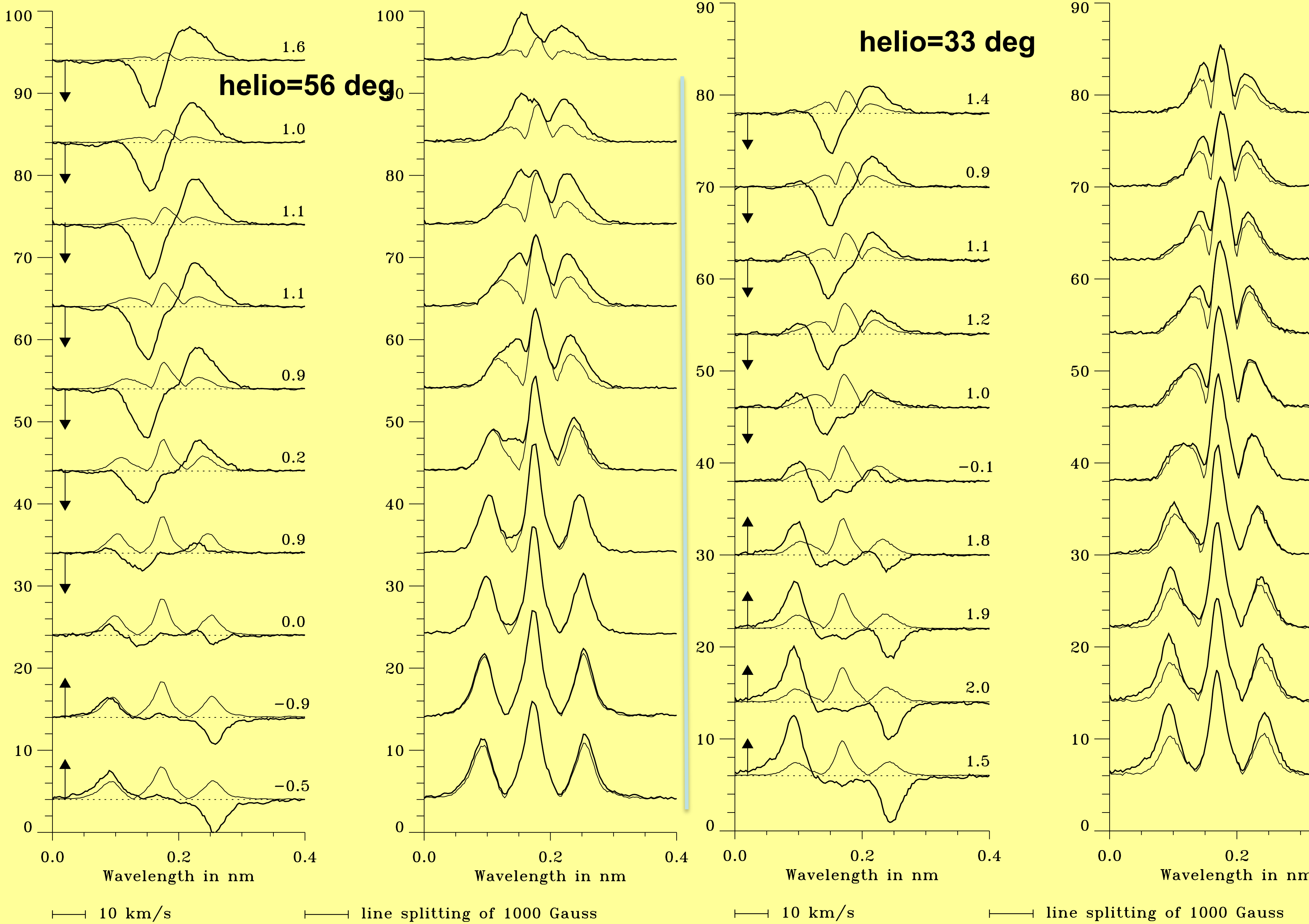

Limb-side penumbra: Profiles along magnetic neutral line

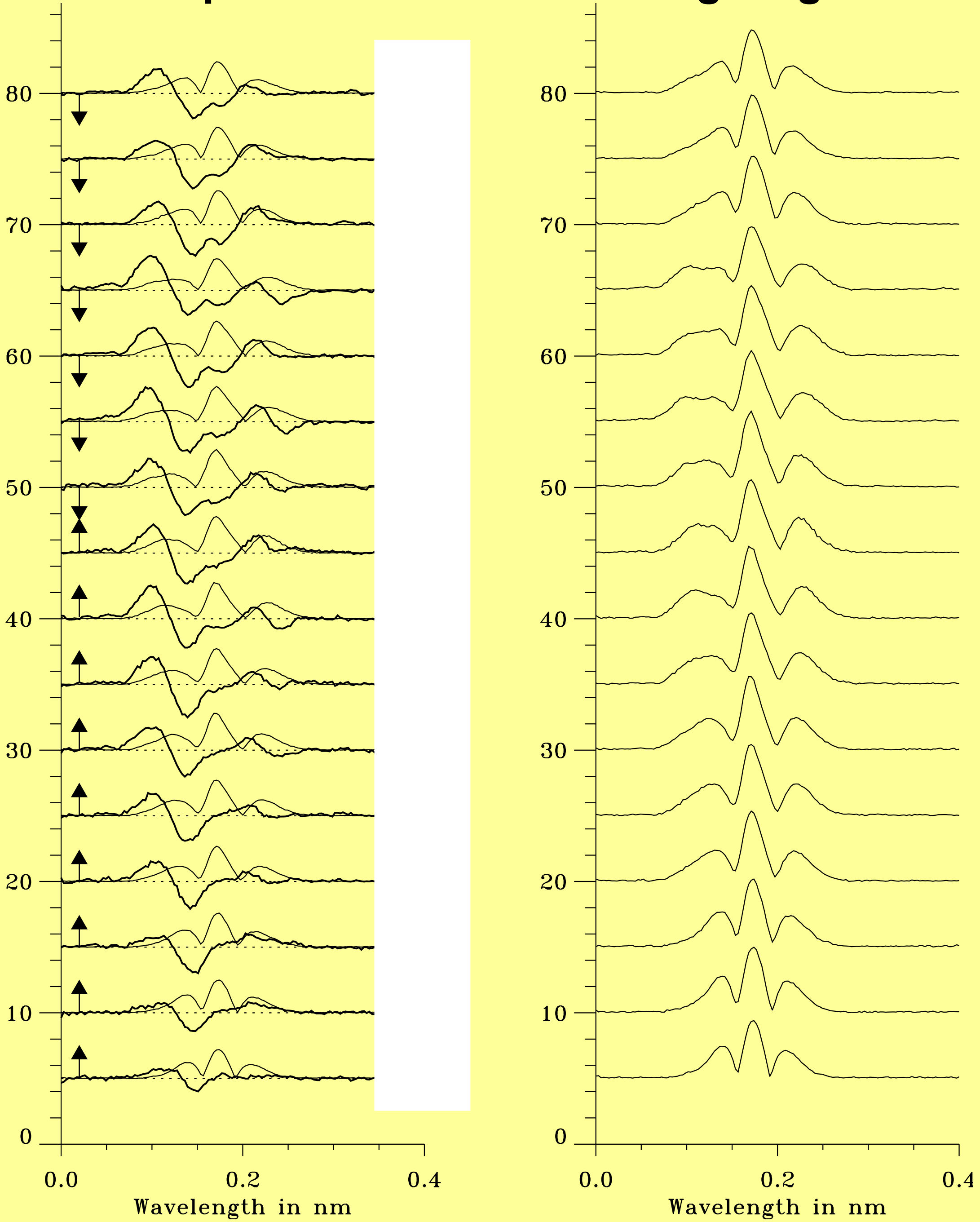

Synthetic forward modelling of 'abnormal' V profiles

Center-side PU:

outer

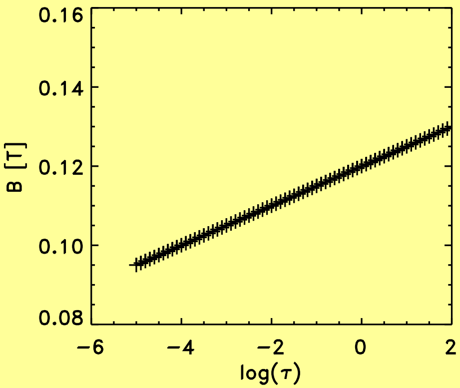

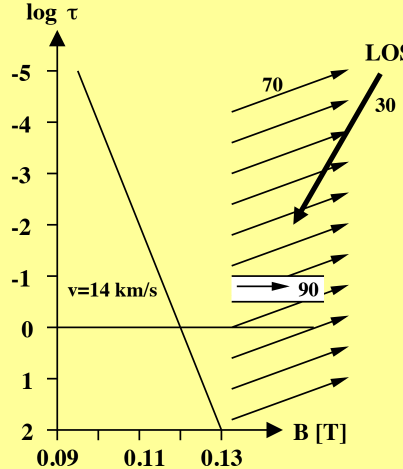

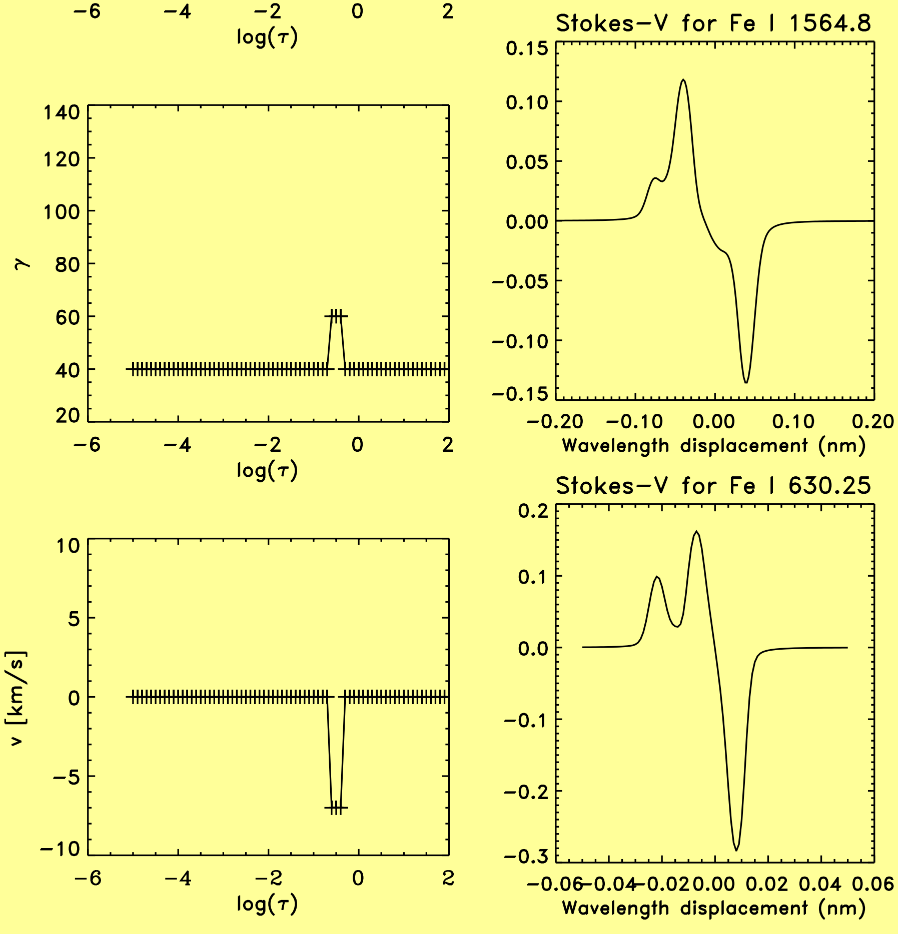

inner

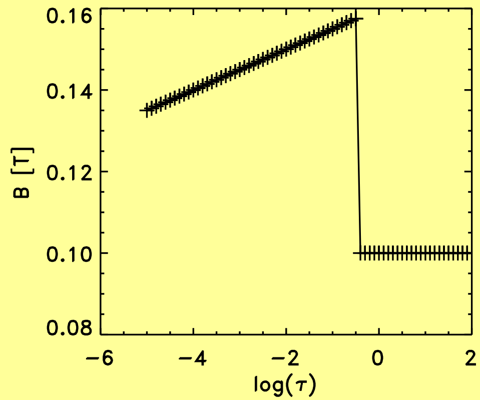

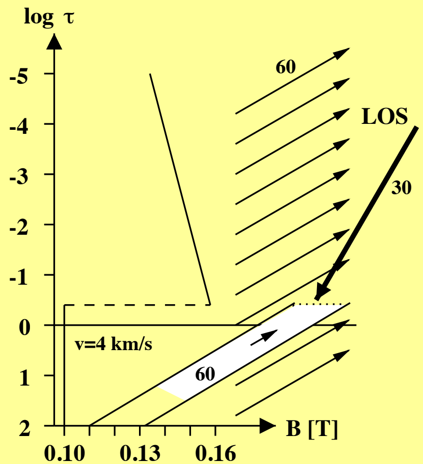

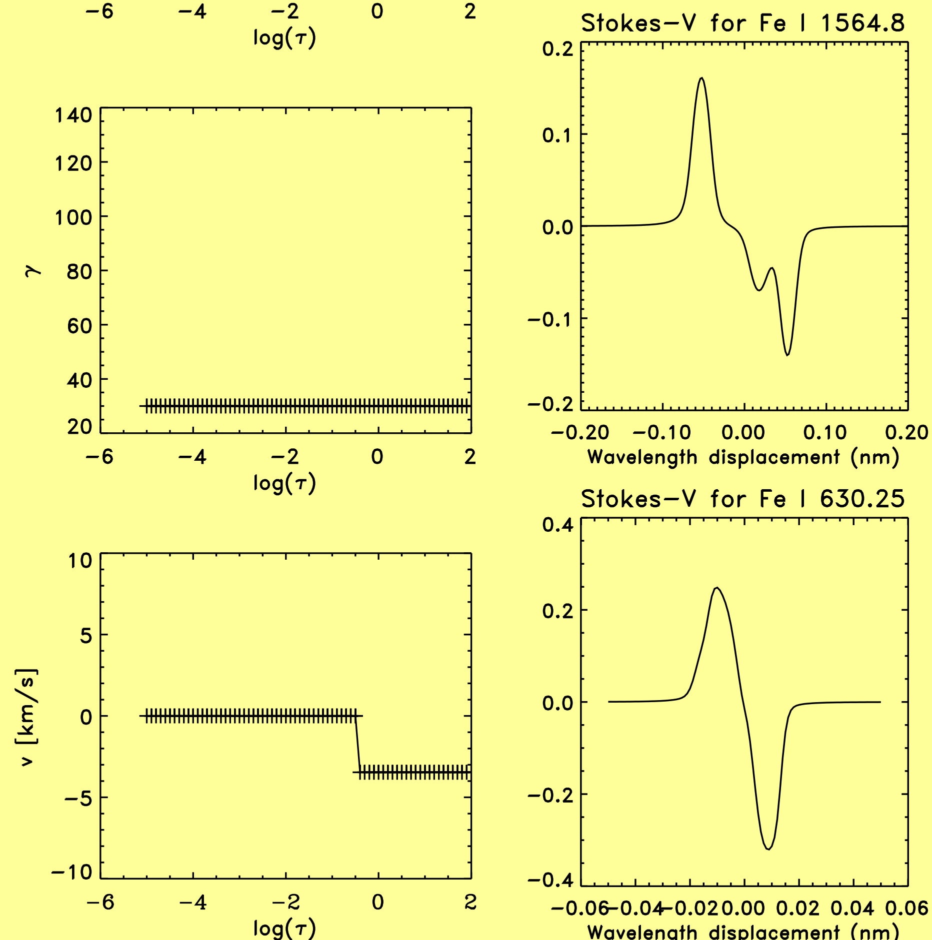

Limb-side PU:

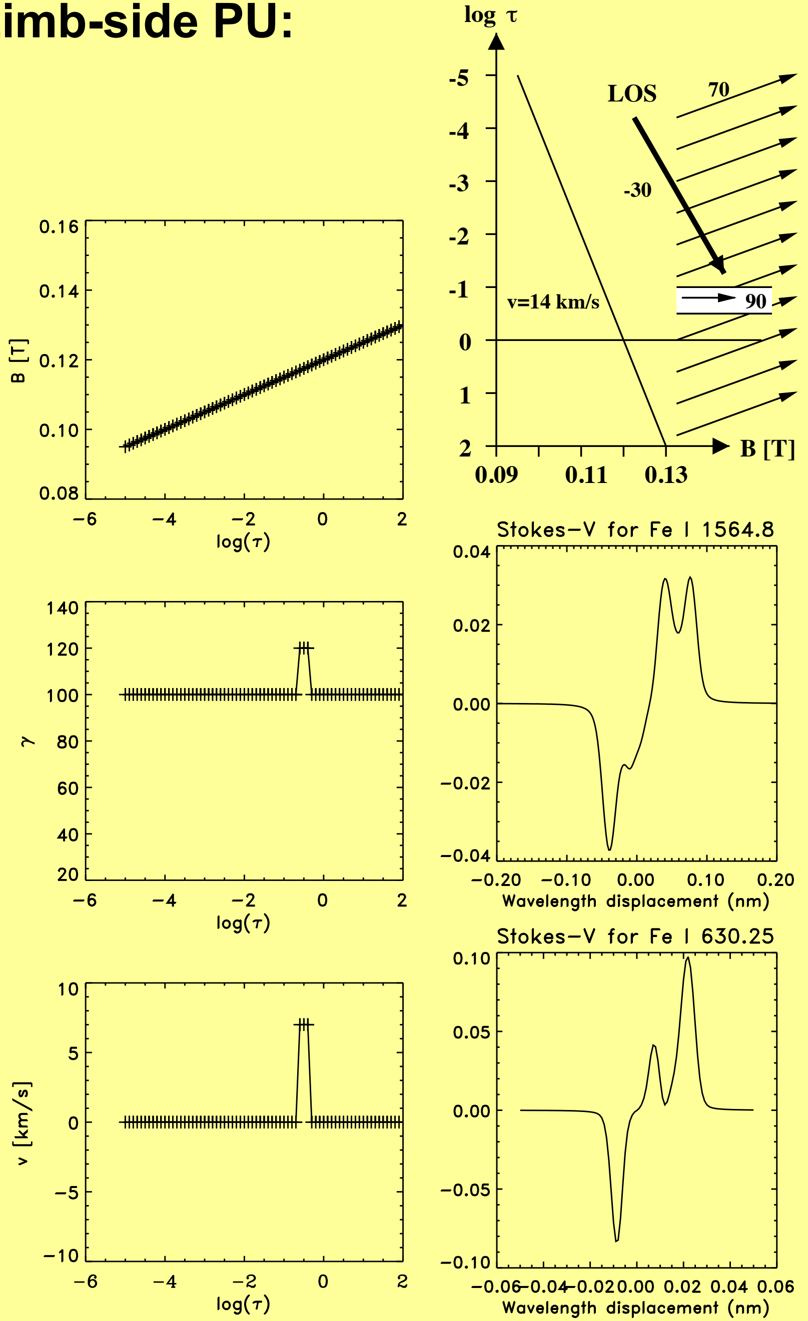

Fig. 11. Model configuration for the outer limb side penumbra (same as Fig. 9).

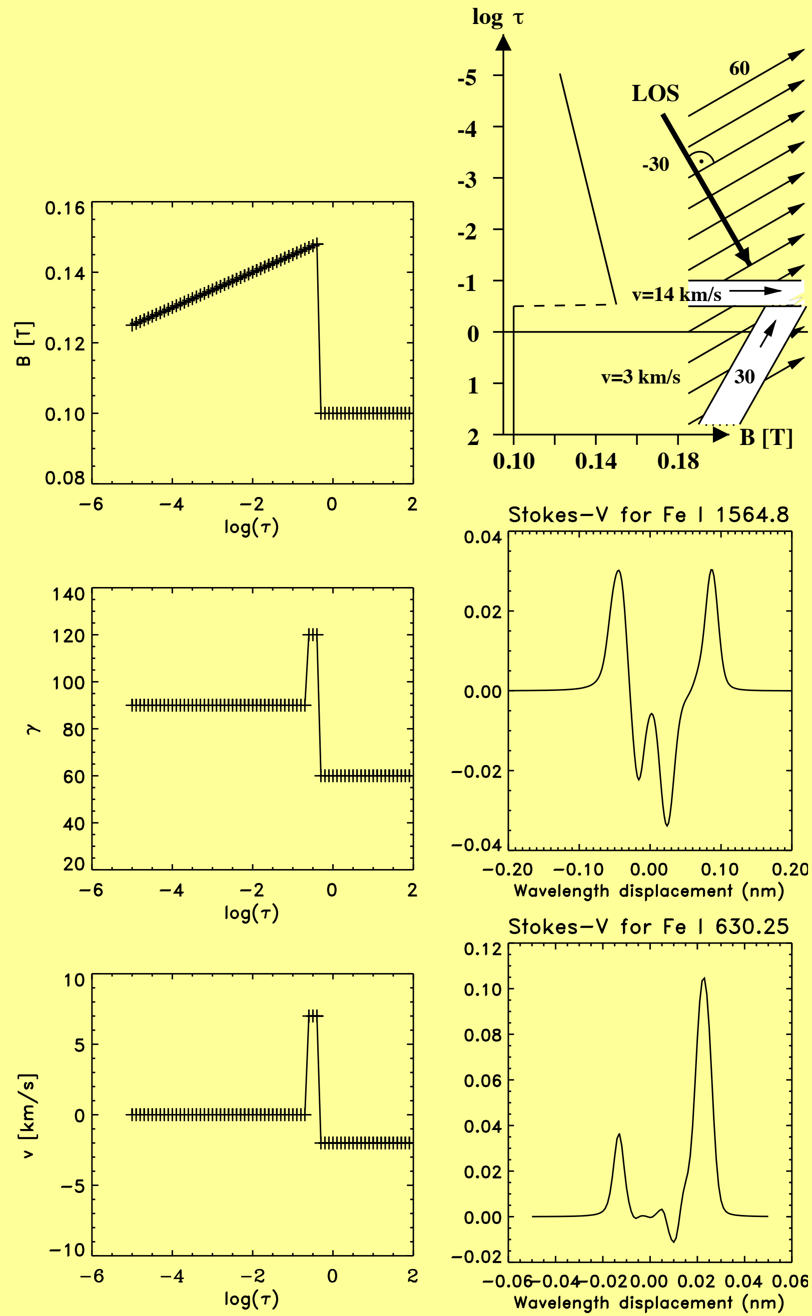

Fig. 12. Model configuration for the magnetic neutral line (same as Fig. 9).

A closer look at Stokes V profiles

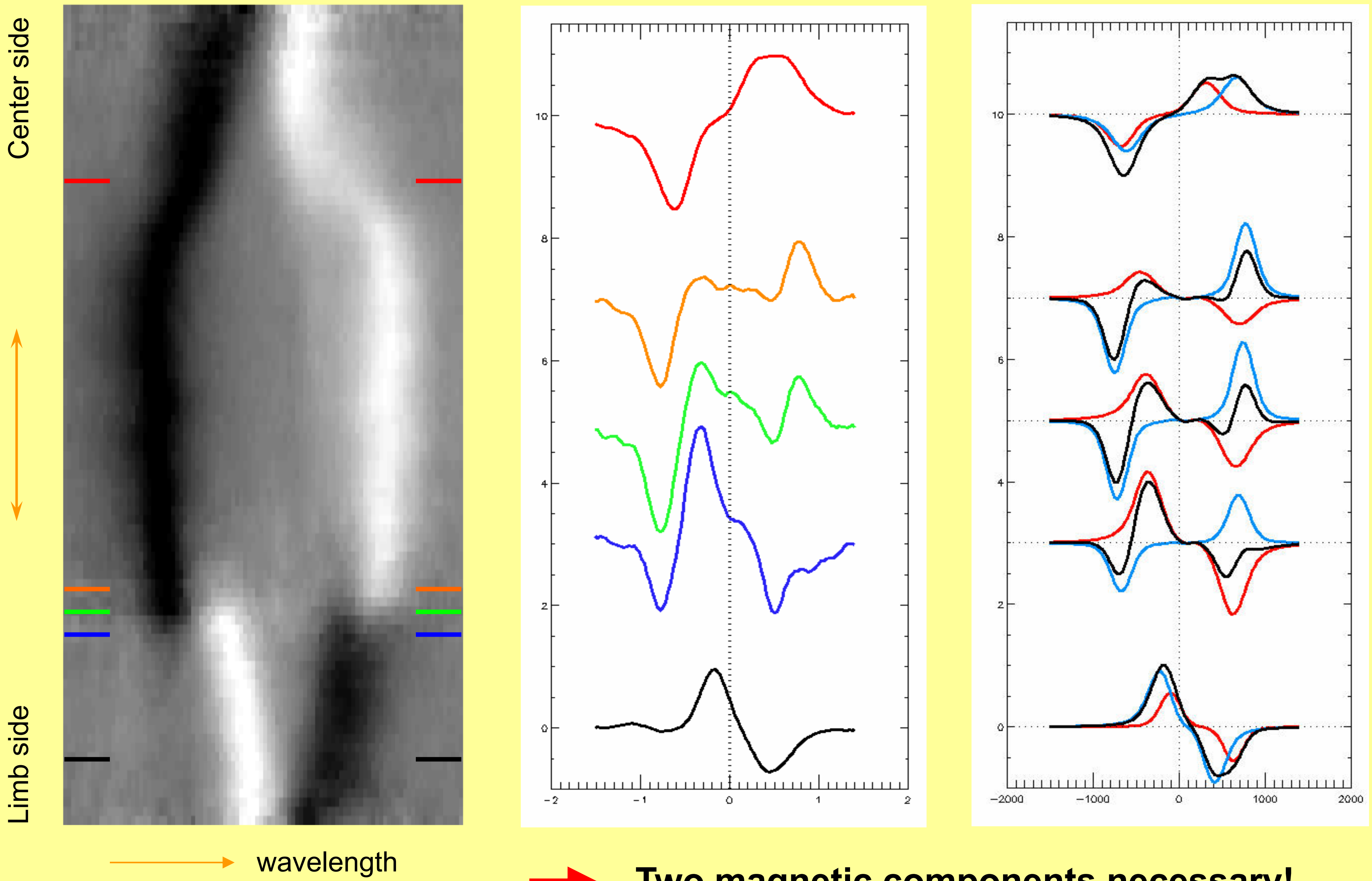

Two magnetic components necessary!

Two-component inversion

Motivation:

- Unresolved structure
- Abnormal Stokes-V profiles along neutral line.
- (Non-zero net circular polarization).

Model:

- Two atmospheric components coexisting in the resolution element.

Free parameters for each component:

- Magnetic field vector
- LOS velocity
- Temperature stratification
- Macro and microturbulence
- Filling factor

A-posteriori justification:

Better fit with two components than with one component.

The magnetic field vector (angle and strength)

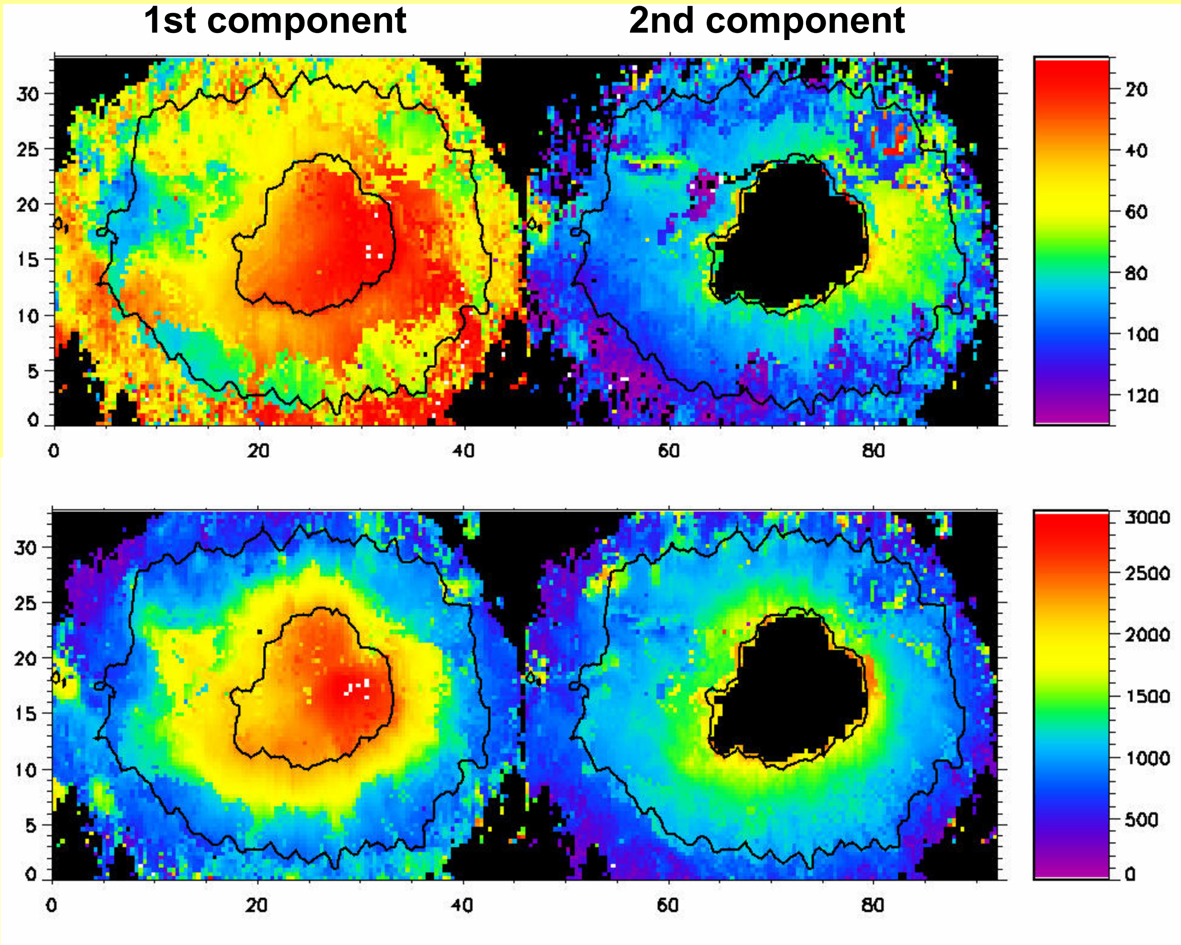

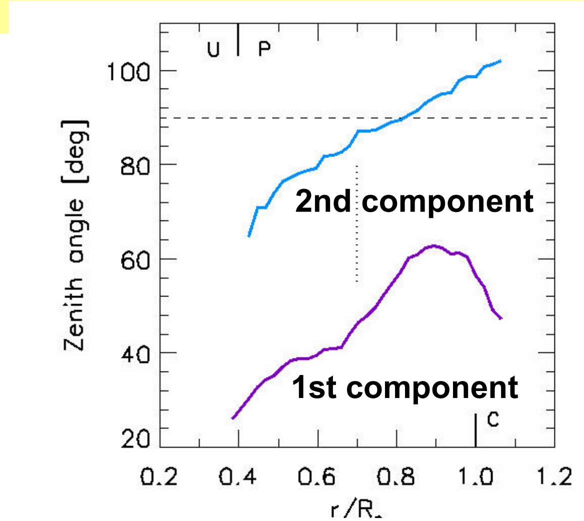

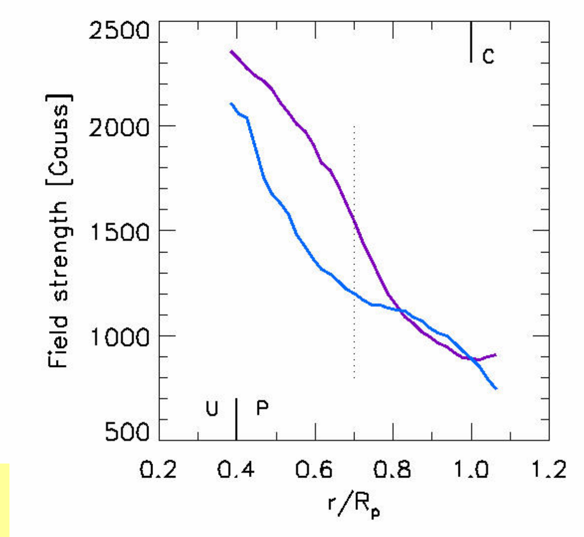

- 2nd component is more inclined than 1st component.
- 2nd component is roughly horizontal, slightly upwards in the inner and downwards in the outer penumbra.

The line-of-sight velocity

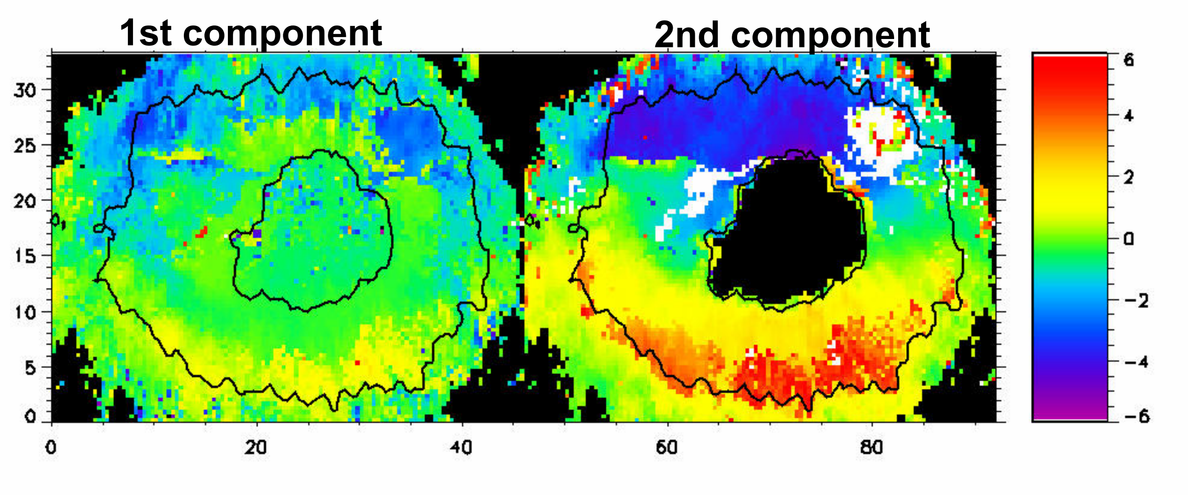

- 1st comp. is almost at rest.
- 2nd comp. carries flow.

Flow geometry of 2nd component:

Axial symmetry $\quad \Rightarrow \quad v_{\mathrm{LOS}}(r,\phi) = v_r(r)\sin\theta\cos\phi + v_z(r)\cos\theta$

ϕ: azimuth around center of sunspot. $\qquad \theta$: heliocentric angle of sunspot.
v_r: horizonal (radial) component of azimuthally averaged velocity vector.
v_z: vertical component of azimuthally averaged velocity vector.

$\Rightarrow$ $\quad v_r$ and v_z is determined by fitting the azimuthal variation, $v_{\mathrm{LOS}}(\phi)$, to the upper formula.

$\Rightarrow$ $\quad$ The zenith angle (inclination) of the flow vector and the flow velocity are inferred from v_r and v_z.

Flow and magnetic field angle of 2nd component

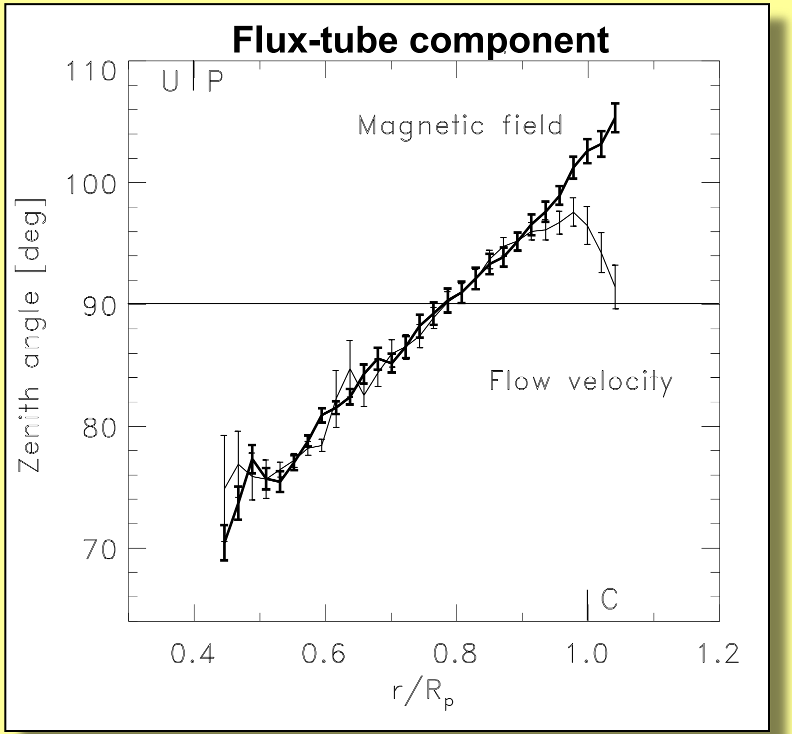

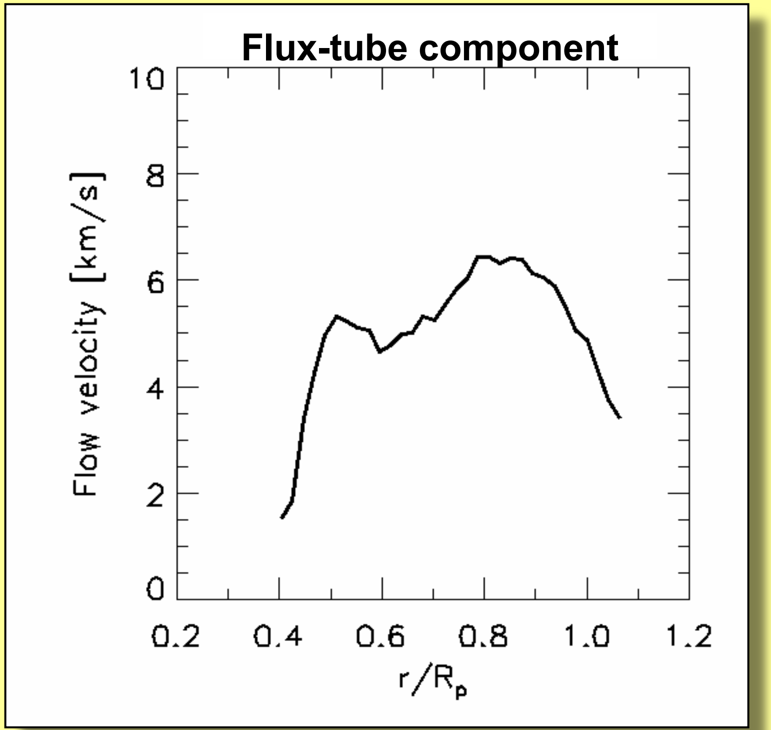

- Magnetic field vector and flow angle of 2nd component are parallel almost throughout the entire penumbra!
- Confirmation that concept of frozen-in magnetic field is applicable in penumbral photosphere.
- Upflow in inner and downflow in outer penumbra!

(Bellot Rubio, Balthasar, Collados, Schl. 2003)

NCP

Net circular polarization

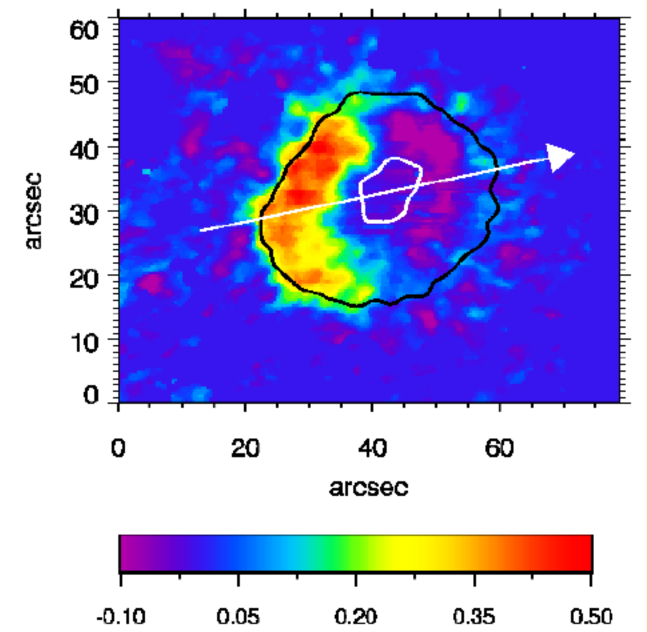

Fe I 630.2 nm (Courtesy: Martinez Pillet)

symmetric

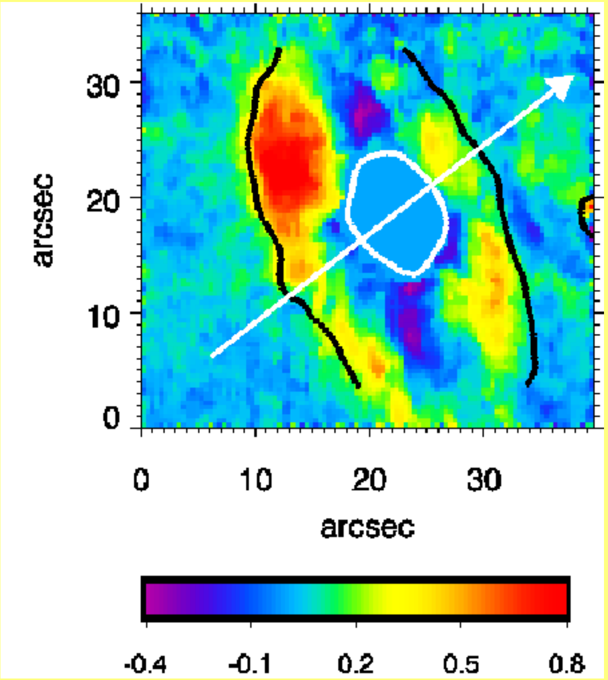

Fe I 1564.8 nm (Schl. & Collados 2002)

antisymmetric !!!??????

$$\mathrm{NCP} = \int V(\lambda)\, \mathrm{d}\lambda \qquad (= 0, \textbf{ if no flow gradients or discontinuities are present})$$

Components with different inclinations and flow velocities must be present

(Müller, Schl., Steiner, & Stix 2002)

The uncombed penumbra

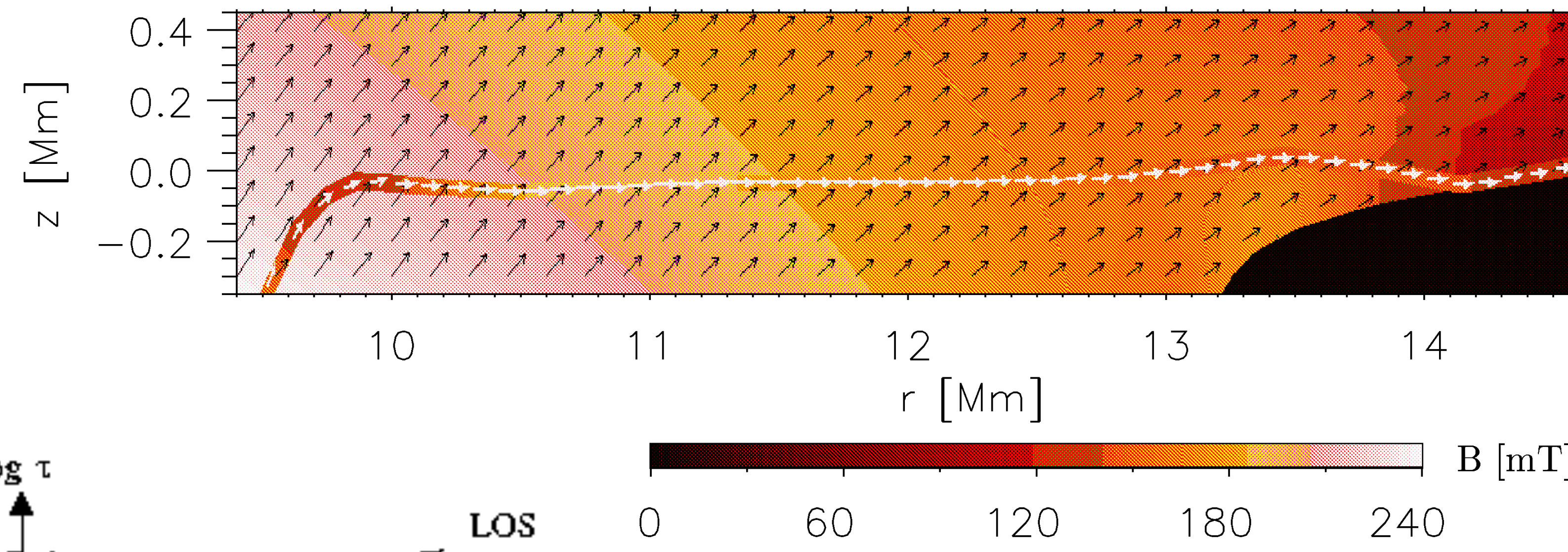

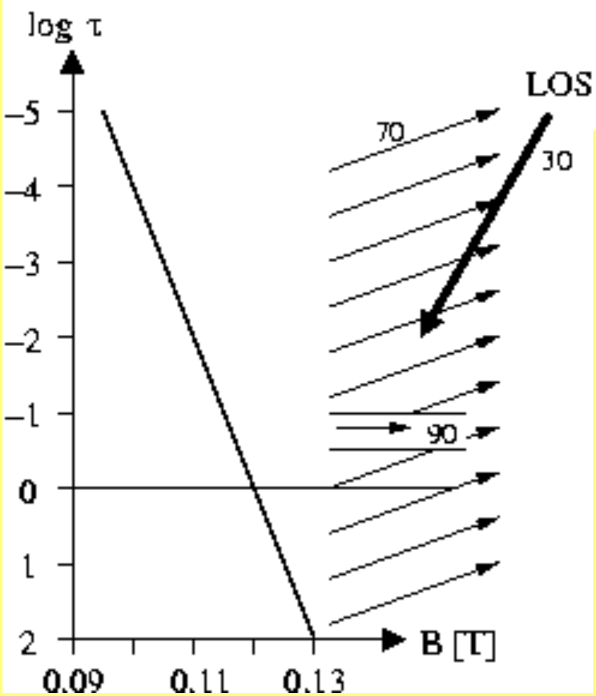

Magnetic field inclination and LOS velocity exhibit discontinuities

“The uncombed penumbra”

The uncombed penumbra

NCP along an mid-penumbral circumference

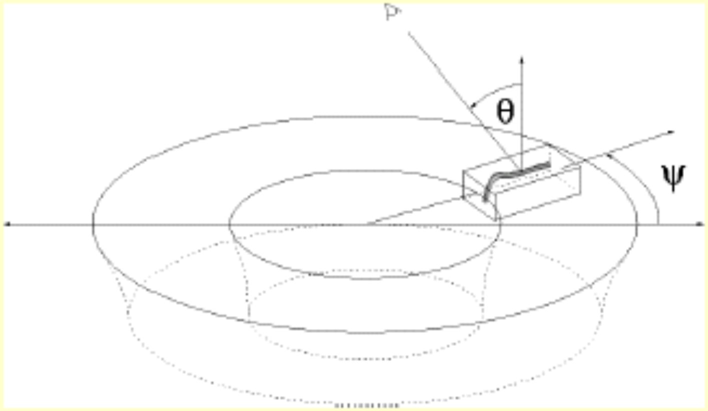

- Radial distance: 12000 km.
- Flow velocity: $v_{\mathrm{t}} = 14$ km/s, $v_{\mathrm{b}} = 0$.
- Inclination: $\gamma'_{\mathrm{t}} = 90°$, $\gamma'_{\mathrm{b}} = 65°$.
- No azimuthal component: $\phi'_{\mathrm{t}} = \phi'_{\mathrm{b}} = \psi$.
- Magnetic field strength: $B_{\mathrm{t}} = B_{\mathrm{b}}$.
- Heliocentric angle: $\theta = 15°$.

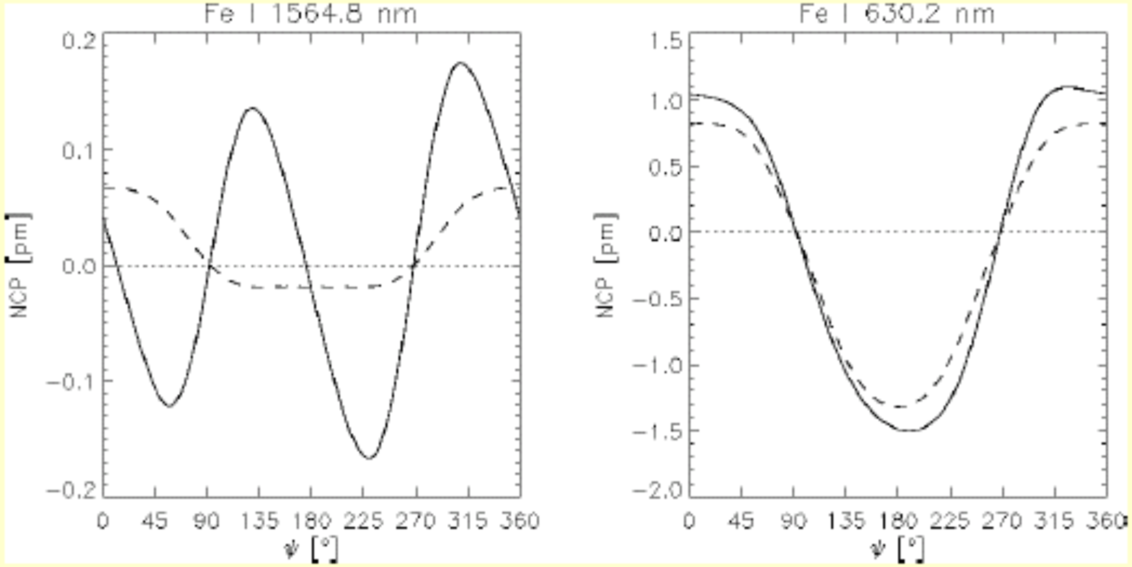

$N(\psi)$ "antisymmetric" $N(\psi)$ "symmetric"

(Müller, Schl., Steiner, Stix 2002)

Dashed line:
without anomalous dispersion

Solid line:
with anomalous dispersion

⇒ Symmetry breaking by anomalous dispersion

Equation of transfer for polarized light

$$\frac{\mathrm{d}}{\mathrm{d}s}\begin{pmatrix} I \\ Q \\ U \\ V \end{pmatrix} = \begin{pmatrix} \eta_I & \eta_Q & \eta_U & \eta_V \\ \eta_Q & \eta_I & \rho_V & -\rho_U \\ \eta_U & -\rho_V & \eta_I & \rho_Q \\ \eta_V & \rho_U & -\rho_Q & \eta_I \end{pmatrix}\begin{pmatrix} I \\ Q \\ U \\ V \end{pmatrix} + \begin{pmatrix} j_I \\ j_Q \\ j_U \\ j_V \end{pmatrix}$$

η_I: Absorption $\longrightarrow$ absorption coefficient for unpolarized light.

η_Q, η_U, η_V: Dichroism $\longrightarrow$ the absorption property of the medium depends on the polarization of radiation.

ρ_Q, ρ_U, ρ_V: Anomalous dispersion $\longrightarrow$ the velocity of propagation of the wave in the medium depends on its polarization properties.

Landi degl'Innocenti in "Astrophysical Spectropolarimetry", (eds.) Trujillo-Bueno, Moreno-Insertis, Sanchez, Cambridge University Press, 2002.

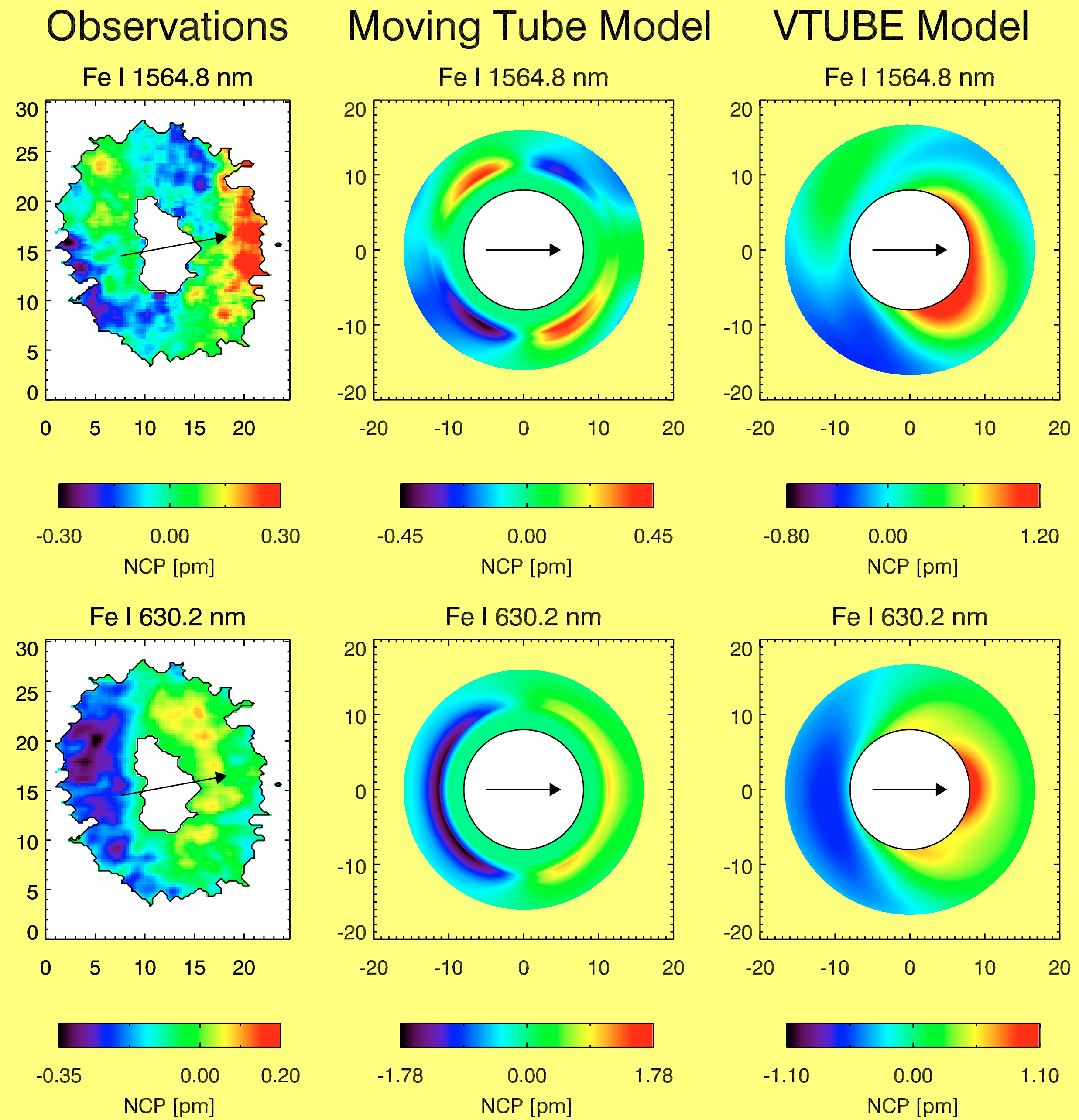

Fig. 5. Maps of net circular polarization (NCP) for an heliocentric angle of $\theta = 30°$. Upper row: infrared line, bottom row: visible line. Columns from left to right: observations (VTT, Tenerife), NCP maps synthesized from the moving tube model, and maps from the new and generalized VTUBE model. The arrows point towards disk center. The absolute magnitude of the NCP is higher for the synthetic maps than for the observations since a filling factor of unity is assumed. The color coding for all maps represents the NCP, measured in pm, and the spatial scales are in Mm.

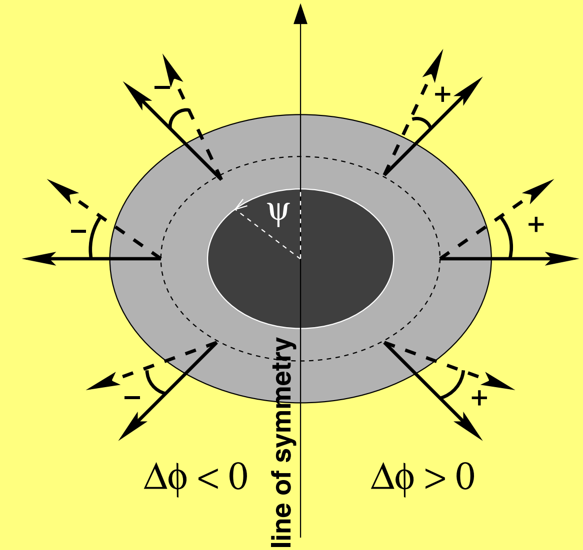

Fig. 1. Pictorial representation of the difference in azimuth, $\Delta\phi(\psi)$, tween the magnetic field vector inside a flux tube (solid arrows) and t of the background field (dashed arrows). The tubes are nearly horiz tal, while the field vector of the background has a steeper inclinati but is also in the plane spanned by the spot axis and the flux tube ax

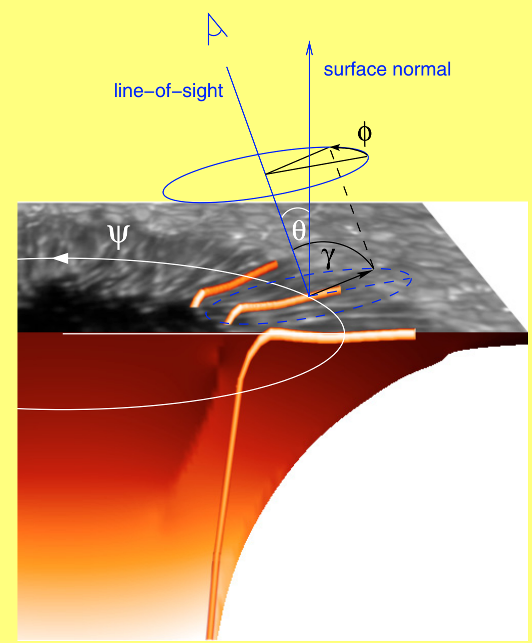

Opposite polarity: 3-lobe profiles

Small-scales dynamics

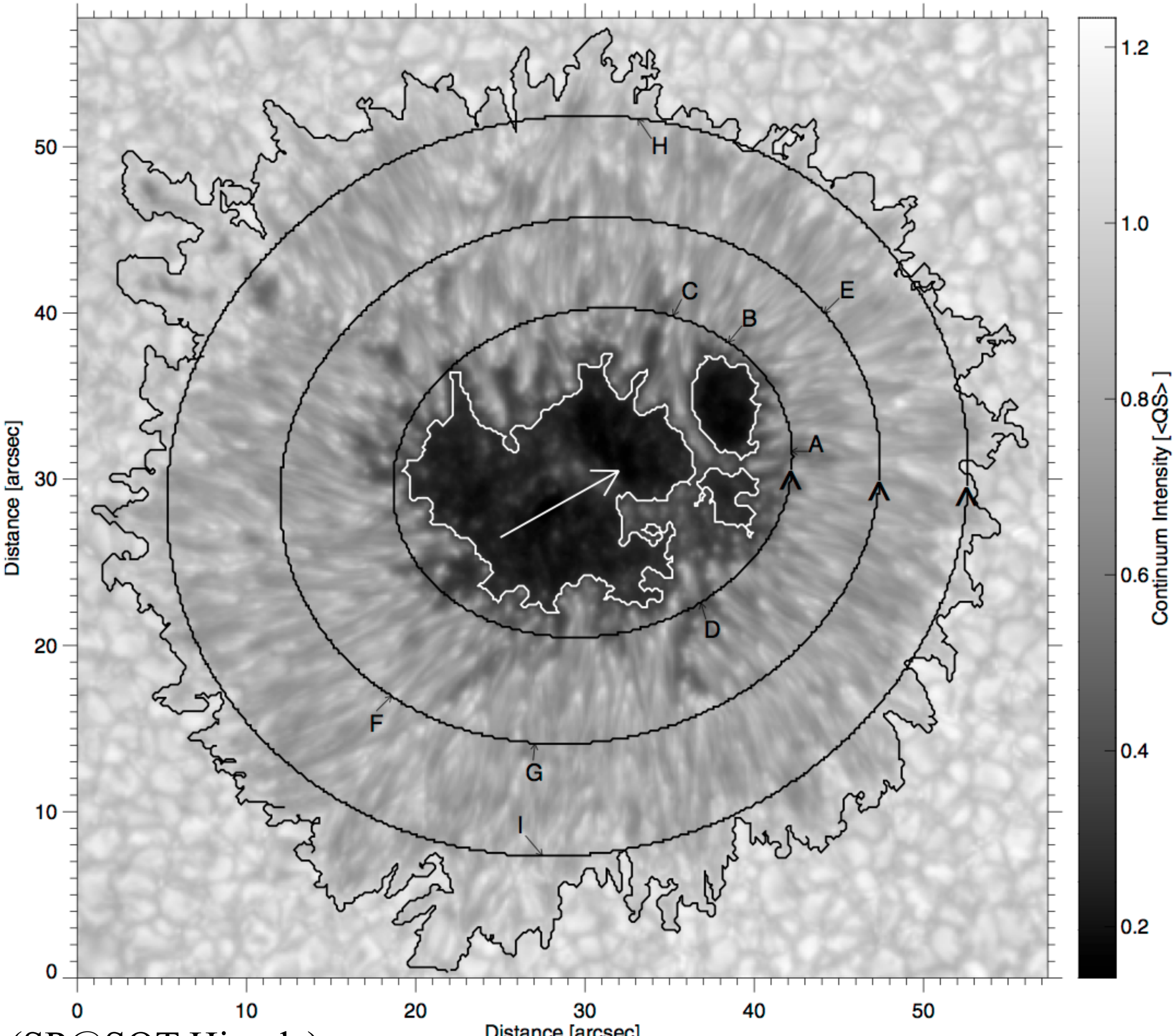

(SP@SOT Hinode)

Intensity fine structure of a Sunspot observed with SP@SOT onboard Hindode

- **Spectral scan**
- **Fe I 630.15 nm**
- **Fe I 630.25 nm**
- **Doppler shift from line wing**

Franz & Schl. 2009

Small-scales dynamics: Up and down flows

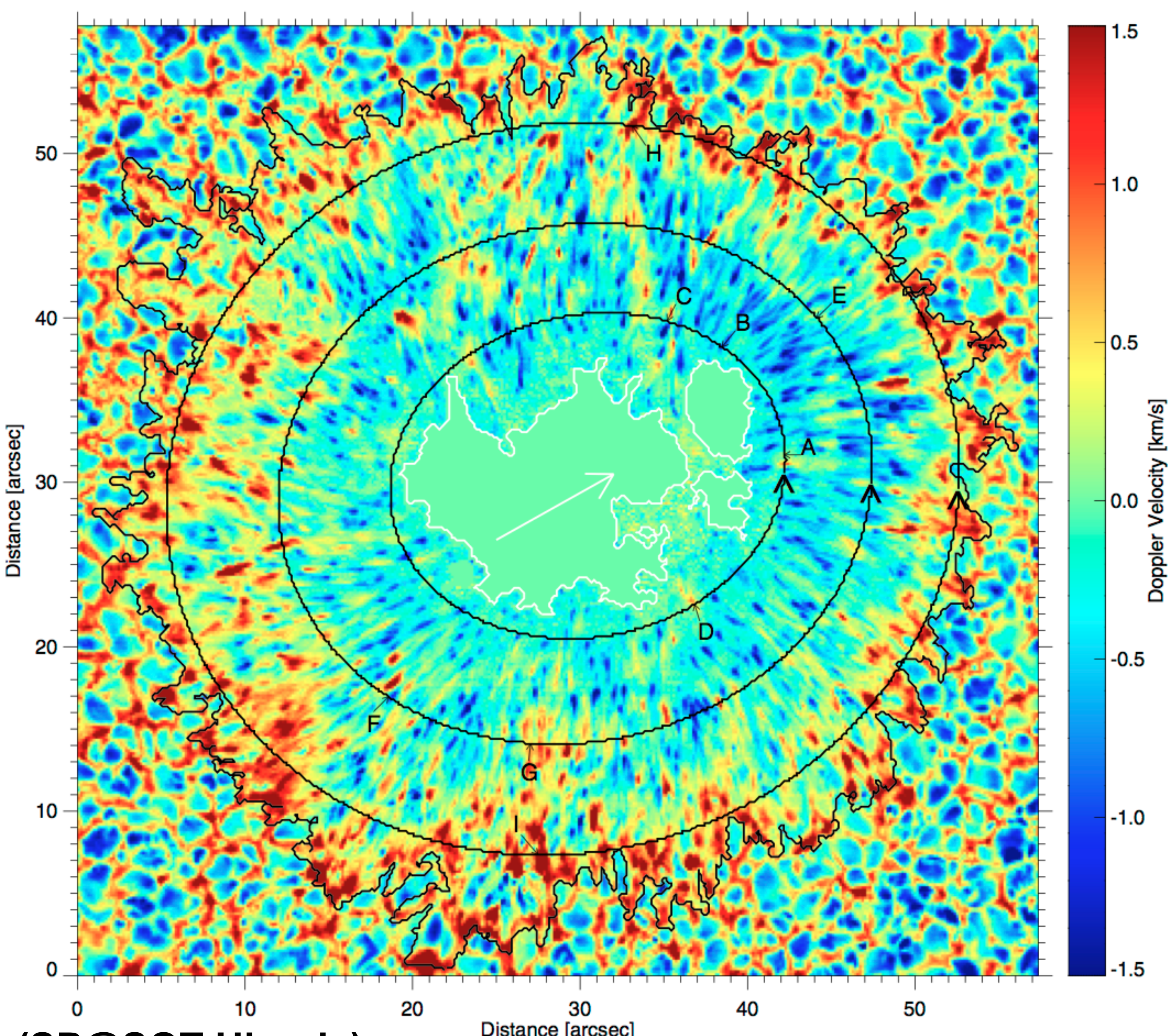

(SP@SOT Hinode)

Flow field of a sunspot at disk center = vertical flow field

Upflows and ! Downflows !

But no elongated downflows next to upflow filaments.

Franz & Schl. 2009

V-profile shapes changing with Doppler shift

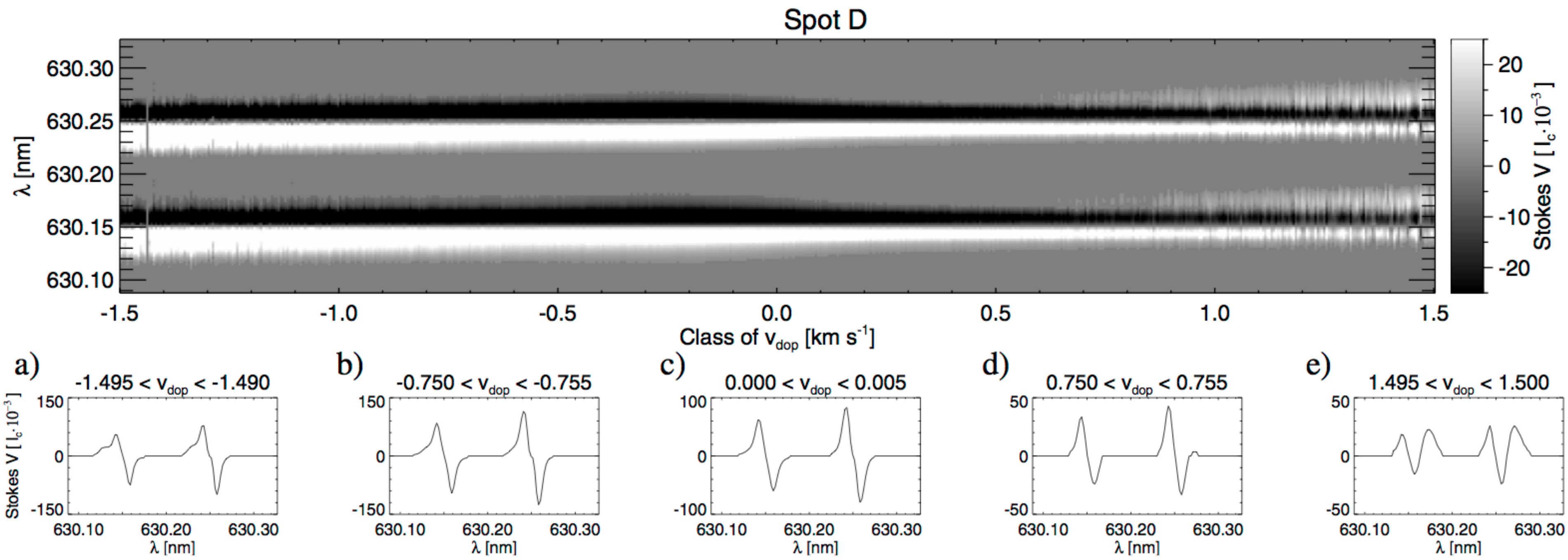

Fig. 4. *Top*: average Stokes *V* profiles of different bins of Doppler velocity for the penumbra of dataset Spot D. White represents the positive lobe, black the negative lobe. The picture is saturated at a continuum intensity of 2.5% and all measurements below the 3σ noise level were artificially set to zero. *Bottom*: examples of averaged profiles in various velocity bins.

- **Blue-shifted V-profiles exhibit blue hump.**
- **Red-shifted V-profiles exhibit 3 lobes.**

(SP@SOT Hinode)

Franz & Schl. 2013

Table 2. Two-layer atmosphere: modification to HSRA.

Optical depth $\log(\tau_{500})$	Field strength B [G]	Zenith angle γ [°]	Velocity v_{dop} [km s^{-1}]
	Upflow case		
0.0 to −0.5	1000	60	−6.5
−0.6 to −3.0	1500	20	0.0
	Downflow case		
0.0 to −0.5	1000	120	8.5
−0.6 to −3.0	700	60	0.0

Table 3. Two-component atmosphere: modification to HSRA.

Filling factor of component [%]	Field strength B [G]	Zenith angle γ [°]	Velocity v_{dop} [km s^{-1}]
	Upflow case		
30	1000	60	−6.5
70	1500	20	0.0
	Downflow case		
30	1000	120	8.5
70	700	60	0.0

Franz & Schl. 2013

V-Profile fine structure

(SP@SOT Hinode)

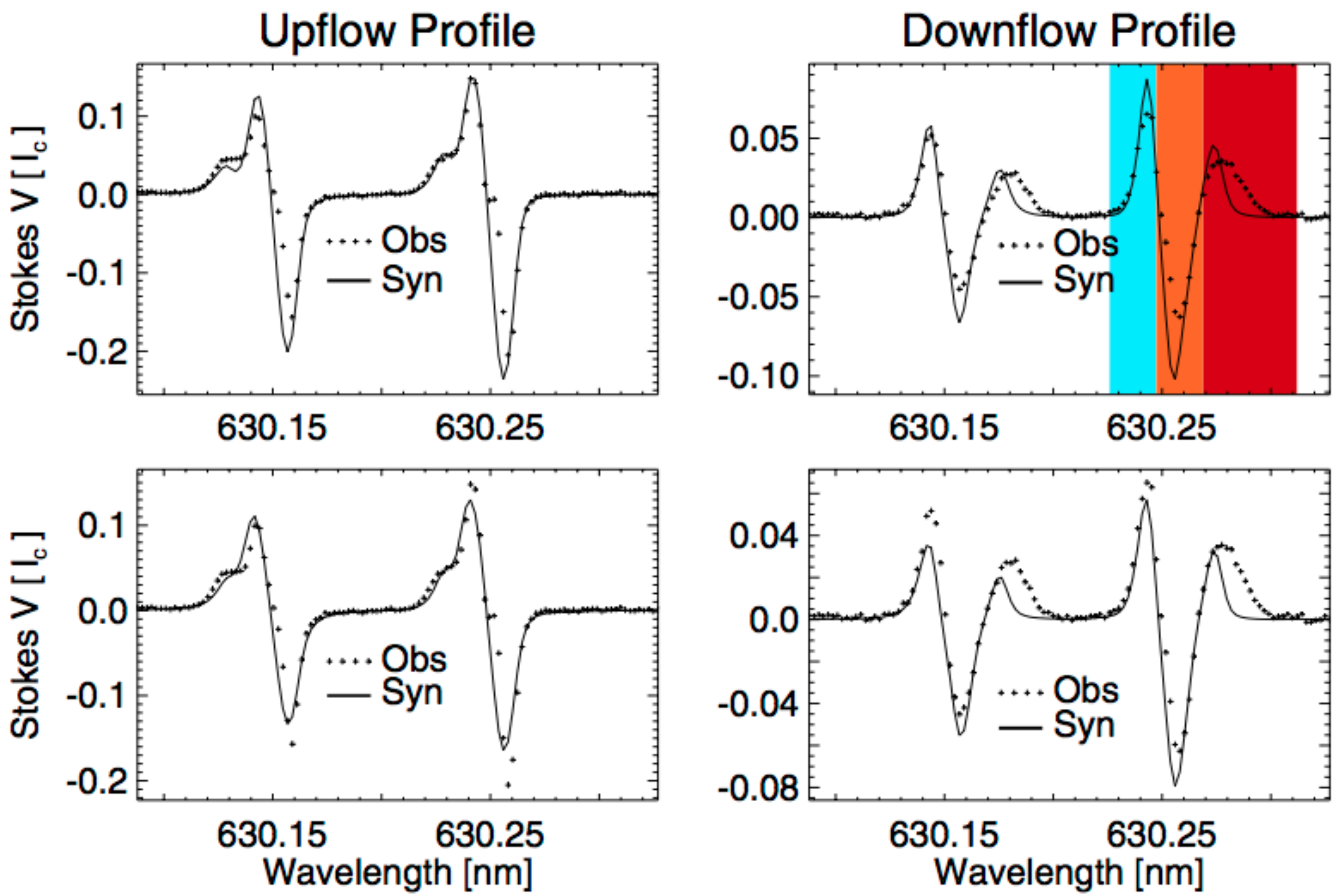

Fig. 1. Stokes *V* profiles from typical penumbral up- and downflows observed with HINODE (crosses). *Top row*: synthetic profiles (solid) radiative transfer calculations within a two-layer atmosphere. The colored regions in the *top right* plot indicate the spectral regions that are used to identify 3-lobe profiles. *Bottom row*: synthetic spectra (solid) originating in a two-component atmosphere.

Franz 2011;
Franz & Schl. 2013

Opposite polarity taking into account 3-lobe profiles

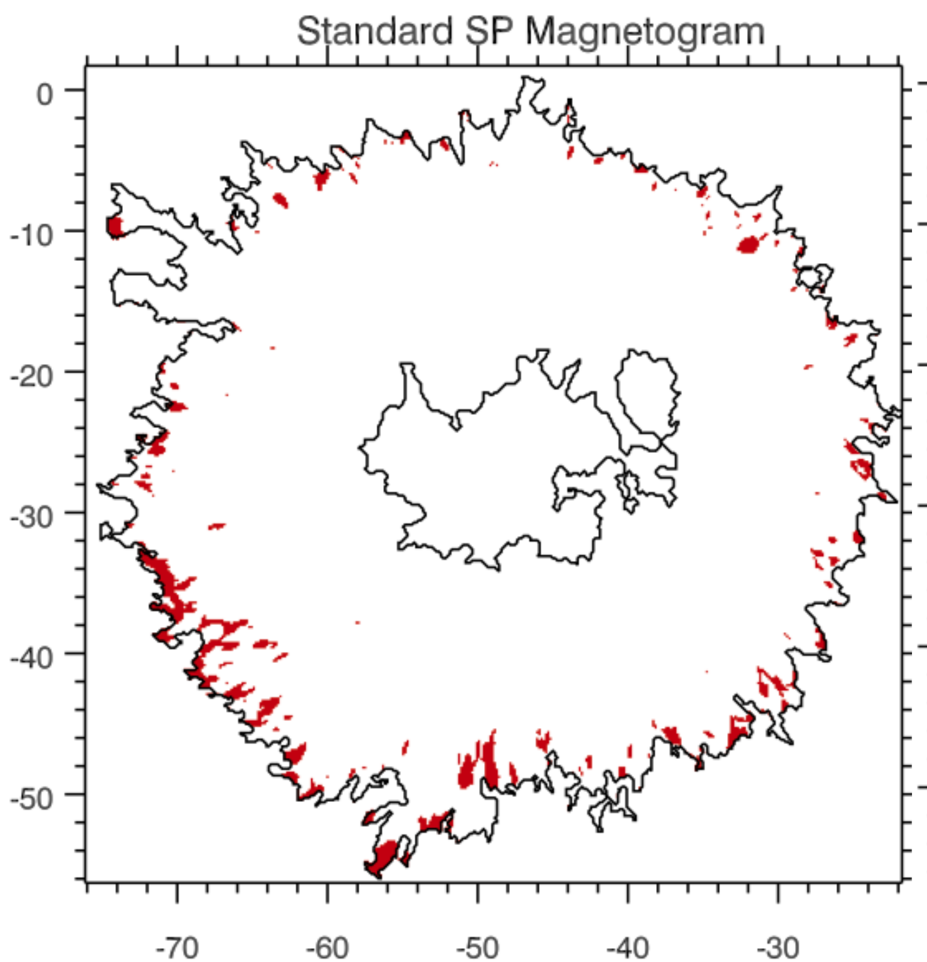

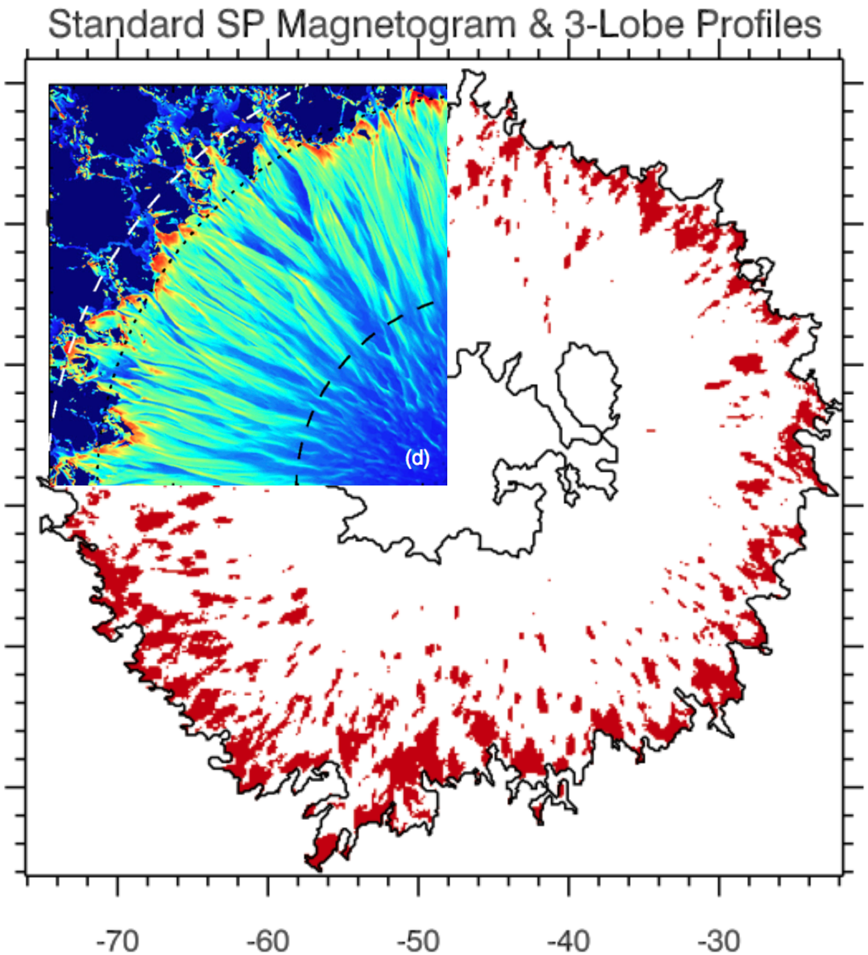

- **Franz & Schl. (2013): 17 % of opposite polarity**
- **see also Sanchez Almeida (2005) and Sanchez A. & Ichimoto (2009).**

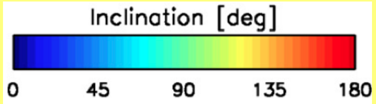

Fig. 6, Rempel 2012

(SP@SOT Hinode)

Franz & Schl. 2013

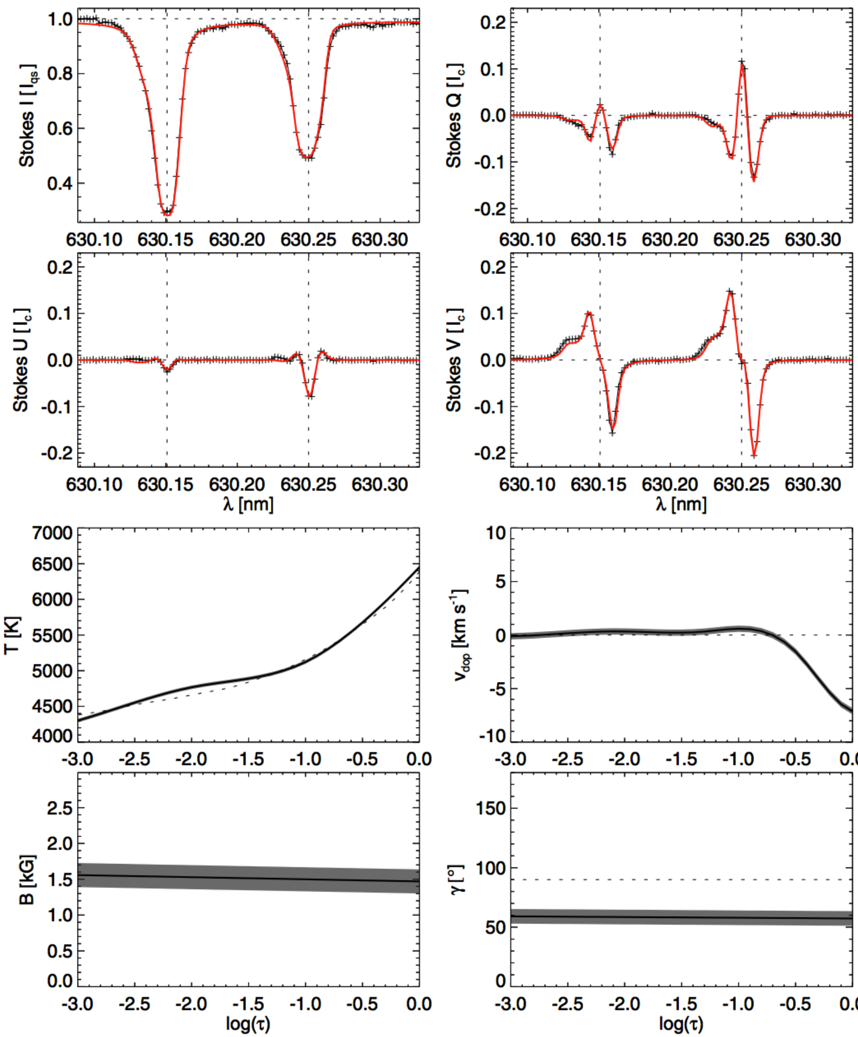

Fig. 2. *Top* part clockwise: representative Stokes *I*, *Q*, *V*, and *U* profiles (black) from an upflow region. The red lines indicate the result of radiative transfer calculations within the atmosphere plotted below and the dashed vertical lines represent the respective vacuum wavelength of the transition. *Bottom* part clockwise: temperature, Doppler velocity, zenith angle, and magnetic field strength (black) with errors (shaded gray) at different optical depth values. The dashed lines indicate the temperature stratification in the HSRA model, plasma at rest, and a zenith angle of 90° in the respective panels.

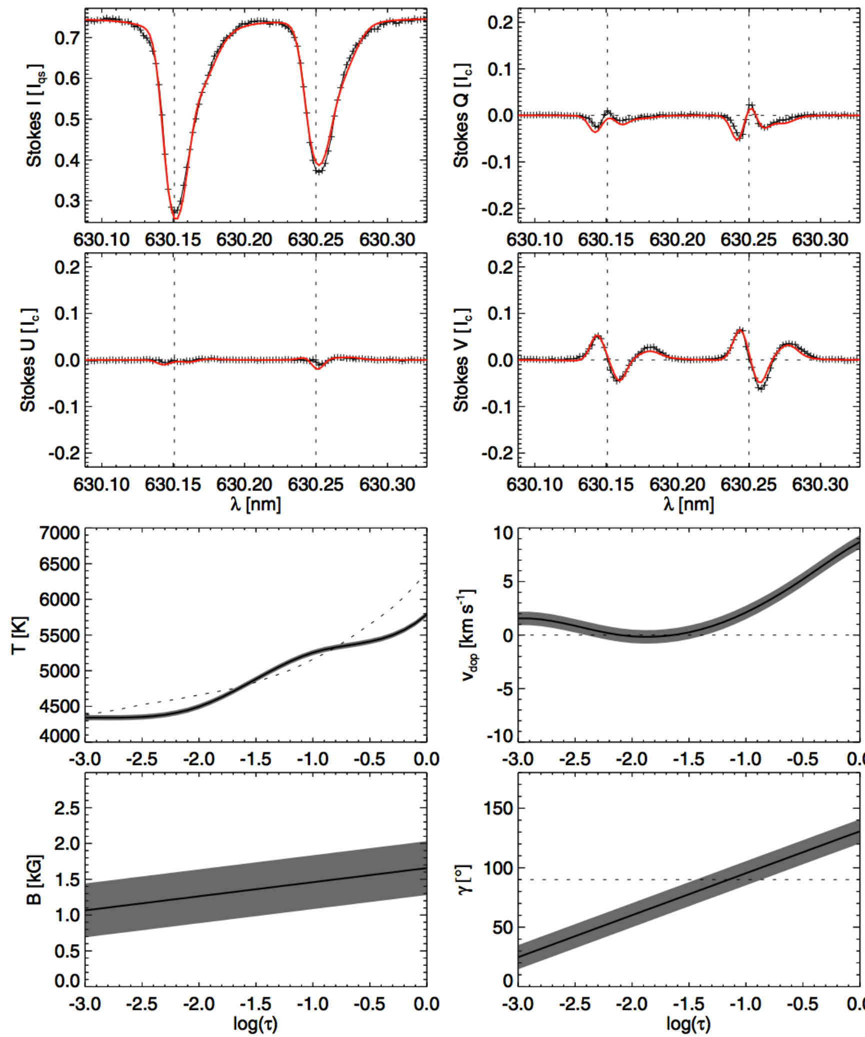

Fig. 3. Same as Fig. 2 but for a representative profiles from a downflow region. The magnetic field changes its polarity in the deep photospheric layers.

atmospheric parameters. Depicted are T, $v_{\rm dop}$, B, and $\gamma_{\rm mag}$ only, because the other parameters where either not inverted ($p_{\rm e^-}$) or remain constant throughout the line-forming region ($v_{\rm mic}$, $v_{\rm mac}$, and ϕ). The variation in the atmospheric parameters along the